Gas absorption into emulsions

Von der Fakultät für Lebenswissenschaften

der Technischen Universität Carolo-Wilhelmina

zu Braunschweig

zur Erlangung des Grades

eines Doktors der Naturwissenschaften

(Dr. rer. nat.)

genehmigte

D i s s e r t a t i o n

von Thanh Hai Ngo

aus Bacninh / Vietnam

1. Referent: Professor Dr. Adrian Schumpe

2. Referent: Professor Dr. Klaus-Dieter Vorlop

eingereicht am: 19.12.2012

mündliche Prüfung (Disputation) am: 05.03.2013

Druckjahr 2013

Vorveröffentlichungen der Dissertation

Teilergebnisse aus dieser Arbeit wurden mit Genehmigung der Gemeinsamen Naturwissenschaftlichen Fakultät, vertreten durch den Mentor der Arbeit, in folgenden Beiträgen vorab veröffentlicht:

Publikationen

Ngo, T. H. and A. Schumpe, "Absorption of CO_2 into alkane/water emulsions in a stirred tank", *Journal of Chemical Engineering of Japan*, **45**, 737-741 (2012).

Ngo, T. H. and A. Schumpe, "Oxygen absorption into stirred emulsions of n-alkanes", *International Journal of Chemical Engineering*, **2012**, 1-7 (2012)
doi:10.1155/2012/265603.

Tagungsbeiträge

Ngo, T. H., N. Golfinger and A. Schumpe, "Oxygen absorption into stirred emulsions"; 10th International Conference on Gas/Liquid and Gas/Liquid/Solid Reactor Engineering (GLS10), Braga, Portugal, 26-29 June, 2011.

Ngo, T. H. and A. Schumpe, "Absorption of CO_2 into alkane/water emulsions in a stirred tank"; 1st International Symposium on Multiscale Multiphase Process Engineering (MMPE), Kanazawa City, Japan, 4-7 October, 2011.

Golfinger, N., T. H. Ngo and A. Schumpe, "Untersuchung der Sauerstoff-Absorption in gerührten Emulsionen mit einer Optode und in der Wasserphase gelöstem Fluorophor"; 10th Dresdner Sensor-Symposium (10. DSS), Dresden, Germany, 5-7 December, 2011.

Acknowledgements

I would like to express my deepest gratitude to my mentor, Prof. Dr. Adrian Schumpe, for his whole-hearted guidance, supervision, support and help throughout this research project.

My sincere thanks are due to Prof. Dr. Klaus-Dieter Vorlop for accepting to be the co-referee of my dissertation. Also, I would like to express my thanks to Prof. Dr. Karl-Heinz Gericke for agreeing to serve as the chairman of the doctoral committee.

My grateful thanks go to Srinivasa Rao Ravella, Nadja Golfinger and Dr. Ajay Mandal for their valuable contributions to the experimental work. In addition, I would like to gratefully acknowledge SOPATec UG (Berlin, Germany) for the opportunity to use its endoscopic photo-probe.

I would like to express my thanks to all members of the Institute of Technical Chemistry, TU Braunschweig, Germany, especially my colleagues in the research group of Prof. Dr. Adrian Schumpe, namely Dr. Marius Rosu, Dr. Jörg Kupka, Dr. Adrian Dobre, Dr. Stoyan Nedeltchev, Oliver Lorenz, Marcel Jatzwauk, and Willy Tchowa Medjiade, for their support, willingness to help, and for a co-operative and friendly working atmosphere.

I am really grateful to my parents in Vietnam, Do Thi Kim Dung and Ngo Dang Tan, for their love, support and unconditional help during my study in Germany. My special thanks go to my wife, Phung Thi Trung, and my son, Ngo Duc Anh, for their love, care, patience and continuous encouragement. Also, I wish to thank Bui Thi Quynh Trang and Quynh Chi for their love and care during the writing phase of my dissertation.

Finally, I am thankful to Hanoi University of Mining and Geology in Vietnam, where I worked as a lecturer at Department of Oil refining and Petrochemicals, for allowing and supporting me to study in Germany.

Table of contents

List of figures

List of tables

Notation

A	Gas-liquid interfacial area, m^2
a	Specific gas-liquid interfacial area (referred to liquid volume), m^{-1}
C^*	Gas solubility in emulsion at a partial pressure of 101325 Pa, mol m^{-3}
c^*_L	Equilibrium concentration of absorbed gas in the liquid phase, mol m^{-3}
C^*_L	Equilibrium concentration of absorbed gas in the (pseudo-homogeneous) liquid phase, mol m^{-3}
$C^*_{O_2,W}$	Equilibrium oxygen concentration in the water phase, mol m^{-3}
c_L	Concentration of absorbed gas in the bulk liquid phase, mol m^{-3}
C_L	Concentration of absorbed gas in the bulk (pseudo-homogeneous) liquid phase, mol m^{-3}
$c_{L,i}$	Liquid phase concentration of absorbed gas at the gas-liquid interface, mol m^{-3}
$C_{O_2,W}$	Oxygen concentration in the water phase, mol m^{-3}
const.	Constant, dimensionless
D	Diffusion coefficient, $m^2\ s^{-1}$
$(D_{AB})_T$	Diffusion coefficient of gas A in liquid B at temperature T, $m^2\ s^{-1}$
d_h	Hole diameter of gas distributor, m
d_i	Impeller diameter, m
D_L	Diffusion coefficient of absorbed gas in liquid, $m^2\ s^{-1}$

d_R	Reactor diameter, m
E	Mass transfer enhancement factor, dimensionless
H	Henry's constant, Pa m^3 mol^{-1}
h	Planck's constant, J s
H_R	Reactor height, m
I	Fluorescence intensity in the presence of oxygen, V
I_0	Fluorescence intensity in the absence of oxygen, V
j	Molar flux, mol m^{-2} s^{-1}
k	Mass transfer coefficient, m s^{-1}
k_G	Gas-side mass transfer coefficient, m s^{-1}
k_L	Liquid-side mass transfer coefficient, m s^{-1}
K_L	Overall liquid-side mass transfer coefficient, m s^{-1}
k_La	Volumetric mass transfer coefficient, s^{-1}
$(k_La)_{GW}$	Gas-water volumetric mass transfer coefficient, s^{-1}
K_{SV}	Stern-Volmer constant, arbitrary unit
m_R	Relative solubility (gas solubility in pure oil compared to pure water), dimensionless
N_S	Stirring speed, s^{-1}
P	Total pressure, Pa

p^*_G	Equilibrium partial pressure of the absorbed gas, Pa
P_f	Final total pressure, Pa
p_G	Partial pressure of absorbed gas in the bulk gas phase, Pa
$p_{G,i}$	Partial pressure of absorbed gas at the gas-liquid interface, Pa
P_i	Initial total pressure, Pa
p_O	Partial pressure of oil, Pa
p_W	Partial pressure of water, Pa
R	Gas constant, Pa m^3 mol^{-1} K^{-1}
R_A	Gas absorption rate, mol m^{-3} s^{-1}
S	Initial spreading coefficient, N m^{-1}
s	Surface renewal frequency, s^{-1}
S^*	Equilibrium spreading coefficient, N m^{-1}
T	Temperature, K
t	Time, s
U	Photomultiplier-voltage in the presence of oxygen, V
U^*_0	Photomultiplier-voltage in the absence of oxygen (measured in external calibration stage), V
U^*_{100}	Photomultiplier-voltage at 100% oxygen saturation (measured in external calibration stage), V
U_0	Photomultiplier-voltage in the absence of oxygen, V

U_{100}	Photomultiplier-voltage at 100% oxygen saturation, V
V	Volume, m^{-3}
$\tilde{V}_A$	Molar volume of gas A at the normal boiling point temperature, $m^3\ mol^{-1}$
$\tilde{V}_B$	Molar volume of liquid A at the normal boiling point temperature, $m^3\ mol^{-1}$
V_G	Gas phase volume, m^{-3}
V_L	Liquid phase volume, m^{-3}
V_R	Reactor volume, m^{-3}

Greek symbols

δ	Film thickness, m
λ	Wavelength, m
λ_{max}	Maximum wavelength, m
μ	Dynamic viscosity, Pa s
μ_B	Dynamic viscosity of liquid B, Pa s
σ	Interfacial tension measured with pure phases, $N\ m^{-1}$
σ^*	Interfacial tension measured with mutually saturated phases, $N\ m^{-1}$
τ	Exposure time, s
τ'	Fluorescence lifetime, s
τ'_0	Fluorescence lifetime in the absence of oxygen, s

υ	Frequency, Hz
Φ_{oil}	Oil volume fraction, dimensionless

Subscripts

atm	Atmosphere
cont.	Continuous liquid phase
disp.	Dispersed liquid phase
E	Excitation light
F	Fluorescent light
G	Gas
L	Liquid
O/W	Oil-in-water
OG	Oil-gas
OW	Oil-water
W	Water
WG	Water-gas

Abbreviations

G	Gas
L	Liquid
LED	Light-emitting diode
O	Oil
O/W	Oil-in-water
O/W/O	Oil-in-water-in-oil
PFC	Perfluorocarbon
PMT	Photomultiplier tube
PTFE	Polytetrafluoroethylene
RuBPY	Tris-(2,2'bipyridyl)-ruthenium (II) chloride
W	Water
W/O	Water-in-oil
W/O/W	Water-in-oil-in-water

1 Introduction and problem statement

Gas-liquid-liquid systems, in which a gas is absorbed into an oil-water emulsion with or without chemical reaction, are of scientific, technical and commercial importance due to their wide industrial application.

Through the development of the aqueous biphasic technique in homogeneous catalysis, gas-liquid-liquid systems have gained increasing attention in various chemical processes, e.g. hydroformylation, carbonylation, hydrogenation and oligomerization (Cornils, 1999). This aqueous biphasic technique involves using water-soluble ligands to solubilize the metal complex catalyst in an aqueous phase, which is easily separated from reactants and reaction products by decantation. Hydroformylation of propene to n-butyraldehyde is a typical example for important industrial applications of gas-liquid-liquid reaction systems. In this process, the reactive gas mixture of carbon monoxide, hydrogen and propylene is converted to n-butyraldehyde in an aqueous solution of rhodium catalyst (Cents *et al.*, 2004). Three different phases therefore exist in the reactor: the gas phase containing CO, H_2, and propylene; the aqueous catalyst phase (water phase); and the dispersed organic butyraldehyde phase (oil phase).

Gas absorption into oil-water emulsions is also frequently encountered in biotechnological processes. Aerobic fermentations are typical examples for industrial applications of gas-liquid-liquid systems with respect to biotechnological engineering. In these processes, oxygen is used as the gas phase (usually from air bubbles). The oil phases, with higher solubilities for oxygen compared to the aqueous phase containing the microorganisms, are mostly liquid hydrocarbons and perfluorocarbons (Dumont and Delmas, 2003; Galaction *et al.*, 2004; Clarke and Correia, 2008). Various useful chemical products have been successfully produced by aerobic fermentations with alkanes as the carbon sources, e.g. amino acids, organic acids, carbohydrates, nucleic acids, vitamins, enzymes, and antibiotics (Fukui and Tanaka, 1980).

In addition, new potential applications of gas-liquid-liquid systems have been considered in gas treatment and separation. The target gases, such as acid gases (H_2S, CO_2); olefins (propylene, isobutylene...) or volatile organic compounds (VOCs: styrene, toluene, benzene…), are removed from a gas stream by chemical or physical absorption into an oil-water emulsion. Park *et al.* (2002) and Mortaheb *et al.* (2012) have recently mentioned a promising technological option for removal of acids gases such as CO_2 and H_2S from a gas stream (e.g. from natural gas or industrial waste gas) based on chemical absorption into water-in-oil emulsions, where an aqueous amine solution is dispersed in a continuous oil phase.

In above mentioned gas-liquid-liquid systems, the gas absorption rate is usually characterized by the volumetric mass transfer coefficient k_La (cf. Chapter 2 for its definition). The addition of a third immiscible liquid phase to a gas-liquid system may affect k_La considerably. An extensive literature review of the experimental investigations on gas absorption into emulsions is presented in Chapter 2, from which the existing problems can be observed:

- The addition of oil to a gas-water system is mostly limited to low oil volume fractions. At high-oil volume fractions, not considered in the previous studies, the high gas solubilities in the oils (high driving force) should have a strong effect on the mass transfer characteristics.

- Most pseudo-homogeneous mass transfer models for evaluating k_La-values have been developed using the assumption that there is no direct contact between oil droplets and gas bubbles. However, these models may not be valid when the oil can spread and cover the gas bubble or when the experiments are carried out at high oil volume fractions.

- The effects of oil addition on the volumetric mass transfer coefficient (k_La) are very complicated: with increasing oil volume fraction, k_La can increase, decrease, or remain unaffected. The reported results are contradictory and the reasons are not clear.

- Understanding the gas transfer mechanisms into emulsions might be attractive to explain the observed results. However, only few studies have addressed this and the mass transfer mechanism is still not well understood due to lack of experimental evidence.

- The oil spreading coefficient (cf. Chapter 2 for its definition) could be a very important clue to identify the mass transfer mechanism. However, the values of spreading coefficient reported in the literature do not agree well.

In the present research, the effects of oil addition on the volumetric mass transfer coefficient k_La are experimentally studied by pressure technique in the full range of oil volume fraction (0-100%). Specifically, absorption of pure oxygen (O_2) and pure carbon dioxide (CO_2) into aqueous emulsions of n-heptane, n-dodecane, and n-hexadecane, respectively, is performed at 0 to 100% oil volume fraction in a stirred tank. At the stirring speed of 1000 min^{-1} used throughout, gas is dispersed into bubbles by surface aeration. A pseudo-homogeneous mass transfer model is developed, which allows evaluating k_La values from the experimental data of pressure decrease under isochoric and isothermal (298.2 K) conditions. With the pressure technique, the information on gas solubility in all studied emulsions is concurrently obtained.

In order to gain more insight into the mass transfer mechanism, the fluorescence technique with an oxygen-sensitive fluorophore, soluble in water but insoluble in the oils, is developed to measure the oxygen transfer to the water phase in aqueous emulsions of n-dodecane and n-hexadecane.

The emulsion phase inversion which might have strong effect on the volumetric mass transfer coefficient is identified by both electrical conductivity and observation methods. In addition, to achieve the correct values of spreading coefficient for the studied systems, interfacial tensions are measured with a tensiometer using the ring method. Finally, an endoscopic photographic technique is used to investigate into the water-in-oil (W/O) emulsion structure.

2 Mass transfer background and literature review

This chapter deals with a detailed discussion of the fundamental theories for mass transfer across gas-liquid interfaces. The experimental investigations on the gas absorption into emulsions reported in the literature are reviewed and discussed. The discussion of the literature results focus on effects of oil addition on mass transfer parameters, spreading coefficient, mass transfer pathways, and mechanisms for mass transfer enhancement.

2.1 Mass transfer across a gas-liquid interface

Mass transfer in gas-liquid systems is the transfer of material through the gas-liquid interface. In gas absorption, as an example, the soluble gas diffuses to the liquid surface, dissolves in the liquid, and then passes into the main body of the liquid. To describe this process, the "two-film theory" and the "surface renewal or penetration theory" are fundamental. They are therefore discussed below.

2.1.1 The two-film theory

The two-film theory of Lewis and Whitman (Lewis and Whitman, 1924) was the first attempt to describe the transfer of a component across the interface between two phases. It is assumed that the total resistance to mass transfer is concentrated in thin stagnant films on both sides of the interface, and that the transfer within these films occurs by molecular diffusion only. Outside the films, in the bulk fluids, the phases are considered as well mixed having no concentration gradients.

The physical absorption of a gas phase component into a liquid on the basis of the two film theory is illustrated in Figure 2.1. The transfer of a component from the bulk of one phase to the interface is characterized by the mass transfer coefficient k (cf. Equation 2.1):

$$j = k\Delta c \tag{2.1}$$

where j is the molar flux of the component (moles per unit area per unit time); Δc is the driving force for mass transfer expressed as the difference between the bulk and the interface concentration.

The mass transfer coefficient k can be written with subscripts L or G which denotes the liquid or gas phase. It should be noted that the driving force is usually expressed as partial pressure difference for the gas phase; therefore k_G has different dimensions from k_L.

From equation 2.1, the molar fluxes in both gas and liquid phases may be written:

$$j_G = k_G(p_G - p_{G,i}) \tag{2.2}$$

$$j_L = k_L(c_{L,i} - c_L) \tag{2.3}$$

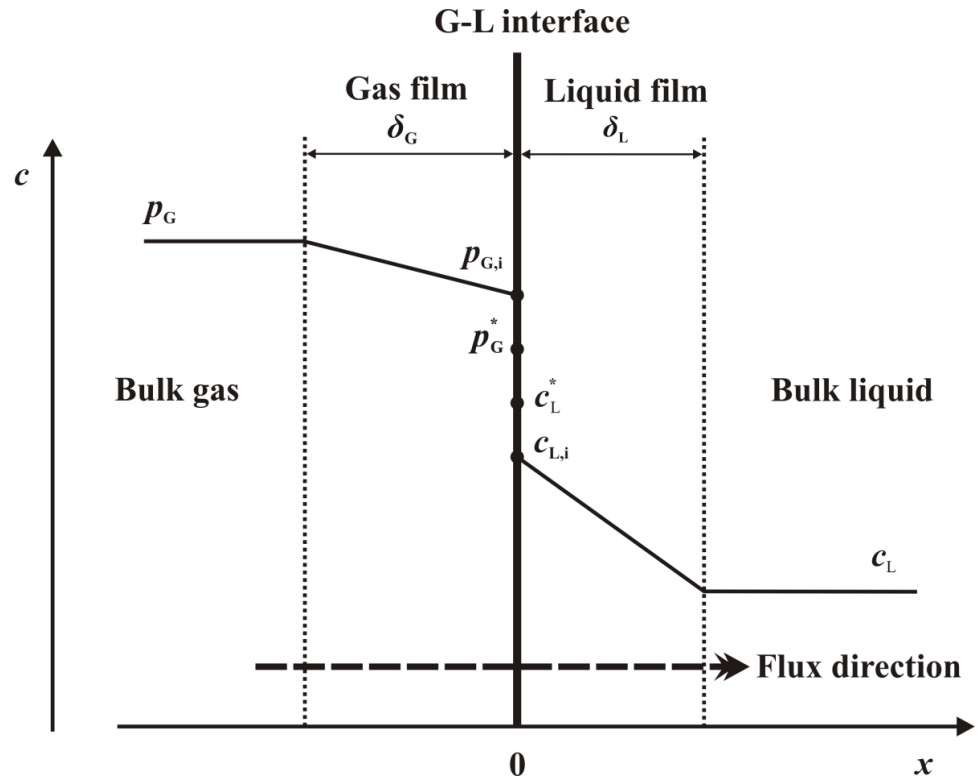

FIGURE 2.1: Concentration profiles in the bulk phases and stagnant films for a gas-liquid system based on the two-film model.

Diffusion in the stagnant films is governed by Fick's first law (cf. Equation 2.4):

$$j = -D\frac{dc}{dx} \tag{2.4}$$

For the liquid phase, using equations 2.3 and 2.4, the relation between the diffusion coefficient D_L and the film thickness δ_L can be derived as follows:

$$j_L = k_L(c_{L,i} - c_L) = -D_L \frac{c_L - c_{L,i}}{\delta_L} \tag{2.5}$$

Thus:

$$k_L = \frac{D_L}{\delta_L} \propto D_L \tag{2.6}$$

Equation (2.6) shows that in the two-film theory, k_L is directly proportional to the diffusion coefficient D_L. According to Taylor and Krishna (1993), usually, the liquid film thickness (δ_L) is in the range 0.01- 0.1 mm and the gas film thickness ($\delta_G = D_G/k_G$) is in the range 0.1- 1 mm. In general, when the level of mixing or turbulence in the fluid phases is increased, the film thicknesses will be decreased, and correspondingly the mass transfer coefficients will be increased.

At steady state the molar fluxes in equations 2.2 and 2.3 must be equal:

$$j = j_L = j_G \tag{2.7}$$

or:

$$j = k_G(p_G - p_{G,i}) = k_L(c_{L,i} - c_L) \tag{2.8}$$

With the assumption of established phase equilibrium at the G/L interface, the relation between $p_{G,i}$ and $c_{L,i}$ is determined by Henry's law:

$$p_{G,i} = Hc_{L,i} \tag{2.9}$$

Equation 2.8 gives:

$$p_{G,i} = p_G - \frac{j}{k_G} \tag{2.10}$$

From equations 2.9 and 2.10, it follows that:

$$c_{\mathrm{L,i}} = \frac{p_{\mathrm{G}}}{H} - \frac{j}{k_{\mathrm{G}} H} \tag{2.11}$$

Substitution of equation 2.11 into equation 2.8 gives:

$$j = k_{\mathrm{L}} \left(\frac{p_{\mathrm{G}}}{H} - \frac{j}{k_{\mathrm{G}} H} - c_{\mathrm{L}} \right) \tag{2.12}$$

From equation 2.12, the molar flux j across the G/L interface is obtained:

$$j = K_{\mathrm{L}} (c_{\mathrm{L}}^{*} - c_{\mathrm{L}}) \tag{2.13}$$

with the overall mass transfer coefficient K_{L} and the equilibrium concentration c^{*}_{L} (in equilibrium with p_{G} in bulk gas phase) given by:

$$\frac{1}{K_{\mathrm{L}}} = \frac{1}{k_{\mathrm{L}}} + \frac{1}{k_{\mathrm{G}} H} \tag{2.14}$$

$$c_{\mathrm{L}}^{*} = \frac{p_{\mathrm{G}}}{H} \tag{2.15}$$

In equation 2.14, the terms $1/k_{\mathrm{L}}$ and $1/k_{\mathrm{G}}H$ are known as liquid-side and gas-side mass transfer resistance, respectively. Compared to the resistance in the liquid phase, the gas-side mass transfer resistance is often negligible because of the much higher diffusion coefficients and lower viscosities prevailing in the gas phase (Nigam and Schumpe, 1996). Then, from equation 2.14, it follows:

$$K_{\mathrm{L}} \approx k_{\mathrm{L}} \tag{2.16}$$

and equation 2.13 can be written as:

$$j = k_{\mathrm{L}} (c_{\mathrm{L}}^{*} - c_{\mathrm{L}}) \tag{2.17}$$

The specific interfacial area a is defined as:

$$a = \frac{A}{V_{\mathrm{L}}} \tag{2.18}$$

Putting the value of a on both sides of equation 2.17, the (volumetric) absorption rate R_A (moles per unit liquid volume per unit time) is obtained:

$$R_A = ja = k_L a(c_L^* - c_L) \tag{2.19}$$

The term $k_L a$ is known as the volumetric mass transfer coefficient. The experimental determination of the interfacial area A, and hence the specific interfacial area a, independent from the liquid-side mass transfer coefficient k_L, is usually difficult, so that the product $k_L a$ is most often reported rather than k_L and a, separately.

2.1.2 The surface renewal theory

In the penetration or surface renewal theory, it is assumed that fluid elements are transported to the interface by turbulence where they are exposed to the second phase for some time, after which the fluid elements return to the bulk fluid phase again and are replaced by fresh fluid elements. During the exposure time that the fluid element resides at the interface, the mass transfer with the second phase takes place by a process of unsteady state molecular diffusion. A pictorial representation of this theory is given in Figure 2.2.

In the surface renewal theory of Higbie (1935), it is assumed that all the fluid elements at the interface would have the same exposure time τ, whereas the basic assumption for Dankwerts (1951) surface renewal theory is that the residence time of each surface element could be subject to a random distribution. However, in both models, the mass transfer coefficient is found to be proportional to the square root of the diffusion coefficient (cf. Equations 2.20 and 2.21):

- Higbie:

$$k_L = 2\sqrt{\frac{D_L}{\pi\tau}} \tag{2.20}$$

- Dankwerts:

$$k_L = \sqrt{D_L\, s} \tag{2.21}$$

here s is known as the surface renewal frequency, which determines the residence time distribution function of each surface element based on equation 2.22 (Coulson and Richardson, 1990):

$$E(t) = s\exp(-st) \tag{2.22}$$

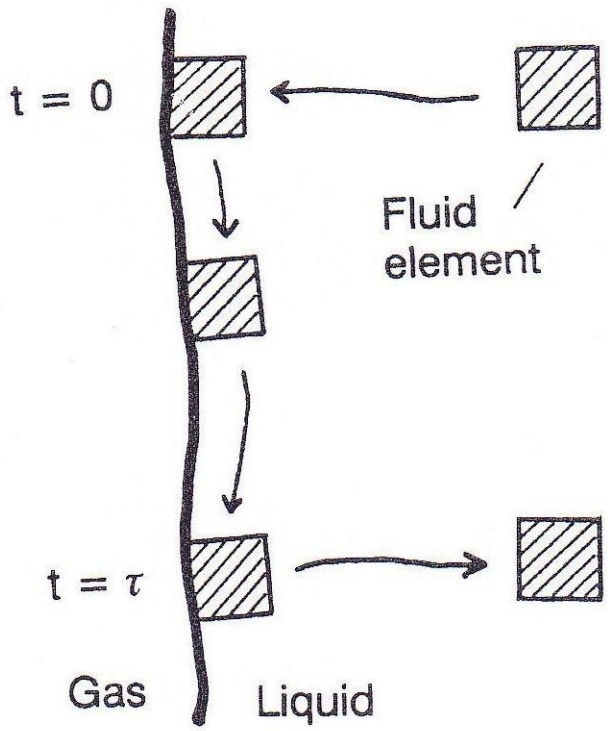

FIGURE 2.2: General representation of the surface renewal theory.

In general, as the degree of turbulence in the liquid phase increases, the exposure time τ will become smaller whereas the surface renewal frequency s will increase. It should be also noted that the two-film and the penetration theory are the limiting cases of the general film-penetration theory suggested by Toor and Marchello (1958).

Despite the different effects of D_L, the application of the two-film and surface renewal theories to predict the mass transfer rates gives relatively close results (Baerns *et al*., 1987). In addition, the results of other theories modeled by more complicated mathematical expressions show only slight differences compared to the two-film theory (Emig and Klemm, 2005). The application of the

two-film theory is therefore most often recommended because of the relative simplicity in computations.

When a second immiscible liquid phase is added to a gas-liquid system, the situation becomes much more complicated. The roles of the dispersed phase should be taken into account when theoretically modeling a gas-liquid-liquid system based on these above fundamental theories. In Chapter 3, the pseudo-homogeneous mass transfer model for the current research will be developed based on the two-film theory.

2.2 Experimental investigations on gas absorption into emulsions

According to the type of absorption (physical absorption, chemical absorption, and physical absorption in biological systems), the experimental investigations on gas absorption into emulsions described in the literature are summarized in Tables 2.1-2.3.

Most investigations on gas absorption into emulsions were aimed at the typical application in industrial bioprocesses, e.g. aerobic fermentations with oil as the carbon source (oxygen absorption). However, new potential applications in industrial gas separation and treatment processes (absorption of CO; CO_2; olefin gases: propylene, isobutylene..; volatile organic compounds (VOCs): styrene, toluene, benzene...) have been also considered.

The oil phase, which is immiscible in the aqueous phase and has higher solubility for the gas components compared to the aqueous phase (cf. m_R-values in Tables 2.1-2.3), could be liquid hydrocarbons, perfluorocarbons or silicon oils. However, as can be seen from the reported experimental results, the addition of these oils to a gas-liquid system with the aim to enhance the gas-liquid mass transfer was mostly limited to low oil volume fractions.

Stirred tank reactors were used extensively to carry out the experiments. This is maybe due to the fact that a better liquid mixing condition which is essential to create or maintain the oil/water emulsions can be more easily established compared to bubble columns or air-lift bioreactors. Moreover, according to Jia *et al.*, (1997), the gas mass transfer rate in stirred tank reactors is usually higher than that in bubble columns or air-lift bioreactors.

To study the effect of the oil addition on the gas-liquid mass transfer, the volumetric mass transfer coefficient (k_La) was measured either in gas or in liquid phase. Some investigators have also attempted to measure the specific interfacial area (a) and the liquid side mass transfer

coefficient (k_L) separately using chemical methods (cf. Table 2.2). The variation of these mass transfer parameters upon oil addition are discussed in detail in Section 2.4.

Some studies have also addressed on the effects of the presence of microorganisms on k_La in fermentation broths (cf. Table 2.3). According to Galaction *et al.* (2005), regardless of the microorganism type, the influence of the cells on oxygen transfer is the result of the increase in broth's apparent viscosity by biomass accumulation, and the blocking effect created by the formation of cell-oil droplet-air bubble associations (i.e. cell could be adsorbed to oil droplet's surface, and the cell-oil droplet association could be further adsorbed to the air bubble's surface).

TABLE 2.1: Physical absorption

Reference	*Apparatus*	*Operating conditions*							*Measurement of mass transfer parameters*	
		T (^{0}C)	*Water phase*	*Oil phase*	*Gas phase*	*Emulsifier or micro-organism*	*Φ_{oil} (-)*	*m_R (-)*	*Measured parameter*	*Phase*
Yoshida *et al.* (1970)	Stirred vessel: d_R = 15 cm, V_L = 2.57 l, turbine agitator (d_i = 6 cm), N_S = 200-650 rpm Bubble column: d_R = 10 cm, H_R = 1 m	30	Water	Kerosene Liquid paraffin Toluene Oleic acid	Oxygen	Tween 85	0-0.22	4.26 3.95 8.17 4.83	k_La	Liquid
Hassan and Robinson (1977)	Stirred vessel: d_R = 15,24 cm, turbine agitator (d_i = 5.08 cm), N_S = 800-1800 rpm	30	Na_2SO_4	n-Dodecane n-Hexadecane	Oxygen		0-0.1	8.12 7.53	k_La	Liquid
Little *et al.* (1994)	Stirred vessel: V_R = 1.25 l, N_S = 0-2500 rpm	25	Water	Toluene	CO_2 Propene	Polyethoxy alkylphenol (Igepal CO-720)	0.0107-0.0385	2.87 103.3	Absorption rate	Gas

TABLE 2.1 (continued)

Cesário *et al.* (1997)	Stirred tank reactor: V_R = 2 l, V_L = 1.3 l, turbine stirrer, N_S = 800 rpm	22	Water	Perfluorocarbon (PFC40)	Oxygen		0-0.2	11.64	k_La	Gas
					Toluene (Vapor)			17.50		
Lekhal *et al.* (1997)	Stirred autoclave: V_L = 0.6 l, N_S = 0-2500 rpm	50	Water	Octene	H_2		0-0.3	10	k_La	Gas
					CO					
Kundu *et al.* (2003)	Bubble column: d_R = 7.6 cm, V_L = 9.2 l, gas distributor (20 holes, d_h = 0.05 cm)	20	Water	Toluene	Oxygen		0-0.1	8.2	k_La	Gas
				Anisole				5.6		
				2-Ethyl-1-hexanol				7.5		
				Decyl alcohol				4.9		
				n-Dodecane				8.1		
				n-Decane				8.8		
				n-Heptane				10.9		

TABLE 2.1 (continued)

Galaction *et al.* (2004)	Stirred bioreactor : V_R = 5 l, V_L = 4 l, two turbine agitators, gas distributor (ring with 14 holes, d_h = 1 mm)	21	CMC solutions with viscosity range: 10-330.5 cP	n-Dodecane	Oxygen		0-0.2		k_La	Liquid
Nielsen *et al.* (2003)	Stirred bioreactor: V_R = 2 l, V_L = 1 l, d_R = 11 cm, turbine imperllers (d_i = 4.95 cm), N_S = 3.33-3.33 rps	30	Aqueous growth medium for Alca-ligenesxyl oxidans Y234	n-Hexadecane	Oxygen		0-0.33		k_La	Liquid
Cents *et al.* (2004)	Stirred autoclave: V_R = 640 ml, gas in-ducing turbine stirrer (d_i = 4.5 cm), N_S = 800 rpm	22-25	Water	Butyraldehyde	CO H_2 Propylene		0-0.4	11.2 4.5 65.3	k_La	Gas

TABLE 2.1 (continued)

Cents *et al.* (2005)	Reactor (d_R = 15 cm, V_R = 3.2 l) operated as both bubble column and stirred vessel, gas distributor (type P1, 90-50 mm), turbine stirrer (d_i = 5 cm)	21	Tap water 0.5 M KCl solution	Toluene Hexadecane Heptane 1- Octanol	Air		0.025 "0-0.06" (for air-water-toluene system)		a	Liquid
Dumont *et al.* (2006 a)	Bubble reactor: H_R = 0.33 m, d_R = 0.21 m, gas distributor (75 x 150 mm) with 50 holes (d_h = 1 mm)	20	Water	n-Dodecane n-Hexadecane Perfluorocarbon (PFC40) Silicone oil 47V5 Silicone oil 47V10	Oxygen		0-0.1	6 5 12 7 7	k_La	Gas

TABLE 2.1 (continued)

Dumont *et al.* (2006 b)	Oxygen absorption: bubble reactor: H_R = 0.33 m, d_R = 0.21 m; gas distributor (75 x 150 mm) with 50 holes (d_h = 1 mm) Styrene absorption: bubble reactor, V_R = 1 or 2 l	20 (for oxygen) 25 (for styrene)	Water	Silicone oil 47V5	Oxygen Styrene (Vapor)		0-0.1	7 633	k_La	Gas
Da Silva *et al.* (2006 a)	Stirred glass reactor: V_R = 2 l, V_L = 1.5 l, four-blade Rushton turbine impeller (d_i = 4.8 cm), gas distributor (ring with 5 holes, d_h = 0.5 mm), N_S = 250 and 500 rpm, aeration rates: 0.5 and 1 vvm	27	Water	n-Dodecane	Oxygen		0-0.1		k_La	Liquid
Shariati *et al.* (2007)	Glass airlift bioreactor: d_R = 0.14 m, draft tube (d_t = 0.1 m, H_t = 1.1 m), gas distributor (25 holes, d_h = 1 mm)	25	Water	Diesel isomax	Oxygen	Kenon 10 Kenon 4	0.71-1.00		k_La	Liquid

TABLE 2.1 (continued)

Boltes *et al.* (2008)	Glass airlift reactor with internal loop: V_L = 2 l, riser height = 0.226 m, riser diameter = 0.055 m, riser wall thickness = 0.001 m, downcomer diameter = 0.084 m	30	Water	n-Dodecane	Oxygen		0-1		k_La	Liquid
Gómez-Díaz *et al.* (2009)	Bubble column: H_R = 65 cm, d_R = 4 cm, gas distributor: 5 holes	?	Water	Methyl ricinoleate (MR)	Oxygen	Tween 80	0-0.011		k_L and a	Liquid

TABLE 2.2: Chemical absorption

Reference	*Apparatus*	*Operating conditions*							*Measurement of mass transfer parameters*	
		T (^{0}C)	*Water phase*	*Oil phase*	*Gas phase*	*Emulsifier or micro-organism*	Φ_{oil} (-)	m_R (-)	*Measured parameter*	*Phase*
Mehta and Sharma (1971)	Stirred contactor (four baffles): d_R = 12.5 cm, V_L = 1.5 l, 6 straight –blade disk turbine impeller, d_i = 5.8 cm, N_S = 750 rpm	?	NaOH	2-Ethyl hexanol	CO_2		0-0.15	4.72	a and k_L	Liquid
Linek and Benes (1976)	Stirred vessel (four baffles): V_L = 0.858 l, d_R = 67 mm; 7 four-blade impellers; N_S = 15.8 s^{-1}	30	Na_2SO_3	n-Alkans (C_{11}-C_{18}) Oleic acid	Oxygen		0-1	11.79 7.57	k_L	Gas
Das *et al.* (1985)	Stirred vessel (four baffles): d_R = 13.5 cm, V_L = 1.5 l, 6 bladed Rushton turbi-ne impeller, N_S = 1300 rpm	?	NaOH	Toluene Methyl isobutyl ketone 2-Ethyl hexanol	CO_2	Tricresyl phosphate (as anti-foaming agent)	0-0.5		a	Gas

TABLE 2.2 (continued)

Mehra and Sharma (1985)	Stirred cell: d_R = 9.2 cm, V_L = 0.2 l, N_S = 60 rpm	27	H_2SO_4	Chlorobenzen	Isobutylene Butene- 1 Propylene	Laury alcohol ethoxylate Nonyl phenol ethoxylate Dimethylcoco-amine oxide	0.02-0.3		Rate of absorption	Gas
Mehra and Sharma (1986)	Stirred cell: d_R = 9.2 cm, V_L = 0.2 l, N_S = 60 rpm	27	H_2SO_4	Chlorobenzen	Butene- 1 Propylene	Laury alcohol ethoxylate (butanol, pen-tanol, hexanol, 2-ethyl hexan ol as co-sur factants)	0.01		Rate of absorption	Gas
Bruining *et al.* (1986)	Stirred cell (four baffles): d_R = 6.1 cm, V_L = 100 ml, d_i = 35 mm, N_S = 440 rpm	26	Na_2SO_3	Decane Cyclohexane Hexadecane	Oxygen	1-Decanol Serdox NNP6	0.005-0.01	11.6	Rate of absorption	Gas

TABLE 2.2 (continued)

Chaudhuri und Sharma (1989)	Stirred cell: d_R = 9.5 cm, V_L = 0.25 l, N_S = 1.33 s^{-1}	30	Aqueous alkaline solutions	Toluene	Carbonyl sulfite (COS)	Tween 40 Laury alcohol ethoxylate	0.1-0.2		Rate of absorption	Gas
Van Ede *et al.* (1995)	Stirred cell: d_R = 0.1282 m, V_L = 1.65 l; N_S = 5 s^{-1}	30	Na_2SO_3	Octene	Oxygen	Mixture of Tween 20 and Tween 85 Sodium dodecyl sulphate	0-0.5	18	Rate of absorption	Gas
Cents *et al.* (2001)	Stirred reactor: V_L = 2.5 l, d_R = 149 mm, 6-bladed Rushton turbine impeller, N_S = 1100 rpm	21	K_2CO_3 / $KHCO_3$	Toluene n-Dodecane n-Heptane 1- Octanol	CO_2		0-0.4		a and k_L (Danckwerts plot technique)	Gas

TABLE 2.3: Physical absorption in biological systems (in the presence of cells)

Reference	*Apparatus*	*Operating conditions*							*Measurement of mass transfer parameters*	
		T (^{0}C)	*Water phase*	*Oil phase*	*Gas phase*	*Emulsifier or micro-organism*	Φ_{oil} (-)	m_R (-)	*Measured parameter*	*Phase*
Jungker *et al.* (1990)	Stirred tank fermentor: V_R = 4 l, V_L = 2.5 l, N_S = 800 rpm	25	Aqueous culture medium	Perfluorocarbon (PFC40)	Oxygen	Baker's yeast	0-1		Oxygen transfer rate (OTR)	Liquid
Rols *et al.* (1990)	Stirred tank fermentor: V_L = 12 l, N_S = 400 rpm, aeration rate = 0.21 vvm	35	Aqueous culture medium	n-Dodecane	Oxygen	Aerobacter - aerogenes Pluronic F68 (emulsifier)	0-0.33	7.9	k_La	Liquid
Ho *et al.* (1990)	Stirred tank fermentor: V_L = 12.5 l, N_S = 1000 rpm	25	Aqueous culture medium	n-Hexadecane	Oxygen	Penicillium chrysogenum	0-0.05		Oxygen transfer rate (OTR)	Liquid

TABLE 2.3 (continued)

Ju *et al.* (1991)	Two stirred bioreactors (surface aeration): "Celstir": V_L = 700 ml, N_S = 100 rpm "BR-05": V_L = 5 l, N_S = 200 rpm	37	Aqueous culture medium	PFC 40 PFC 77	Oxygen	Escherichia-coli (with two non-ionic emulsifiers)	0-0.25		k_La and oxygen transfer rate (OTR)	Liquid
Cesário *et al.* (1996)	Stirred tank fermentor: V_R = 2 l, V_L = 1.3 l, N_S = 800 rpm	30	Aqueous culture medium	Perfluorocarbon (PFC40)	Ethene (in air)	Mycobacterium parafortuitum E3	0-0.28	9.78	k_La	Gas
Jia *et al.* (1997)	Air-lift bioreactor: V_L = 5 l, d_R = 120 mm, draft tube (d_t = 80 mm, H_t = 350 mm), aeration rate = 0.5-2 vvm	34	Aqueous culture medium	n-Dodecane Perfluorocarbon	Oxygen	Saccharomyces cerevisiae	0-0.16		k_La	Liquid
Galaction *et al.* (2005)	Stirred bioreactor : V_R = 5 L, V_L = 4 l, two turbine agitators; gas distributor (ring with 14 holes, d_h = 1 mm)	21	Aqueous culture medium	n-Dodecane	Oxygen	Propionibacterium shermanii	0-0.2		k_La	Liquid

2.3 Spreading coefficient and mass transfer mechanisms

2.3.1 Spreading coefficient (*S*)

The oil spreading coefficient *S* is defined as in equation 2.23:

$$S = \sigma_{WG} - \sigma_{OG} - \sigma_{OW} \tag{2.23}$$

S can be either positive or negative. If *S* is positive, whenever the three phases of gas, oil, and water come into contact, the oil tends to totally spread as continuous film on the gas bubbles (Figure 2.3). On the other hand, if *S* is negative (non-spreading), the oil tends to form discrete droplets at the gas-water interface. The velocity of the spreading process increases as the spreading coefficient increases and decreases as the oil viscosity increases (Grattoni *et al.*, 2003).

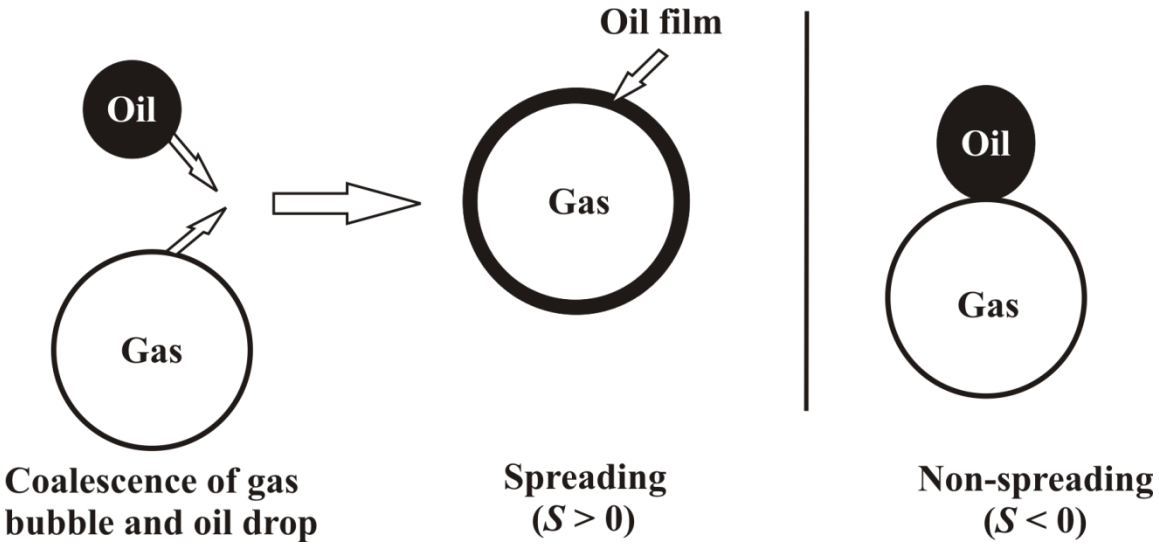

FIGURE 2.3: Spreading behavior of oil on water-gas interface.

According to Brilman (1998), the "initial" spreading coefficient *S* (cf. Equation 2.23), which exists in an early state of contact between pure phases, is often reported in the literature. However, in most practical applications, the phases are mutually saturated, and therefore the "equilibrium" spreading coefficient (S^*), which is established after mutual saturation of the

phases, should be used. The equilibrium spreading coefficient S^* can be calculated based on the values of the surface (interfacial) tensions of mutually saturated phases using equation 2.24:

$$S^* = \sigma^*_{WG} - \sigma^*_{OG} - \sigma^*_{OW} \quad (2.24)$$

Table 2.4 represents several reported values of spreading coefficient (S) for some n-alkanes. Very surprisingly, different authors reported quite different or even contradictory values. For n-dodecane, at the same temperature of 298.15 K, Oliveira *et al*. (1999) and Rols *et al*. (1990) reported positive spreading coefficients (S = + 3.7 and S = + 0.6 mN m^{-1}, respectively), whereas negative values (-5.3 to -5.9 mN m^{-1}) have been reviewed by Pinho and Alves (2010).

TABLE 2.4: Literature values of spreading coefficient S for some n-alkanes

Oil	*T [K]*	*S [mN m^{-1}]*	*Authors*
n-Heptane	298.15	+1.2 to +2.3	Pinho and Alves (2010)
n-Dodecane	298.15	-5.3 to -5.9	Pinho and Alves (2010)
	303.15	-2.6	Hassan and Robinson (1977)
	298.15	+3.7	Oliveira *et al*. (1999)
	?	+8.7	Wei and Liu (1998)
	298.15	+0.6	Rols *et al*. (1990)
n-Hexadecane	303.15	-9.3	Hassan and Robinson (1977)
Mixture of n-alkanes (C_{11}-C_{18})	303.15	-3.6	Linek and Benes (1976)

2.3.2 Mass transfer mechanisms

- **Mechanisms for gas transfer into O/W emulsions**

When a gas is absorbed into an oil-in-water (O/W) emulsion (i.e. oil dispersed in continuous water phase), three possible mass transfer pathways, illustrated in Figure 2.4, have been generally proposed (Cesário *et al*., 1997).

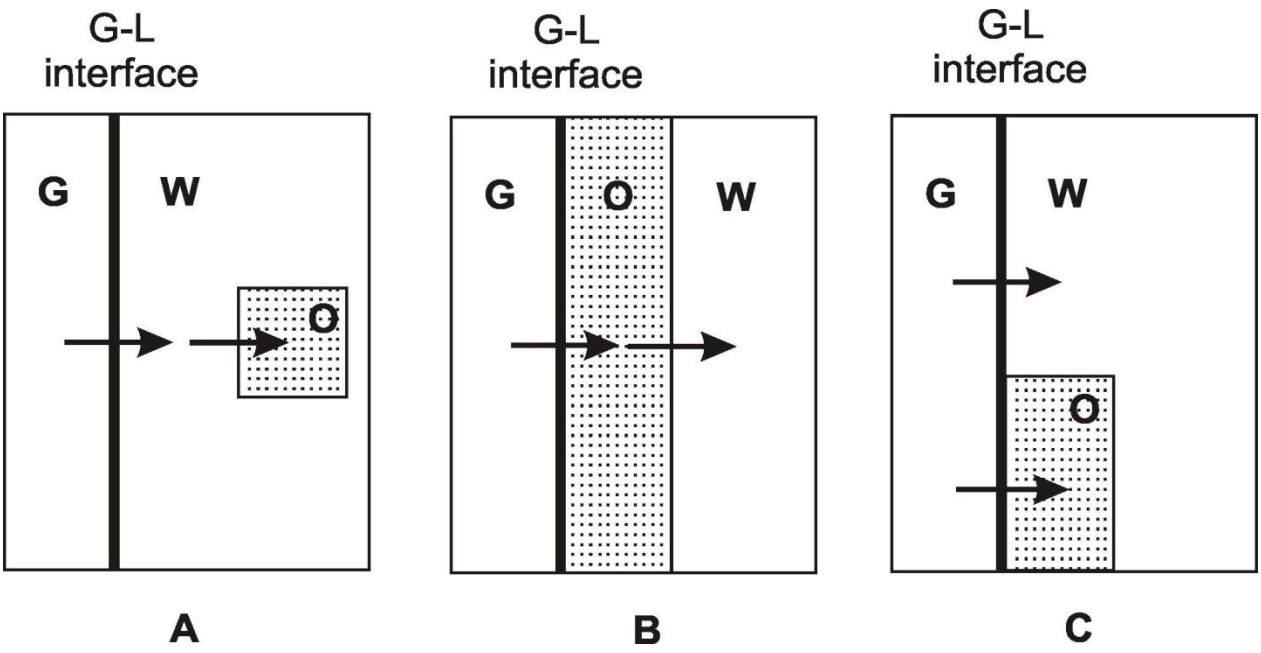

FIGURE 2.4: Possible mechanisms for gas transfer into O/W emulsions.

According to Cesário *et al*., (1997), all three mass transfer pathways are possible, depending on the value of the spreading coefficient *S*. If $S < 0$ (non-spreading), the oil remains as droplets dispersed in the water phase and does not contact directly with the gas bubble, and thus the mechanism is preferably serial transport: gas → water → oil (case A). If $S > 0$ (spreading), the oil tends to spread as a thin film covering totally or partially the gas/water interface; therefore the mechanism could follow case B (serial transport: gas → oil → water) or case C (parallel transport: gas → oil and gas → water), respectively.

Linek and Benes (1976) concluded from their study that there is no direct contact between the oil and the gas phase in O/W emulsions with $S < 0$ and the transfer mechanism is gas → water → oil. In addition, they suggested that the direct contact between the oil and the gas phase is even lacking in systems with $S > 0$. Similarly, MacMillan and Wang (1990) reported that the serial

transport gas → water → oil is the most probable mechanism for systems with $S < 0$, whereas the occurrence of direct gas/oil contact for systems with $S > 0$ remains speculative. In contrast, Rols *et al.* (1991) confirmed the existence of the direct gas-oil contact for the systems with S > 0 and the proposed mass transfer mechanism in their study is gas → oil → water → cells.

Regardless of the spreading coefficient, Das *et al.*, (1985) concluded that the oil phase can provide a parallel mechanism of transport (i.e. case C) when the gas has high solubility in it. On the other hand, according to Dumont and Delmas (2003), the mass transfer from the gas phase to O/W emulsions may not occur as in case B or C and that the case A which is used extensively in the literature is a more logical explanation.

- **Mechanisms for gas transfer into W/O emulsions**

Figure 2.5 illustrates two possible mass transfer pathways considered by Linek and Benes (1976) for the case of gas absorption into water-in-oil (W/O) emulsion (i.e. water dispersed in continuous oil phase). The gas might be transported to the W/O emulsion following either serial transport: gas → oil → water (case D) or parallel transport: gas → oil and gas → water (case E). These authors concluded that the mass transfer mechanism in W/O emulsions (both with negative and positive spreading coefficient) is case E (i.e. there is a parallel transfer of gas to both phases), whereas case D was rejected as improbable.

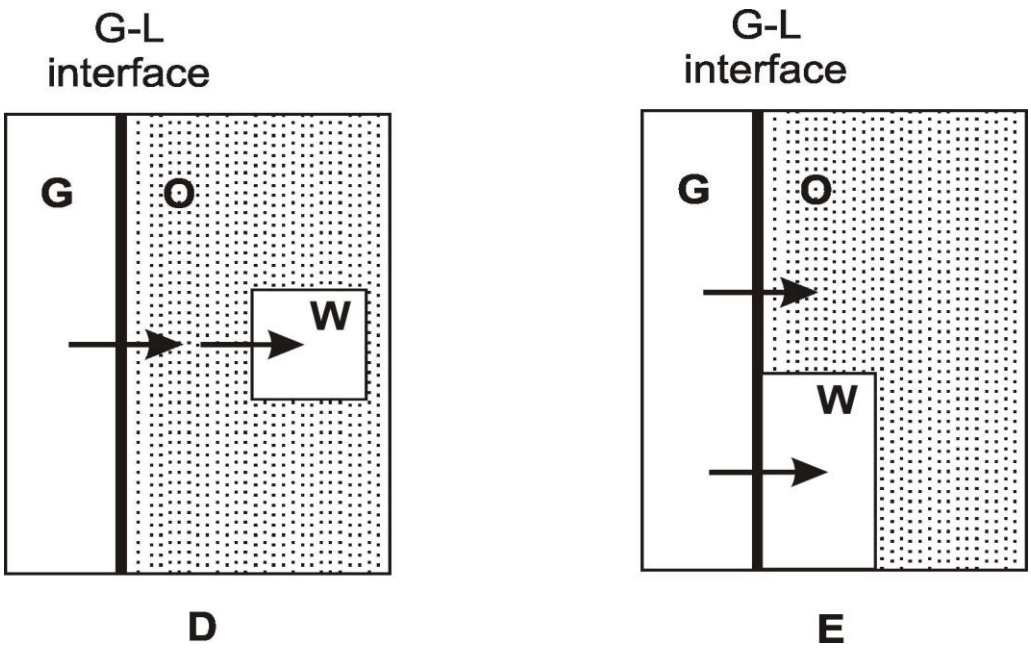

FIGURE 2.5: Possible mechanisms for gas transfer into W/O emulsions.

2.4 Effect of oil addition on mass transfer parameters

2.4.1 Effect of oil addition on volumetric mass transfer coefficient (k_La)

Table 2.5 summarizes some experimental results reported in the literature showing the effect of oil addition on the mass transfer parameters: k_La, k_L, and a. As the oil volume fraction increases, no general trends in the variation of the volumetric mass transfer coefficient (k_La) could be derived from the reported results whether the concept of spreading coefficient S (positive or negative) was mentioned or not.

On the addition of toluene and oleic acid (both with positive S-values) to an oxygen-water system in a stirred tank, Yoshida *et al.* (1970) found a minimum in k_La: it initially decreased and then increased with increasing oil volume fraction. These authors mentioned that this variation of k_La might be attributed to opposite changes in both k_L and a: the oil phase ($S > 0$) decreases the mass transfer coefficient (k_L) by increasing the liquid phase mass transfer resistance, but increased gas-liquid interfacial area a owing to spreading as a thin film on the gas-liquid interface, lowering the surface tension, thus decreasing the bubble size. Conversely, Rols *et al.* (1990) found a maximum in k_La for oxygen in aqueous emulsions of n-dodecane ($S > 0$): as the oil volume fraction increased, k_La first increased rapidly and then above 15 vol. % it decreased. These authors proposed the "bubble covering" mechanism (cf. Section 2.5) to explain the increase in k_La with increasing the oil hold-up, but this mechanism was not able to elucidate the decay of k_La at high oil hold-ups. Surprisingly, Dumont *et al.* (2006 a) reported that k_La remained practically constant upon addition of PFC 40 (also with $S > 0$).

In the case of negative spreading coefficient (kerosene and liquid paraffin), Yoshida *et al.* (1970) found that k_La decreased linearly with increasing oil volume fraction and explained that the effective interfacial area of gas bubbles for oxygen transfer might decrease due to partial blanketing of the bubble surface with lens-like oil droplets and slower diffusion of oxygen through oil droplets. Hassan and Robinson (1977) performed oxygen absorption experiments into aqueous emulsions of n-dodecane and n-hexadecane (both with negative S-values) in a stirred tank. With increasing n-hexadecane volume fraction, k_La initially increased (until $\Phi_{oil} = 0.06$), then remained approximately constant. Surprisingly, a sharp initial decrease in k_La (until $\Phi_{oil} = 0.01$) was found in case of n-dodecane. Unfortunately, these authors were not able to explain the opposing trends.

Regardless of spreading coefficient (*S*), some studies have been also carried out with the aim of finding other factors to explain the variations of k_La with the oil addition more persuasively. Unfortunately, the reported experimental results are contradictory. For instance, Lekhal *et al.* (1997) studied the absorption of H_2 and CO into octene/water emulsions in a stirred autoclave. They observed a clear maximum in k_La at 3-4% oil volume fraction; the effect was somewhat stronger at higher stirring speed. They suggested that this interesting maximum should be explained by coalescence inhibition by small oil droplets or by the "shuttle" mechanism (cf. Section 2.5). In contrast, Dumont *et al.* (2006 b) found that k_La for oxygen initially decreased rapidly and then increased rather slowly with increasing volume fraction of silicone oil 47V5; the effects are particularly marked for low volume fractions of silicone oil (1-2%). Similarly, Boltes *et al.* (2008) who recently studied the absorption of oxygen into aqueous emulsions of n-dodecane in an airlift reactor reported that k_La first decreased with increasing oil volume fraction, increased afterwards for higher oil volume fractions.

It should be noted that the peak-type in k_La (minimum or maximum) was not always observed by other authors. Kundu *et al.* (2003) who studied the oxygen absorption in aqueous emulsions of several oils in a bubble column observed that k_La increased with increasing oil volume fractions for n-heptane, n-dodecane, and n-decane. According to these authors, addition of 1% n-dodecane or n-heptane could enhance oxygen transfer in a bubble column up to fourfold. Similar trend in k_La (i.e. k_La increase) was also reported by Galaction *et al.* (2004). Quite differently, Ju *et al.* (1991) found the opposite trend in k_La for oxygen: with increasing the volume fraction of both studied oils (PFC 40 and PFC 77), k_La decreased only. According to these authors, this trend in k_La can be at least partly attributed to the increase in the emulsion viscosity with increasing PFC volume fraction, which slows down the surface-renewal rate of the liquid elements.

Figure 2.6 presents additionally the variation of relative k_La for oxygen (i.e. ratio of the k_La in the emulsions to one in the water phase) upon the addition of some n-alkanes with paying attention also to the reactor types. As can be seen from Figure 2.6, compared to the k_La-value in water: Kundu *et al.* (2003) and Da Silva *et al.* (2006 a) reported mass transfer enhancement (k_La higher than in water); Yoshida *et al.* (1970) and Nielsen *et al.* (2003) found mass transfer depression (k_La lower than in water); whereas "no effect" on mass transfer was reported by Dumont *et al.* (2006 a). It should be noted that the k_La results of Kundu *et al.* (2003) and Dumont *et al.* (2006 a) are surprisingly contradictory, although the same oil phase (n-dodecane) and a bubble column were used in both studies for the absorption of oxygen.

2.4.2 Effect of oil addition on gas-liquid specific interfacial area (*a*)

Some authors have attempted to study the effects of oil addition on the gas-liquid specific interfacial area, *a* (cf. Table 2.5). Mehta and Sharma (1971), who studied CO_2 absorption in NaOH solution with the oil phase of 2-ethyl hexanol in a stirred tank reactor, found that the interfacial area (*a*) increased marginally with an increase in the volume fraction of 2-ethyl hexanol. These authors supposed that the presence of small oil droplets could result in a decrease in coalescence rates of gas bubbles and hence increased the value of *a*. Conversely, the recent experimental results in a bubble column of Gómez-Díaz *et al.* (2009) showed a decrease in the value of *a* when oil volume fraction increased and this effect was more pronounced at high values of gas flow rate.

Linek and Benens (1976) suggested from their study that an oil phase with a positive spreading coefficient *S* (oleic acid) caused an increase of the interfacial area (more significant at higher agitator speeds), whereas one with a negative *S*-value (n-alkans) caused a decrease of the interfacial area. However, Cents *et al.* (2005) observed from their study that adding 2.5% of both n-hexadecane and n-heptane to an air-electrolyte (0.5 M KCl solution) system had no significant effect on the interfacial area *a.*

Interestingly, Das *et al.* (1985) found that the presence of oil phase influences the interfacial area in a more complex way: as the oil volume fraction was increased, the interfacial area first increased, and then decreased (passed through a maximum). They explained that the initial increase in interfacial area would be due to the prevention of bubble coalescence by oil droplets, while at higher oil hold-ups a diminished level in turbulence would prevent bubble breakage, hence decrease the interfacial area.

TABLE 2.5: Effect of oil addition on mass transfer parameters: k_La, a, k_L

Oil volume fraction	k_La	a	k_L	*Oil phase*	*Authors*
Φ_{oil} ↗ (*S:* not mentioned)		↗		2-Ethyl hexanol	Mehta and Sharma (1971)
		↗↘		Toluene Methyl isobutyl-ketone 2-Ethyl-hexanol	Das *et al.* (1985)
	↘			PFC 40 PFC 77	Ju *et al.* (1991)
	↗↘			Octene	Lekhal *et al.* (1997)
	↗			n-Heptane n-Dodecane n-Decane	Kundu *et al.* (2003)
	↗			n-Dodecane	Galaction *et al.* (2004)
	↘↗			Silicone oil 47V5	Dumont *et al.* (2006 b)
	↘ ↗			n-Dodecane	Boltes *et al.* (2008)
		↘	↗	Methyl ricinoleate	Gómez-Díaz *et al.* (2009)
Φ_{oil} ↗ ($S > 0$)	↘↗			Toluene Oleic acid	Yoshida *et al.* (1970)
			↘↗	Oleic acid	Linek and Benes (1976)
	↗↘			n-Dodecane	Rols *et al.* (1990)
	→			PFC 40	Dumont *et al.* (2006 a)
Φ_{oil} ↗ ($S < 0$)	↘			Kerosene Liquid paraffin	Yoshida *et al.* (1970)
			↗	n-Alkanes (C_{11}-C_{18})	Linek and Benes (1976)
	↗			n-Hexadecane	Hassan and Robinson (1977)
	↘↗			n-Dodecane	
	→			n-Dodecane n-Hexadecane	Dumont *et al.* (2006 a)

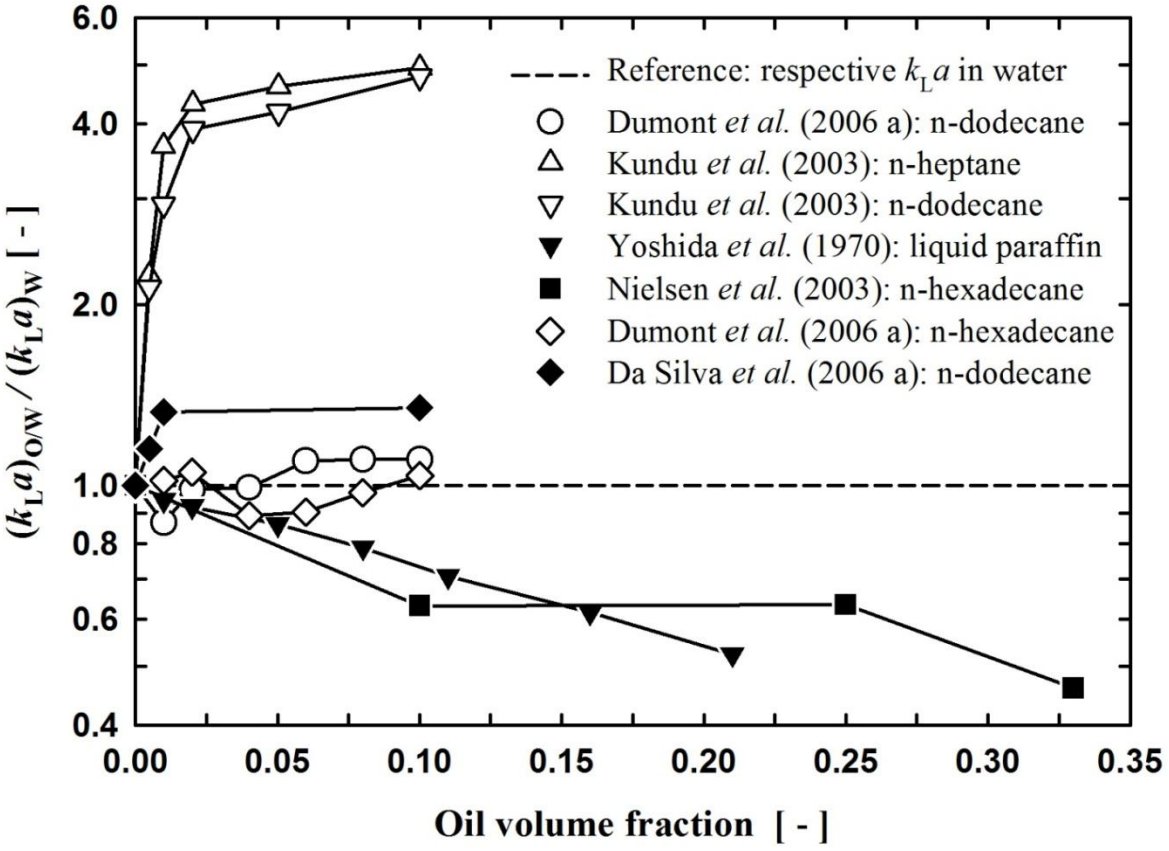

FIGURE 2.6: Variation of $k_L a$ for oxygen upon n-alkane addition reported in the literature for stirred tanks (filled symbols) and bubble columns (open symbols).

2.4.3 Effect of oil addition on liquid-side mass transfer coefficient (k_L)

The liquid-side mass transfer coefficient k_L was the objective of a study by Linek and Benens (1976) for the absorption of oxygen and argon in aqueous emulsions of n-alkans ($S < 0$) and oleic acid ($S > 0$) in an agitated vessel. They found that, with increasing the oil volume fraction, k_L remained essentially constant for O/W type emulsions of n-alkanes, whereas a sharp initial decrease, followed by a slight increase in k_L was found for O/W type emulsions of oleic acid (cf. Table 2.5). According to these authors, the rapid initial drop of k_L at low concentration of oleic acid can be attributed to the surface activity effects of oleic acid (i.e. oleic acid can accumulate at the gas-liquid interface where it acts like a surface active contaminant, which increases the liquid-side mass transfer resistance). On the contrary, Gómez-Díaz *et al.* (2009) who studied the effects of oil addition (methyl ricinoleate) on k_L for oxygen absorption at very low oil volume fractions (Φ_{oil} = 0-0.0054), reported an increase in k_L as the oil volume fraction increased.

In case of W/O type emulsions of both oils (i.e. at contents of n-alkanes and of oleic acid beyond 18 and 35%, respectively), Linek and Benens (1976) also found that k_L increased linearly with increasing oil volume fraction.

2.5 Mechanisms for mass transfer enhancement

When an oil phase with a strong affinity for the solute gas is added to a gas-liquid system, significant gas-liquid mass transfer enhancement could be expected. In the literature, the "bubble covering" mechanism and the "shuttle" mechanism have been proposed to explain the mass transfer enhancement in gas-liquid-liquid systems. These two mechanisms will be discussed below.

2.5.1 "Bubble covering" mechanism

The "bubble covering" mechanism was proposed by Rols *et al.* (1990, 1991). The basic idea of this mechanism is that, when a gas bubble is submerged in the emulsion, the oil will cover the gas bubble as a thin film; this thin oil film will be loaded with the gas as long as the gas bubble has not disrupted.

According to Rols *et al.* (1991), the detailed "bubble covering" mechanism can be divided into three steps (as presented in Figure 2.7):

- Step 1: As the gas bubble is generated in the emulsion, the bubble surface becomes enveloped by an oil film.

- Step 2: While the bubble is rising, the gas is transferred from the bubble to the oil film; the higher the gas solubility in the oil phase, the higher the transfer rate.

- Step 3: After bubble disruption (e.g. at the liquid free surface), the oil film may be re-dispersed into droplets. These gas-rich droplets will then release their absorbed gas towards the water phase; the more finely the oil is dispersed, the greater is the transfer efficiency.

Based on the "bubble covering" mechanism, Rols *et al.* (1991) developed a mathematical model to evaluate the volumetric mass transfer coefficient $k_L a$ for their specific mass-transfer experiments. However, their model is not able to explain the experimentally observed decay of

$k_L a$ at high oil volume fraction in their previous paper (Rols et al., 1990). Moreover, their model seems to be very difficult to apply because of the lack of important information concerning surface properties, frequency of bubble-droplet collisions, coalescence time, etc.

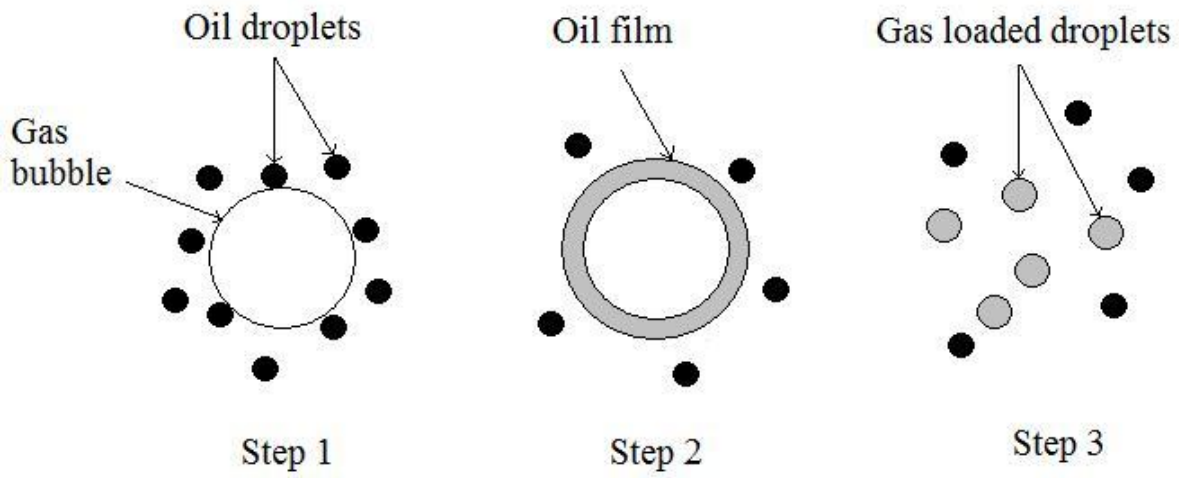

FIGURE 2.7: Physical description of "bubble covering" mechanism (Rols *et al.*, 1991).

In the light of the discussion in Section 2.3, it is likely that the oils with positive spreading coefficients *S* have high potential to enhance gas-liquid mass transfer by the 'bubble covering' mechanism (cf. Figure 2.3).

2.5.2 "Shuttle" mechanism

Like in gas-liquid-solid systems, the "shuttle" or "grazing" mechanism has been considered as one possible way to explain mass transfer enhancement in gas-liquid-liquid systems. According to this mechanism, oil droplets can travel frequently between the stagnant mass transfer zone (hydrodynamic mass transfer film) at the gas-liquid interface and the liquid bulk. In the mass transfer zone, the oil droplets absorb the gas leading to an increased absorption rate owing to their higher solubility for the gas. After a certain contact time, the oil droplets return to the liquid bulk where the absorbed gas is discharged. The "shuttle" mechanism requires that the oil droplet size is smaller than the film thickness δ_L (cf. Figure 2.1), so that the oil droplets can enter the mass transfer zone for mass transfer enhancement.

The "shuttle" mechanism has been theoretically analyzed as well as experimentally tested in some studies. Typical example comes from the work of Bruining *et al.* (1986) in which oxygen absorption into an O/W emulsion was investigated (cf. Table 2.2). When decane was added as the oil phase (0.5-1 vol. %), the oxygen absorption rate increased and when decane and the emulsifier 1-decanol were added together, the oil droplets became considerably smaller (10 μm or less) and the absorption rate increased even more. On the other hand, experiments in which the oil droplets were large (of the order of 50 μm or larger) showed no significant effect on the absorption rate. According to these authors, the enhancement factor (or grazing factor, E_{shuttle}) based on pseudo-homogeneous model of shuttle mechanism can be estimated by following equation:

$$E_{\text{shuttle}} = \sqrt{1 + \Phi_{\text{disp.}}\,(m_{\text{R}} - 1)} \tag{2.25}$$

where $\Phi_{\text{disp.}}$ and m_{R} are the volume fraction of the dispersed phase and the relative solubility (i.e. gas solubility in the pure oil compared to pure water), respectively.

Testing the "shuttle" mechanism on the CO_2 absorption to 0.5 M K_2CO_3/ 0.5 M $KHCO_3$ buffer solution catalyzed by sodium hypochlorite, Cents *et al.* (2001) found that mass transfer is enhanced by the addition of toluene and 1-octanol, which could be well described by their pseudo-homogeneous model of shuttle mechanism. However, this mechanism fails to explain no enhancement of mass transfer when n-dodecane and n-heptane were added in their experiments.

Lekhal *et al.* (1997) observed a clear maximum in $k_{\text{L}}a$ at low oil volume fractions (3-4 vol. %) (cf. Tables 2.1 and 2.5). According to these authors, this interesting maximum could be explained by "shuttle" mechanism or by coalescence inhibition by small oil droplets.

2.6 Concluding remarks

Gas-liquid-liquid systems have applications in biphasic catalysis (e.g., hydroformylation) and in industrial bioprocesses (e.g., aerobic fermentations with oil as the carbon source). In addition, new potential applications in industrial gas separation and treatment processes, e.g. separation of CO, CO_2, olefin gases (e.g. propylene, isobutylene) as well as volatile organic compounds (e.g. styrene, toluene, benzene) have been mentioned. In these processes, the addition of oil (e.g. hydrocarbon, perfluorocarbon, or silicon oil) with strong affinity for the gas to a gas-liquid system is to enhance the gas-liquid mass transfer. However, most studies reported in the literature are limited to low oil volume fractions.

Some possible mechanisms for the gas transfer in both O/W and W/O emulsions have been proposed, in which the gas can be transferred to emulsions by either serial transport (e.g. gas → water → oil) or parallel transport (e.g. gas → oil and gas → water, simultaneously). However, the correct mechanism is still questionable and no unique mechanism could be confirmed because of lack of experimental evidence.

The spreading coefficient (S or S^*) could be a very important clue to the mass transfer mechanism. In practical applications, the "equilibrium" spreading coefficient (S^*) might be more important than the "initial" value (S). However, the "initial" spreading coefficient (S) is mostly reported in the literature and the values do not agree well.

Most mathematical mass transfer models for evaluating k_La-values were developed using assumption that there is no direct contact between oil droplet and gas bubble (i.e. serial mechanism: gas → water → oil). However, these models may not be valid when the oil can spread and cover the gas bubble or when the experiments are carried out at high oil volume fractions.

The effects of oil addition on the volumetric mass transfer coefficient (k_La) are very complicated: with increasing oil volume fraction, k_La can increase, decrease, or even remain unaffected. The reported results in k_La are contradictory and the reasons are not clear.

3 Mass transfer models for the present research

Development of an appropriate model, which allows to experimentally evaluate the volumetric mass transfer coefficient $k_L a$ for the full range of oil volume fraction (0-100%), is a challenging task in the present study. In this chapter, a pseudo-homogeneous mass transfer model is developed, by which the $k_L a$ values can be determined using the pressure measurement technique. Further, gas-water mass transfer in gas-oil-water systems using fluorescence technique is described and discussed in which a linear regression approach for the modified Stern-Volmer equation is proposed.

3.1 General considerations

Various mass transfer models have been reported in the literature for gas absorption into emulsions. They can generally be categorized into "pseudo-homogeneous" and "heterogeneous" models.

In the pseudo-homogeneous models (Bruining *et al.*, 1986; Lekhal *et al.*, 1997; Cents *et al.*, 2001; Kundu *et al.*, 2003), the emulsion is treated as a homogeneous phase with the same mean solution capacity for the gas component (Mehra, 1999). The following assumptions are usually made for the pseudo-homogeneous models:

- The dispersed phase droplets are much smaller than the liquid film thickness at the gas-liquid interface.
- The dispersed phase is homogeneously distributed throughout the continuous phase.
- The mass transfer of the gas occurs only through the continuous phase (there is no direct gas-dispersed phase contact).
- Liquid-liquid mass transfer resistances are neglected.

Obviously some of the above assumptions are questionable, for example, in case of O/W surfactant-free emulsions, the oil droplet size might be larger than the film thickness. At high oil volume fractions or with spreading oils as discussed earlier in Chapter 2 (i.e. positive *S*-values), gas-oil direct contact should be possible.

Differently, some proposed heterogeneous models (Nagy, 1995; Lin *et al.*, 1999; Mehra, 1999; Brilman *et al.*, 1998, 2000) considered geometric aspects of the dispersed droplets (e.g. droplet size and droplet location from the gas-liquid interface), concentration gradients of the solute gas

inside the droplets and droplet-droplet interactions. It appears that the heterogeneous models give the better level of understanding of the mass transfer enhancement phenomena at the gas-liquid interface. However, it is not sure that the currently available experimental results could give accurate values of many parameters used in these models (Dumont and Delmas, 2003). For this reason, although being subject to several constraints, the pseudo-homogeneous models are more widely used. In addition, the results obtained with the pseudo-homogeneous models can predict reasonably well the trends with changing operating conditions, such as the gas-liquid contact time, the relative solubility and the dispersed phase volume fraction (Brilman *et al.*, 2000).

The pseudo-homogeneous mass transfer model is selected for the present research in conjunction with the dynamic pressure measurement technique. The main advantage of the pressure technique is that it can give information on both the volumetric mass transfer coefficient ($k_L a$) and the gas solubility (C^*).

3.2 Pseudo-homogeneous mass transfer model

The homogeneous mass transfer model proposed by Albal *et al.* (1983) has allowed evaluating successfully the gas-liquid volumetric mass transfer coefficient ($k_L a$) based on the dynamic pressure measurement technique for gas-liquid and gas-liquid-solid systems. Similarly, in the present study (i.e. gas-liquid-liquid system), it is assumed that the oil-water emulsion behaves like a single, homogenous liquid phase (i.e. a pseudo-homogeneous liquid) with mean physicochemical properties, specifically, mean gas solubility.

At isothermal and isochoric conditions, the absorption rate can be calculated from the decline of the total pressure (P) in the reactor as follows:

$$-\frac{V_G}{V_L RT}\frac{dP}{dt} = k_L a(C_L^* - C_L) \tag{3.1}$$

The bulk concentration C_L of the solute gas in the liquid phase can be expressed as:

$$C_L = \frac{V_G}{V_L RT}(P_i - P) \tag{3.2}$$

Equilibrium at the gas-(pseudo-homogeneous) liquid interface obeys Henry's law:

$$C_{\mathrm{L}}^{*} = \frac{(P - p_{\mathrm{W}} - p_{\mathrm{O}})}{H} \tag{3.3}$$

where p_{W} and p_{O} are the vapor pressures of water and oil, respectively.

Substitution of equations 3.2 and 3.3 into equation 3.1 gives:

$$-\frac{dP}{dt} = k_{\mathrm{L}}a\left[\frac{V_{\mathrm{L}}RT}{V_{\mathrm{G}}H}(P - p_{\mathrm{W}} - p_{\mathrm{O}}) - (P_{\mathrm{i}} - P)\right] \tag{3.4}$$

At saturation equilibrium, the final pressure is P_{f} and the final concentration of the solute gas is $C_{\mathrm{L,eq}}^{*}$ which can be calculated from equation 3.2 as:

$$C_{\mathrm{L,eq}}^{*} = \frac{V_{\mathrm{G}}}{V_{\mathrm{L}}RT}(P_{\mathrm{i}} - P_{\mathrm{f}}) \tag{3.5}$$

Also, from equation 3.3:

$$C_{\mathrm{L,eq}}^{*} = \frac{(P_{\mathrm{f}} - p_{\mathrm{W}} - p_{\mathrm{O}})}{H} \tag{3.6}$$

From equations 3.5 and 3.6, it follows that:

$$\frac{V_{\mathrm{L}}RT}{V_{\mathrm{G}}H} = \frac{(P_{\mathrm{i}} - P_{\mathrm{f}})}{(P_{\mathrm{f}} - p_{\mathrm{W}} - p_{\mathrm{O}})} \tag{3.7}$$

Substitution of equation 3.7 into equation 3.4 gives:

$$-\frac{dP}{dt} = k_{\mathrm{L}}a\left[\frac{(P_{\mathrm{i}} - P_{\mathrm{f}})}{(P_{\mathrm{f}} - p_{\mathrm{W}} - p_{\mathrm{O}})}(P - p_{\mathrm{W}} - p_{\mathrm{O}}) - (P_{\mathrm{i}} - P)\right] \tag{3.8}$$

or:

$$-\frac{P_{\mathrm{f}} - p_{\mathrm{W}} - p_{\mathrm{O}}}{P_{\mathrm{i}} - p_{\mathrm{W}} - p_{\mathrm{O}}} \cdot \frac{dP}{(P - P_{\mathrm{f}})} = k_{\mathrm{L}}a \cdot dt \tag{3.9}$$

Integrating both sides of equation 3.9 gives:

$$-\frac{P_\mathrm{f}-p_\mathrm{W}-p_\mathrm{O}}{P_\mathrm{i}-p_\mathrm{W}-p_\mathrm{O}}\cdot\ln(P-P_\mathrm{f})=k_\mathrm{L}a\cdot t+C \tag{3.10}$$

The volumetric mass transfer coefficient ($k_\mathrm{L}a$) for gas absorption into emulsions can be experimentally determined by using equation 3.10 and the experimental data on the pressure decrease with time in the reactor (cf. Chapter 5 for more details).

In addition, the overall gas solubility (C^*) in the emulsion at a partial pressure of 101325 Pa can be calculated from the total pressure decrease ($\Delta P = P_\mathrm{i} - P_\mathrm{f}$) as follows (cf. Equation 3.5):

$$C^* = \frac{V_\mathrm{G}}{V_\mathrm{L}}\cdot\frac{1}{RT}\cdot\Delta P\cdot\frac{101325\ \mathrm{Pa}}{P_\mathrm{f}-p_\mathrm{W}-p_\mathrm{O}} \tag{3.11}$$

3.3 Mass transfer enhancement factor

It might be argued that the driving force should be based on the gas solubility $(C^*)_\mathrm{cont.}$ in the continuous phase rather than the mean gas solubility as assumed in the pseudo-homogeneous mass transfer model. This will shift the $k_\mathrm{L}a$ values in O/W emulsions upwards (lower driving force) while those in W/O emulsions will be shifted downwards (higher driving force). Concerning this aspect, Nielsen *et al.* (2003) suggested a comparison with the volumetric mass transfer coefficient in the respective continuous phase $(k_\mathrm{L}a)_\mathrm{cont.}$ in the form of the mass transfer enhancement factor *E*, which can be expressed as:

$$E = \frac{k_\mathrm{L}a}{(k_\mathrm{L}a)_\mathrm{cont.}}\cdot\frac{C^*}{(C^*)_\mathrm{cont.}} \tag{3.12}$$

3.4 Gas-water mass transfer in gas-oil-water systems using fluorescence technique

The main objective of the present research is to study the gas-emulsion mass transfer using the dynamic pressure measurement technique, in which no distinction can be made between the gas transport to the water or to the oil but only towards the overall emulsion. To gain more information about the mass transfer mechanism in our gas-oil-water systems, the fluorescence technique has been employed. Specifically, oxygen transfer to the water phase was studied in aqueous emulsions of n-dodecane and n-hexadecane using a fluorescence-based oxygen optode. To this end, an oxygen-sensitive fluorophore, namely, tris-(2,2'-bipyridyl)-ruthenium(II) chloride

(RuBPY), soluble in water but insoluble in the oils, was selected to assess the dissolved oxygen concentrations in the water phase (cf. Figure 3.1; Table 3.1 below). By direct dissolution of the fluorophore in the liquid, the response time of the oxygen optode can be much improved as compared to fluorophore fixation at the sensor tip (Terasaka *et al.*, 1998; Jordan *et al.*, 2001; Jordan and Schumpe, 2001). This section contains the basic principles of the fluorescence-based oxygen optode, a description of the fiber optic oxygen sensor system used in the present study, followed by the mass transfer model for evaluation of the gas-water volumetric mass transfer coefficient, $(k_L a)_{GW.}$

3.4.1 Basic principles of fluorescence-based oxygen sensing

Fluorescence occurs in certain molecules which are called fluorophores or fluorescent dyes. When a fluorophore absorbs a photon of energy ($h\upsilon_E$) supplied by an external light source (e.g. light-emitting diode-LED), it is excited from electronic ground state (S_0) to a higher energy excited electronic singlet state. This excited state is usually either the first (S_1) or the second (S_2) excited singlet state (Lakowicz, 2006). The fluorophore exists in its excited state for a finite time, called the fluorescence lifetime τ'. During this time, the fluorophore rapidly relaxes to the lowest vibrational energy level of the first excited singlet state (S_1) after undergoing some non-radiative processes (e.g. vibrational relaxation, internal conversion) which results in some energy losses. After that, it emits a photon of energy ($h\upsilon_F$) and returns to its ground electronic state (S_0); this process is called "fluorescence".

Due to energy dissipation during the excited-state lifetime, the energy of the fluorescence photon ($h\upsilon_F$) is lower (i.e. longer wavelength) than the excitation photon ($h\upsilon_E$). In addition, the fluorescence quantum yield of a fluorophore is defined as the number of photons emitted through fluorescence relative to the number of absorbed photons. Figure 3.1 and Table 3.1 present the chemical structure and photochemical characteristics of the fluorescent dye (RuBPY) used in the present study.

TABLE 3.1: Photochemical characteristics of Tris-(2,2'bipyridyl)-Ruthenium (II) chloride (RuBPY) in water (Mills, 1997)

Dye	*Lifetime, τ'_0 (μs)*	*λ_{max}-absorption (nm)*	*λ_{max}-emission (nm)*	*Quantum yield, Q (-)*
RuBPY	0.60	452	613; 627	0.042

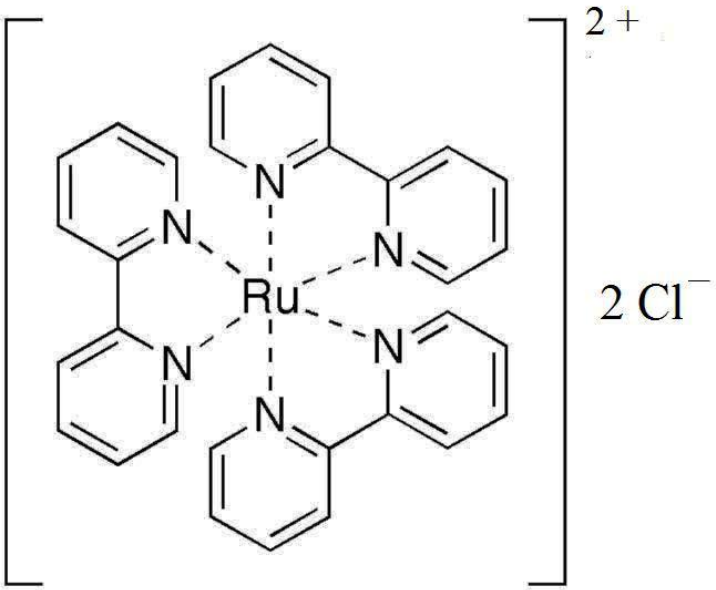

FUGURE 3.1: Chemical structure of Tris-(2,2'bipyridyl)-Ruthenium (II) chloride (RuBPY).

The intensity of fluorescence decreases when the excited-state fluorophore is deactivated upon collisional contact with molecular oxygen. Such decreases in intensity are called "fluorescence quenching", and molecular oxygen is called the "quencher". In this way, the oxygen concentration in a solution can be monitored by measuring the fluorescence intensity. It can be therefore said that, the basic principle of fluorescence-based oxygen sensing (or fluorescence-based oxygen optode) is based on the fluorescence quenching by the presence of oxygen molecules. The actual fluorescence quenching step can be written as follows (Mills, 1998; Badocco, 2011, 2012):

$$[\text{Fluorophore}]^* + O_2 \overset{k_Q}{\rightarrow} \text{Fluorophore} + [O_2]^* \tag{3.13}$$

where the symbol (*) indicates the electronic excited state, and k_Q is the quenching rate constant. In most oxygen optical sensors, the rate of the reaction in equation 3.13 is diffusion-controlled (Mills, 1998), and hence k_Q depends directly on the oxygen diffusion coefficient D_{O_2}.

The mathematical relationship between fluorescence intensity and oxygen concentration is described by the well-known Stern-Volmer equation (Lakowicz, 2006):

$$\frac{I_0}{I} = 1 + k_Q \cdot \tau_0' \cdot C_{O_2,W} = 1 + K_{SV} \cdot C_{O_2,W} \tag{3.14}$$

In this equation, I_0 and I are the fluorescence intensities in the absence and presence oxygen, respectively; $K_{SV} = k_Q \cdot \tau'_0$ is the Stern-Volmer constant; τ'_0 is the fluorescence lifetime of the fluorophore in the absence of oxygen (see above); $C_{O_2,W}$ is oxygen concentration in the water phase. In general, the higher the value of K_{SV}, the greater the sensitivity of the optical oxygen sensor (Mills, 1998).

Equation 3.14 shows that a plot of I_0/I versus oxygen concentration, called the Stern-Volmer plot, gives a straight-line with K_{SV} as the slope, and 1 as the intercept. Oxygen optodes have usually a polymer matrix, in which the fluorophore is immobilized, coated on the tip of an optical fiber. In such matrices, the Stern-Volmer plots are mostly no longer linear but rather downward curved (Gouin *et al.*, 1997; Hartmann *et al.*, 1995; Demas *et al.*, 1995). Two common explanations for the non-linearity are either the multiple quenching sites or the non-linear solubility of oxygen in the polymer matrix (Demas *et al.*, 1995). On the other hand, when the fluorophore is freely dissolved in a solution, as in the present study, a linearity of the Stern-Volmer plot can be expected (Gouin *et al.*, 1997; Lakowicz, 2006).

3.4.2 Fiber optic oxygen sensor system based on fluorescence intensity

The fluorescence intensity based fiber optic oxygen sensor (MOPS, Comte-Moderne Analysesysteme GmbH, Hannover, Germany), shown in Figure 3.2, was used to measure the oxygen concentration in only the water phase. The optical fiber tip, provided by the manufacturer, was originally coated with the fluorophore (tris(4,7-diphenyl-1,10-phenantrolin)-ruthenium(II)-chloride) immobilized in silicone matrix. This optode was not suitable for the present study because of its high response time. So the coated layer was left out and the excited light was guided directly into the emulsion where a different fluorophore (RuBPY) was dissolved in the water phase (cf. Figure 3.2). A number of external calibrations had to be performed (cf. Chapter 5 for details), because the provided calibration software stored in the measurement unit was no longer valid. To this end, a Labview 7.1 based software was developed allowing reading and recording the output voltage (U) on the photomultiplier used as fluorescence intensity detector (cf. Figure 3.2).

The fiber optic oxygen sensor system contains a dichroitic mirror at a 45^o angle for splitting the excitation and fluorescent light. The excitation light (λ_E = 470 nm), emitted from a blue light-emitting diode (LED), reflexes off the dichroitic mirror, and is focused onto the optical fiber core by the objective lens; the excitation light then propagates through the optical fiber to the emulsion where it excites the dissolved RuBPY in the water phase. The backward fluorescent light is

collected by the same fiber, and passed back through the objective lens and the dichroitic mirror to the photomultiplier tube (PMT) where it is detected. The fluorescence intensity is measured in terms of the voltage of the photomultiplier as output signal.

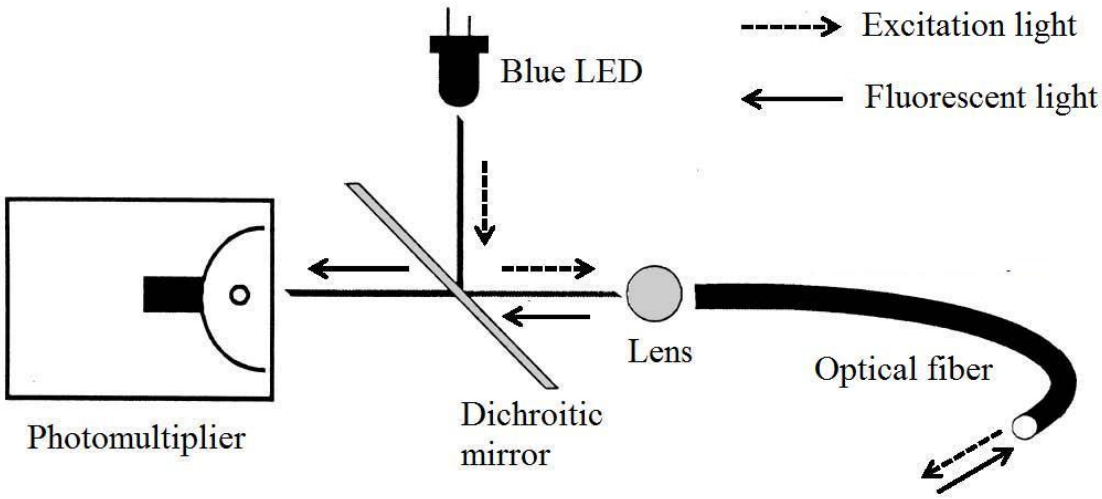

FIGURE 3.2: Fiber optic oxygen sensor system with modified optode (Köneke *et al.*, 1999).

3.4.3 Evaluation of gas-water volumetric mass transfer coefficient, $(k_L a)_{GW}$

With fluorescence intensity based instruments, it is always necessary to minimize the effects of stray and ambient light. Considering these effects, the relationship between the true signals (I, I_0) and the measured signals (U, U_0) for the used oxygen optode (MOPS) can be expressed as follows (Comte, 1993):

$$I_0 = \frac{U_0 - U_{100}}{const.} \tag{3.15}$$

$$I = U - U_0 + I_0 \tag{3.16}$$

where U_0 and U_{100} are the photomultiplier voltages corresponding to the oxygen concentrations in the water phase of 0% and 100% saturation, respectively.

Substitution of equations 3.15 and 3.16 into equation 3.14 gives:

$$C_{O_2,W} = \frac{1}{K_{SV}} \cdot \left(\frac{\frac{U_0 - U_{100}}{const.}}{U - U_0 + \frac{U_0 - U_{100}}{const.}} - 1 \right) \tag{3.17}$$

Using the modified Stern-Volmer equation 3.17, the oxygen concentration ($C_{O_2,W}$) can be converted from the output voltage of the photomultiplier, as long as the values of U_0, U_{100}, K_{SV}, and *const.* are known.

Equation (3.17) that it can be rearranged as follows:

$$\frac{1}{U_0 - U} = \frac{1}{K_{SV}} \cdot \frac{const.}{U_0 - U_{100}} \cdot \frac{1}{C_{O_2,W}} + \frac{const.}{U_0 - U_{100}} \tag{3.18}$$

Equation 3.18 shows a linear relationship between $1/(U_0 - U)$ and $1/C_{O_2,W}$. Therefore, the values of U_0, U_{100}, K_{SV}, and *const.* can be obtained by linear regression method based on the external calibrations mentioned above in Subsection 3.4.2. The slope (A) and the intercept (B) of the linear plot of $1/(U_0 - U)$ against $1/C_{O_2,W}$ are given by:

$$A = \frac{1}{K_{SV}} \cdot \frac{const.}{U_0 - U_{100}} \tag{3.19}$$

$$B = \frac{const.}{U_0 - U_{100}} \tag{3.20}$$

The gas-water volumetric mass transfer coefficient $(k_L a)_{GW}$ can be calculated based on the two-film theory (cf. Equation 2.19 in Chapter 2) as follows:

$$\frac{dC_{O_2,W}}{dt} = (k_L a)_{GW} \cdot (C^*_{O_2,W} - C_{O_2,W}) \tag{3.21}$$

or:

$$\frac{dC_{O_2,W}}{(C^*_{O_2,W} - C_{O_2,W})} = (k_L a)_{GW} \cdot dt \tag{3.22}$$

Integrating both sides of equation 3.22 gives:

$$\ln\left(C^{*}_{O_2,W} - C_{O_2,W}\right) = -\left(k_L a\right)_{GW} \cdot t + C \tag{3.23}$$

The equation (3.23) allows to experimentally evaluate the gas-water volumetric mass transfer coefficient $(k_L a)_{GW}$ in gas-water-oil systems whereby the oxygen concentration in the water phase ($C_{O_2,W}$) is calculated from the modified Stern-Volmer equation 3.17 (cf. Chapters 5 and 6 for more details).

4 Some important properties of surfactant-free emulsions

Upon addition of oil to a gas-water system in a stirred tank, phase inversion and associated phenomenon (e.g. double emulsion), described and discussed in this chapter, might have strong effect on mass transfer. In addition, the viscosities of aqueous emulsions of n-alkanes used in the mass transfer experiments are estimated.

4.1 Phase inversion

In a system of two immiscible liquids (e.g. water and an oil), two general types of emulsions can be formed: oil-in-water (O/W) emulsion where the oil phase is dispersed in the continuous water phase and water-in-oil (W/O) emulsion where the water phase is dispersed in the continuous oil phase. Phase inversion refers to the phenomenon in which O/W emulsion becomes W/O emulsion, and vice versa (i.e. the dispersed phase becomes the continuous phase. At a constant stirring speed, the phase inversion in surfactant-free emulsions in a stirred tank generally occurs when the volume fraction of the dispersed phase exceed a critical limit. This critical limit of dispersed phase volume fraction is usually known as the phase inversion point.

Several investigators have suggested the physical mechanism for phase inversion phenomenon (Vaessen *et al.*, 1996; Groeneweg *et al.*, 1998; Hu *et al.*, 2005). According to these authors, the phase inversion occurs as the result of a dynamic imbalance between drop breakup and coalescence processes. Before phase inversion, there exists a dynamic equilibrium between the two processes: coalescence and breakup (too large drops tend to break up easily, while too small drops tend to coalesce). With increasing volume fraction of the dispersed phase, the coalescence rate increases faster than the breakup rate (Vaessen *et al.*, 1996). At a certain volume fraction, the dynamic balance between coalescence and breakup will collapse, and then the phase inversion will occur (i.e. rapid coalescence of dispersed drops throughout the whole system leads to form the new continuous phase). In other words, the phase inversion occurs at a certain volume fraction of the dispersed phase where the drop coalescence process dominates over the drop breakup process. Figure 4.1 illustrates a phase inversion process from W/O to O/W emulsion as increasing the water volume fraction.

Experimental results reported in the literature have suggested that all the factors which affect drop coalescence and breakup characteristics, e.g. agitation speed, impeller type, liquid

properties, electrostatic interaction etc., can affect the phase inversion phenomenon (Yeo *et al.*, 2000).

Mostly, the phase inversion is experimentally detected by measuring the electrical conductivity of the emulsion. By increasing the oil volume fraction in an O/W emulsion, the conductivity of the emulsion will gradually decrease because of the decrease in the volume fraction of the conductive aqueous phase. At a certain point, there will be a sudden decrease in conductivity to near zero, indicating the phase inversion to W/O emulsion (oil as continuous phase). In addition, it should be mentioned that the phase inversion in a stirred tank could be identified by simply observing the de-emulsification after switching-off the agitator as suggested by Noui-Medihi *et al.* (2004). Both methods were used in the present study to identify the phase inversion for aqueous emulsions of n-alkanes (cf. Chapter 5-6 for more details).

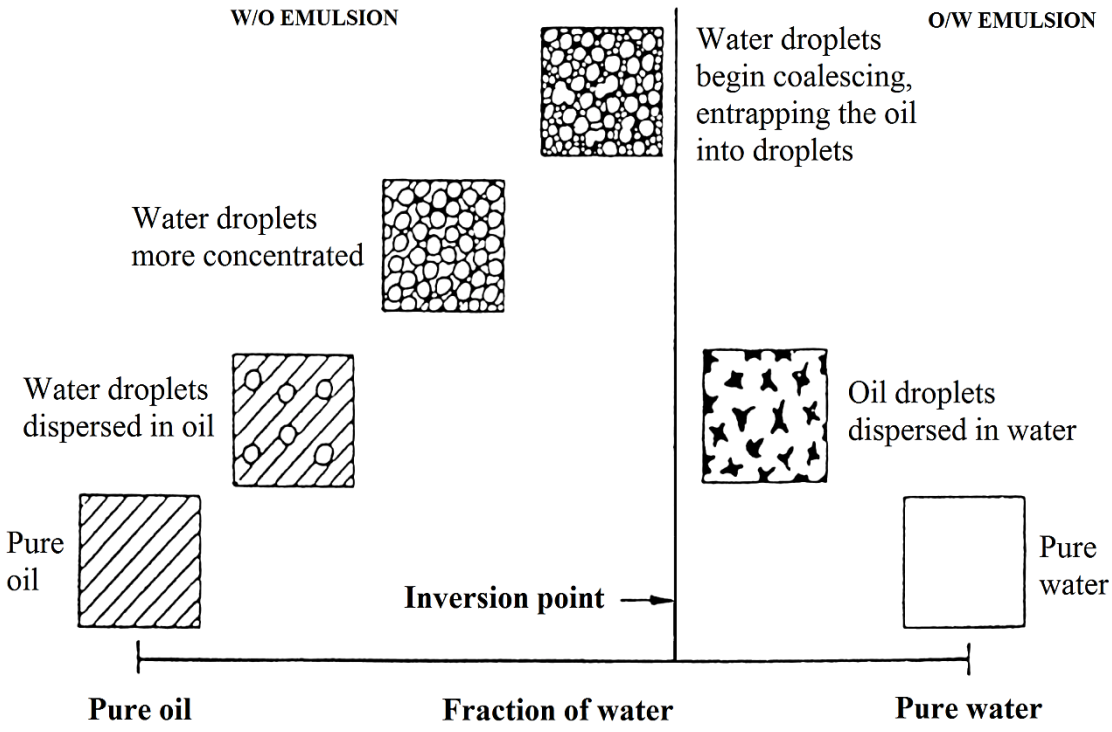

FIGURE 4.1: Description of a phase inversion process (Yeo *et al.*, 2000; Xu, 2007).

4.2 Double emulsions

Double emulsions (also known as secondary emulsions or multiple emulsions) mean "emulsions of emulsions". The dispersed drop of a double emulsion itself contains one or more smaller droplets inside. In general, double emulsions can be classified as either oil-in-water-in-oil (O/W/O) emulsion or water-in-oil-in-water (W/O/W) emulsion. In the case of O/W/O emulsion, for instance, the dispersed phase is an oil-in-water (O/W) emulsion, and the continuous phase is oil.

The existence of double emulsions in some liquid-liquid systems has been observed by several investigators (Pacek *et al*., 1994; Groeneweg *et al.*, 1998; Liu *et al.*, 2005 and 2006). On the study of the phase inversion (from W/O to O/W) for emulsions of water or glycerol-water solutions in chlorobenzene, in a stirred tank, using video technique, Pacek *et al.* (1994) observed the formation of O/W/O emulsions (chlorobenzene/glycerol-water/chlorobenzene emulsions), just before phase inversion (cf. Figure 4.2).

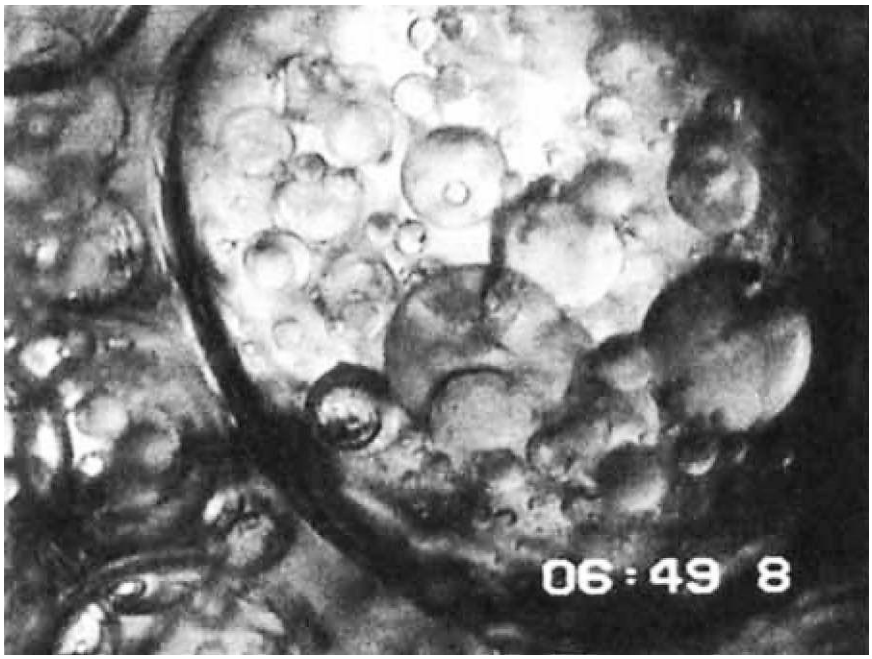

FIGURE 4.2: Image of O/W/O emulsion for a glycerol-water and chlorobenzene system reported by Pacek *et al.* (1994).

Liu *et al.* (2005) recorded the phase inversion process (from O/W to W/O) for emulsions of Exxol D80 Oil and $CaCl_2$ solution, in a stirred vessel, using laser-induced fluorescence technique

(LIF). These authors reported that a great number of the O/W/O emulsions appeared during and after phase inversion, whereas the W/O/W emulsions before phase inversion were extremely rare.

Kuma (1996) suggested the mechanism for the formation of double emulsions (i.e. droplets inside drops) as illustrated in Figure 4.3. Simultaneous collision and coalescence between drops could enable the entrapment of the interfacial continuous phase film as droplets. Successive coalescence of such drops would result in drops containing several droplets. If the entrapped droplets would be sufficiently stable to prevent their escape back to the continuous phase, the double emulsions then would be observed.

It appears that O/W/O emulsions are much more likely to occur than W/O/W emulsions. According to Kumar (1996), this phenomenon might be attributed to the fact that oil drops in water experience repulsion forces due to the overlapping of the electrical double layers leading to low coalescence efficiencies, whereas water drops in oil of low dielectric constant do not experience such repulsion forces and are therefore associated with high coalescence.

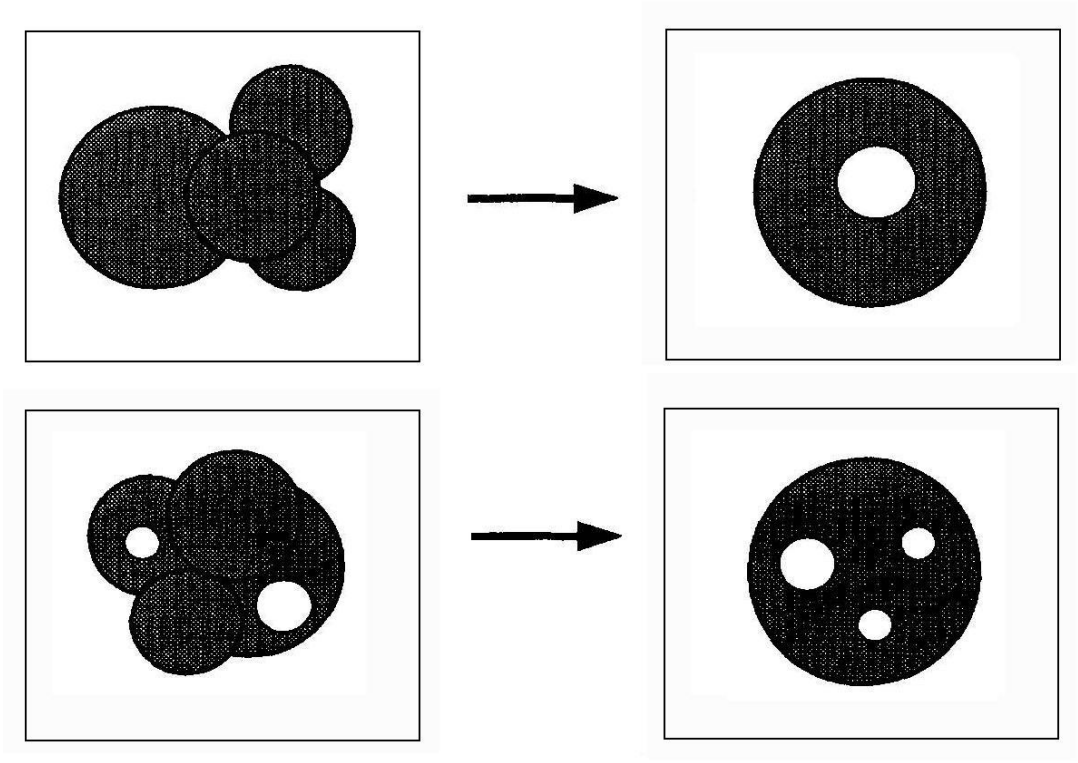

FIGURE 4.3: A simplified representation of the entrapment of continuous phase droplets (in white color) in a dispersed phase drop (in black color) by Kumar (1996).

The presence of double emulsions might have strong effects on the volumetric mass transfer coefficient $k_L a$. Therefore, the structure of a W/O emulsion has been investigated and discussed using an endoscopic photographic technique (cf. Chapters 5 and 6).

4.3 Emulsion viscosity

The viscosity of liquid-liquid dispersion (μ) was first suggested by Einstein (1906) pertaining to the limiting conditions of spherical droplets in infinitely dilute dispersion (cf. Equation 4.1):

$$\mu = \mu_{\text{cont.}}\left(1 + 2.5\, \Phi_{\text{disp.}}\right) \tag{4.1}$$

Obviously, this equation would not be valid at high concentration of the dispersed phase where the droplets can interact and deform from the original shape. To overcome this problem, a number of viscosity expressions have been developed and reported in the literature, which can be found in Hu *et al.* (2005) and Ngan *et al.* (2009). Among them, equation 4.2 proposed by Vermuelen *et al.* (1955) is one of the most commonly used equations for estimating the viscosity of a liquid-liquid system (Guilinger *et al.*, 1988).

$$\mu = \frac{\mu_{\text{cont.}}}{1 - \Phi_{\text{disp.}}}\left(1 + \frac{1.5\, \Phi_{\text{disp.}} \cdot \mu_{\text{disp.}}}{\mu_{\text{disp.}} + \mu_{\text{cont.}}}\right) \tag{4.2}$$

where $\Phi_{\text{disp.}}$ is the volume fraction of dispersed phase, $\mu_{\text{disp.}}$ and $\mu_{\text{cont.}}$ are the viscosities of dispersed and continuous phases, respectively.

Guilinger *et al.* (1988) also reported that the viscosity predictions using equation 4.2 for a water-kerosene system agreed well with their experimental results. Equation 4.2 was used in the present study to estimate the viscosities for aqueous emulsions of n-alkanes, because measuring the viscosity was not possible for our studied systems.

The estimated viscosities corresponding to the oil volume fractions used in the mass transfer measurements are shown in Figures 4.4-4.5 for aqueous emulsions of n-heptane, n-dodecane, and n-hexadecane, respectively (cf. Chapters 5-6 for phase inversion and viscosity-values of pure liquids).

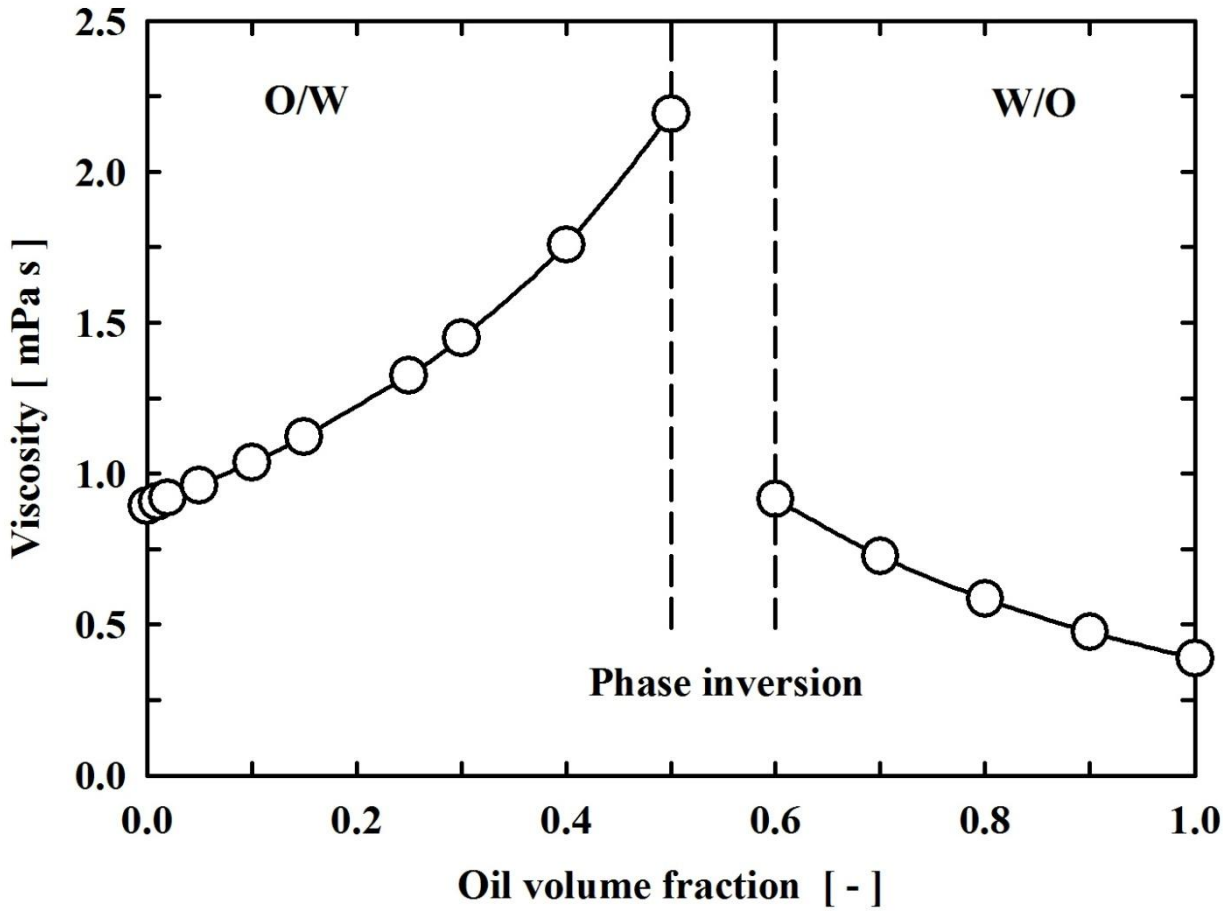

FIGURE 4.4: Variation of viscosity with oil volume fraction for aqueous emulsion of n-heptane (estimated using Equation 4.2).

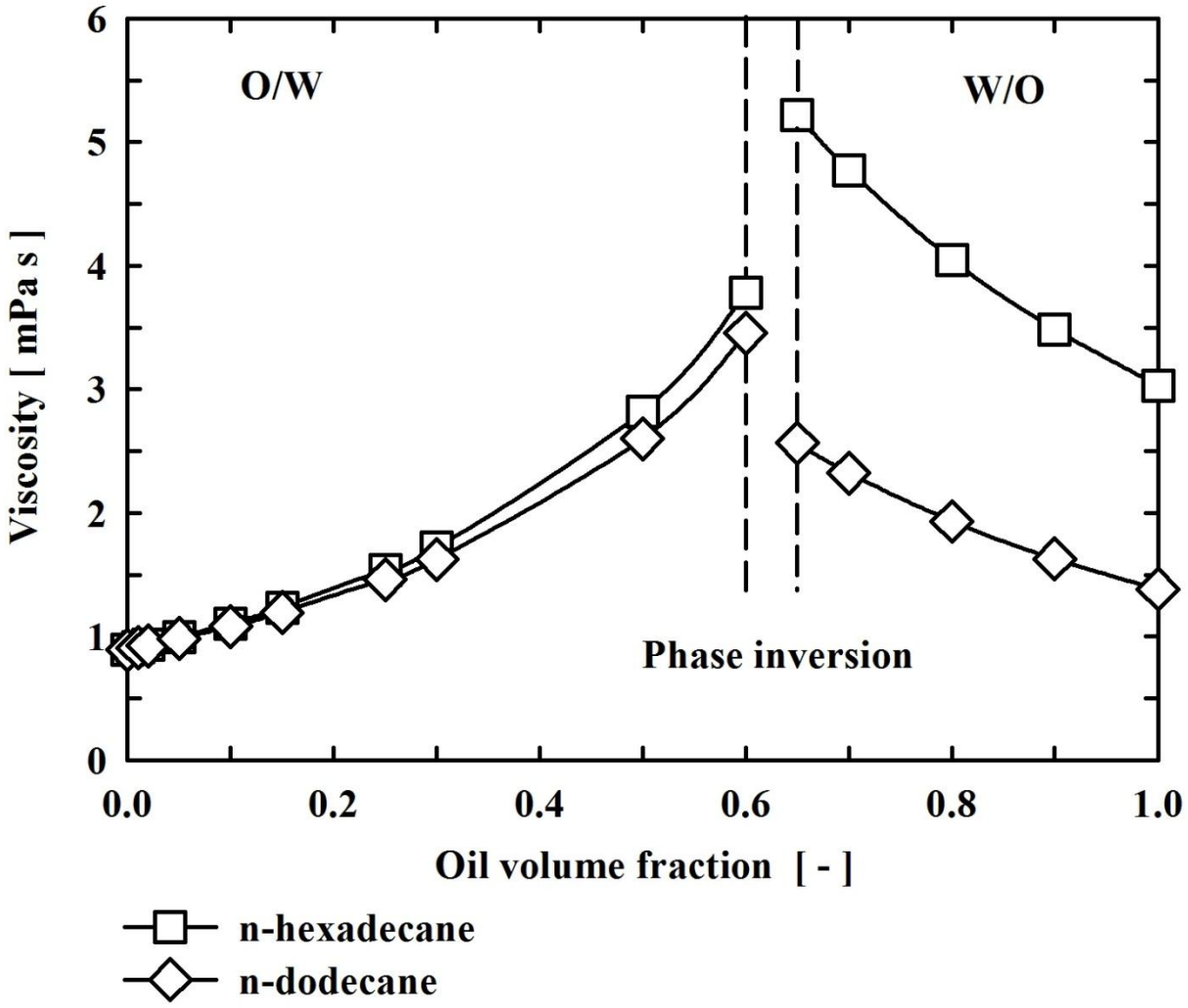

FIGURE 4.5: Variation of viscosity with oil volume fraction for aqueous emulsions of n-dodecane and n-hexadecane (estimated using Equation 4.2).

It can be seen from Figures 4.4-4.5 that starting from O/W emulsion, the emulsion viscosity increases with an increase in oil volume fraction. However, after inverting to W/O emulsion, the emulsion viscosity decreases with increasing the oil volume fraction. The effect of these trends on the volumetric mass transfer coefficient $k_L a$ is discussed in detail in Chapter 6.

5 Experimental

5.1 Chemicals

The following chemicals were used in the experiments:

- Water phase: double-distilled water.
- Gas phase: oxygen (O_2) and carbon dioxide (CO_2) with technical standard 5.0 (purities of 99.999%), bought from Westfalen AG, Germany.
- Oil phase: n-heptane, n-dodecane and n-hexadecane with purities ≥ 99%, bought from Merck, Germany.
- Tris-(2,2'bipyridyl)-Ruthenium (II) chloride (RuBPY): bought from Sigma-Aldrich Chemie GmbH, Germany (cf. Chapter 3 for chemical structure and some photochemical properties of RuBPY).

Some physical properties of the used liquids at 298.15 K, which were taken from Lide and Kehiaian (1994), are shown in Table 5.1.

TABLE 5.1: Physical properties of the liquids at 298.15 K

Name	*Molecular formula*	*Vapor pressure [kPa]*	*Density [g cm^{-3}]*	*Viscosity [mPa s]*	*Surface tension [mN m^{-1}]*
Water	H_2O	3.17 *	0.997	0.893	71.99
n-Heptane	C_7H_{16}	6.09	0.680	0.387	19.65
n-Dodecane	$C_{12}H_{26}$	0.02	0.745	1.383	?
n-Hexadecane	$C_{16}H_{34}$	?	0.769	3.032	27.05

* taken from Haynes and Lide (2010).

5.2 Measurement of k_La

5.2.1 Experimental setup

Figure 5.1 shows the schematic diagram of the experimental setup for measuring the volumetric mass transfer coefficient k_La for absorption of O_2 or CO_2 into aqueous emulsions of three n-

alkanes: n-heptane, n-dodecane and n-hexadecane, respectively. The stirred reactor was made of glass with a total volume of 1830 ml, an inner diameter of 100 mm, and a total height of 21 cm (cf. Subsection 5.2.2 for the reactor volume determination). With a working liquid volume of 700 ml, the liquid height in the reactor was approximately 8 cm. The reactor was jacketed with a jacket height of 17 cm and the temperature in the reactor was controlled to 298.2 $\pm$ 0.1 K by the thermostat TIC 1 (Model F32, Julabo Labortechnik GmbH, Germany). Four baffles, each with a width of 10 mm, were mounted to the reactor wall to prevent vortex formation and liquid rotation.

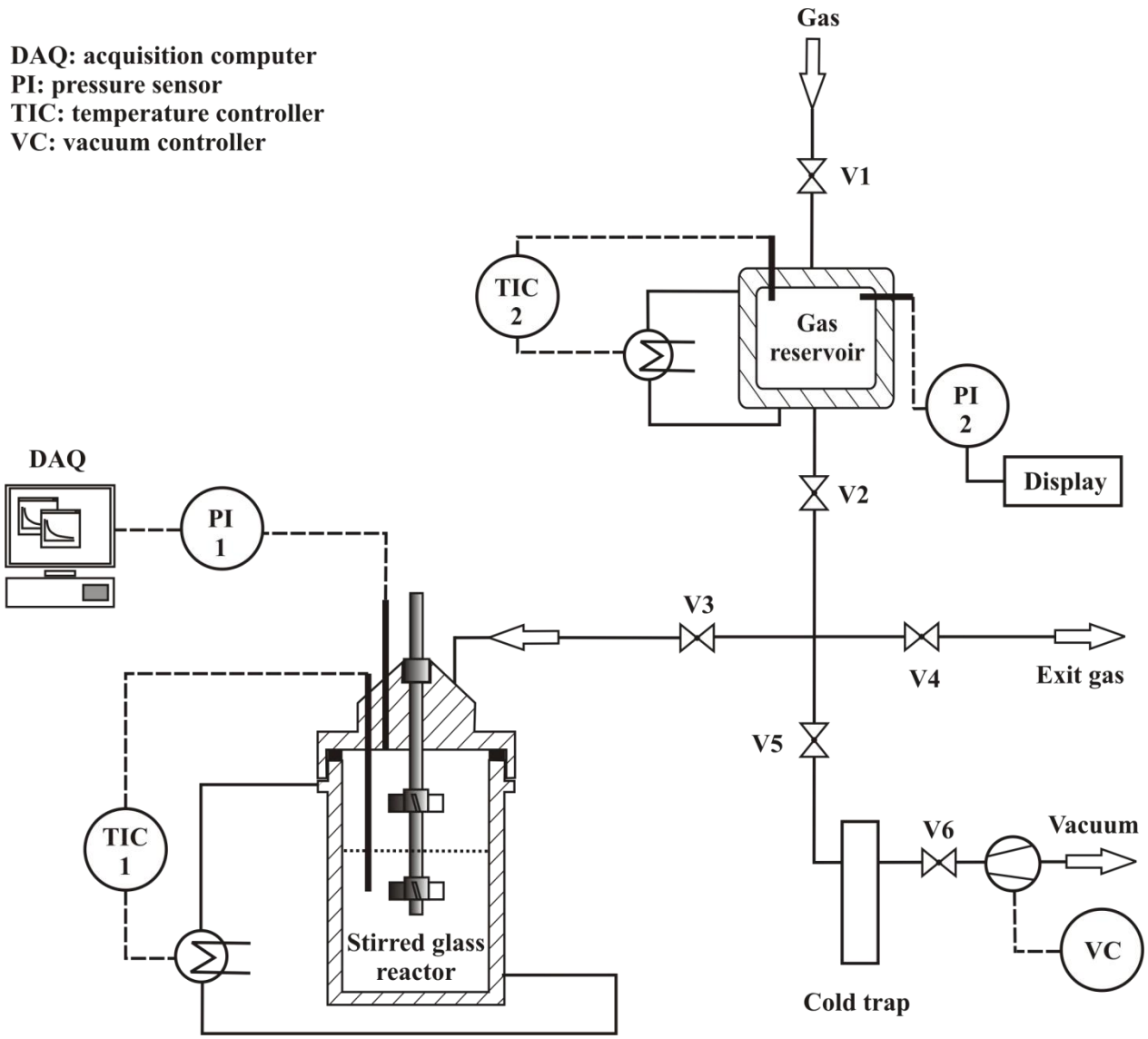

FIGURE 5.1: Experimental setup for $k_L a$ measurement by pressure technique.

The PTFE-jacketed stainless steel stirrer shaft was equipped with two upward 45^{o} pitched-blade PTFE impellers (Bohlender GmbH, Germany). Further characteristics of the stirrer shaft and impellers are presented in Table 5.2. The stirrer shaft was connected to the motor (RZR 2102 control, Heidolph Elektro GmbH, Germany) through a magnetic stirrer bearing (Type MRK 1/20, Buddeberg GmbH, Germany). Using this type of stirrer bearing has allowed avoiding leakage at the studied high stirring speed (1000 min^{-1}).

TABLE 5.2: Characteristics of the stirrer shaft and impellers

	Dimensions [mm]
Stirrer shaft diameter	8
Impeller diameter-blade height-blade thickness	50-18-4
Off-bottom clearance of lower impeller (for liquid phase)	20
Off-bottom clearance of upper impeller (for gas phase)	140

The pressures in the reactor were measured by the pressure sensor PI 1 (Model: STJE-Honeywell, pressure range: 0-5 bar, accuracy of 0.05%, Althen GmbH, Germany). The measured pressures could be read on the digital display PAX S (Althen GmbH, Germany) and recorded using an A/D-Converter KPCI 3108 (Keithley instrument GmbH, Germany) and a data acquisition software written in Labview 7.1. The digital display PAX S was connected to the A/D-Converter though a screw terminal connector STP-36 (Keithley instrument GmbH, Germany).

Characteristics of some other important apparatuses are as follows:

- Gas reservoir: jacketed, made of stainless steel, total volume of 630 ml, operating pressure up to 9 bar.
- Thermostat (TIC 2): Model F33, Julabo Labortechnik GmbH, Germany.
- Pressure sensor (PI 2): Model STJE (Honeywell), pressure range: 0-14 bar, accuracy of 0.05%, Althen GmbH, Germany.
- Digital display for the pressure sensor (PI 2): PAX S, Althen GmbH, Germany.
- Temperature sensors (for both reactor and gas reservoir): Pt 100, Julabo Labortechnik GmbH, Germany.
- Vacuum controller (VC): Type VCZ 224, ILMVAC GmbH, Germany.

5.2.2 Determination of reactor volume

After setting up the experimental system for k_La measurement, the total volume of the glass reactor must be determined in order to calculate accurately the gas solubility in emulsions based on equation 3.11 in Chapter 3. To this end, the reactor volume was measured using a soap film flowmeter (1-10-100 ml, Hewlett Packard); the principle of this measurement is shown in Figure 5.2.

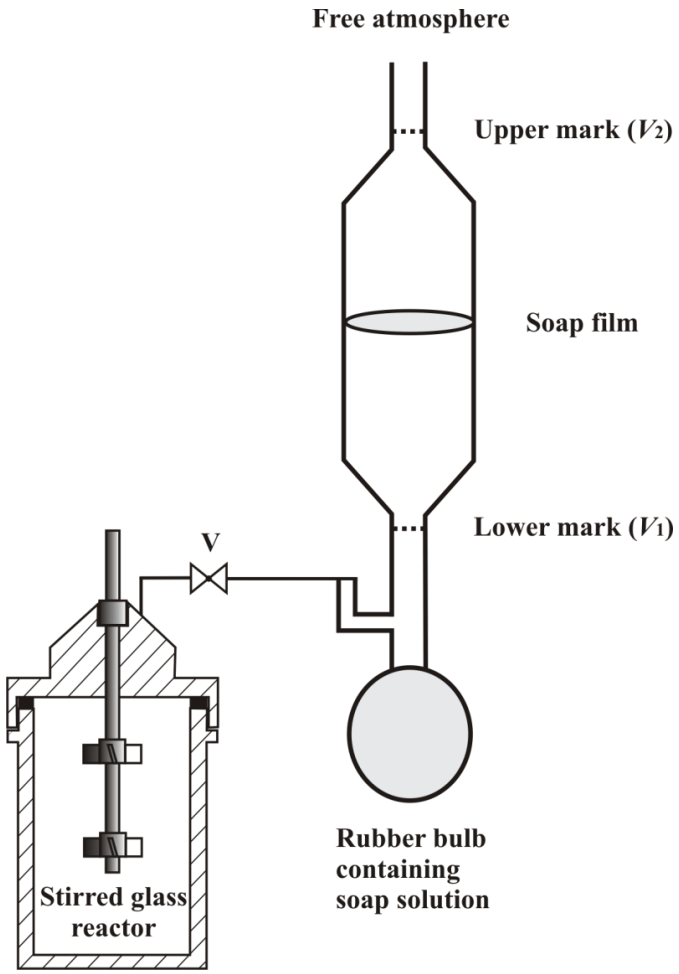

FIGURE 5.2: Measuring principle of the reactor volume using a soap film flowmeter.

The empty glass reactor was charged with a gas up to about 1.3 (bar); the temperature in the reactor (T_R) was usually controlled to 298.2 $\pm$ 0.1 K. The soap film in the glass tube was initially produced by squeezing the rubber bulb to push the soap solution into the tube above the side arm (gas inlet), then releasing the bulb to lower the soap solution. By opening the valve (V), the soap film traveled slowly upwards through a fixed volume between two marks on the glass tube (ΔV =

V_2 - V_1). When the soap film reached the lower mark V_1 and the upper one V_2, the corresponding pressures P_1 and P_2 in the reactor were read on the digital display. The reactor volume (V_R) could be determined from the pressure decrease ($\Delta P = P_1 - P_2$) as follows:

$$V_R = \Delta V \cdot \frac{P_{atm}}{\Delta P} \cdot \frac{T_R}{T_{atm}} \tag{5.1}$$

where P_{atm} and T_{atm} are the pressure and temperature of the surrounding atmosphere.

The glass reactor volume was determined as 1830 ml; therefore, with a working liquid volume V_L of 700 ml, the gas volume V_G in the reactor was 1130 ml.

5.2.3 Experimental procedure

All experiments were carried out under surface aeration with gas entrainment into bubbles at the same high stirring speed (1000 min^{-1}). The experimental operation was batchwise with respect to both gas and liquid phases. The experimental procedure consisted of the following steps:

- **Sample preparation**

The gas (O_2 or CO_2) was charged from the gas bottles into the gas reservoir up to a pressure of about 8-9 bar by opening the valve V1; after charging, the valve V1 was closed. The mixture of oil and water (total volume 700 ml) with desired oil volume fractions (0-100%) was placed in the reactor which had been thoroughly cleaned with acetone and double-distilled water. The temperature in both the gas reservoir and the glass reactor was then controlled to the same temperature of 298.2 $\pm$ 0.1 K by the thermostates TIC 2 and TIC 1, respectively. This took about three hours.

- **Degassing by applying vacuum and agitation**

After the operation temperature (298.2 $\pm$ 0.1 K) was attained, the oil-water emulsion was mechanically created by stirring at 1000 min^{-1} in about 3 minutes. Still keeping the stirring speed at 1000 min^{-1}, the emulsion was degassed by applying vacuum (V3, V5 and V6 were opened while V2 and V4 were closed). The liquid losses during degassing were determined using a cold trap with liquid nitrogen as the coolant. The n-heptane loss was about 1.3 ml for O_2 and 1.7 ml for CO_2 respectively; these losses were compensated by adding the respective volumes in excess

before each measurement. On the other hand, the losses were negligible for n-dodecane and n-hexadecane.

- **Absorption**

After degassing, the valves V5, V6, V3 were closed and the valve V2 was opened. The agitator was then stopped. When the liquid surface had become stable (no movement), the reactor was pressurized in about 10-12 s to approximately 0.15 MPa (1.5 bar) with pure O_2 or to approximately 0.17 MPa (1.7 bar) with pure CO_2 by opening slowly the valve V3. After about 20 s, when the pressure reading had become constant, the absorption experiment was started by switching on the agitator again. The time course of the pressure decrease in the reactor head space, measured with pressure sensor PI 1, was recorded by the Labview 7.1 data acquisition software. The data recording rate of 2.5 s^{-1} was used for emulsions of n-dodecane and n-hexadecane, whereas that of 3.0 s^{-1} was used for emulsions of n-heptane. A typical experimental record is shown in Figure 5.3.

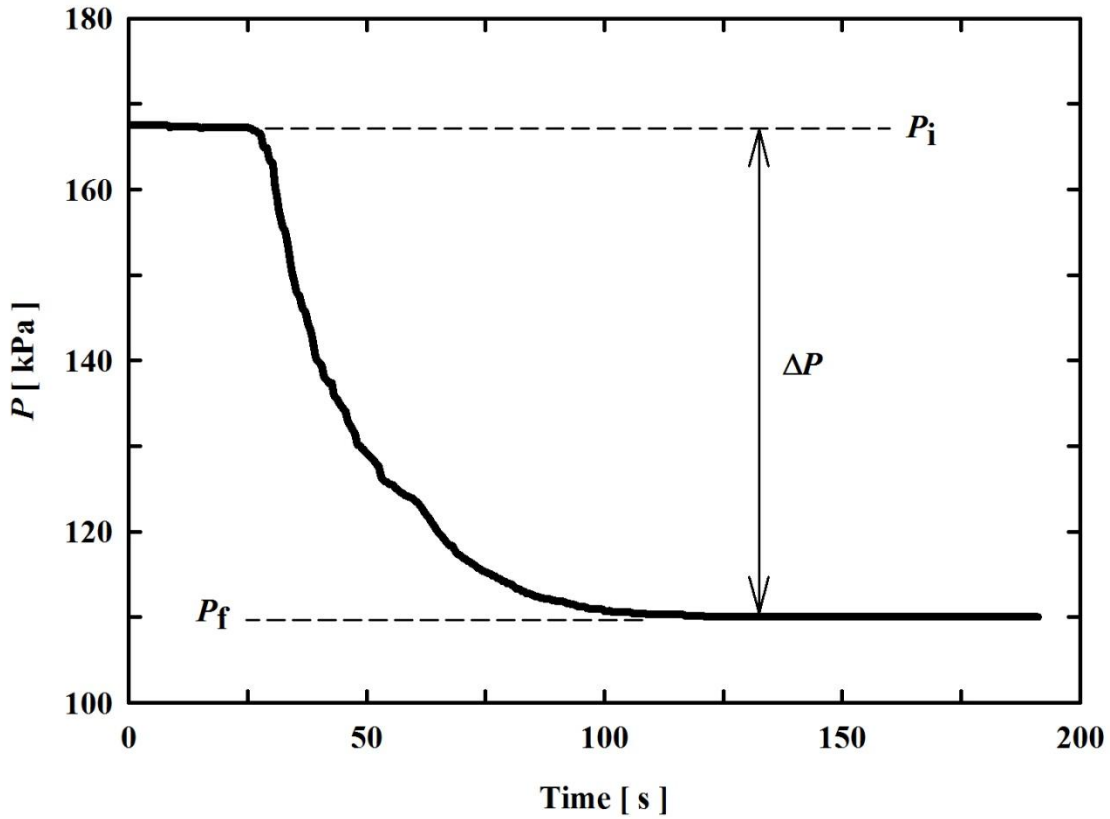

FIGURE 5.3: Example for pressure decrease during gas absorption into emulsions (CO_2/water/n-hexadecane system, Φ_{oil} = 30%).

After each measurement, the agitator was stopped, the valve V4 was opened to release the pressure in the reactor to atmospheric pressure. After about 30 minutes when the water and oil phases were completely separated, the above experimental procedures were repeated for a new measurement. For each oil volume fraction, the experiment was repeated at least five times.

5.2.4 Evaluation of $k_L a$

The equation 3.10 of the pseudo-homogeneous model, which has been developed in Chapter 3, is shown here once again:

$$-\frac{P_f - p_W - p_O}{P_i - p_W - p_O} \cdot \ln(P - P_f) = k_L a \cdot t + C$$

Using this equation, in conjunction with the experimental record of the pressure decrease with time in the reactor (cf. Figure 5.3), the volumetric mass transfer coefficient $k_L a$ can be determined by plotting $f(t) = -\ln(P - P_f) \cdot (P_f - p_W - p_O)/(P_i - p_W - p_O)$ versus time t. The slope of the resulting linear line gives the value of $k_L a$.

For all determinations of $k_L a$ in the present study, the data at 15% to 90% saturation was used in order to exclude the initial re-emulsification phase as well as the final phase with low driving force. Figure 5.4 presents a typical example for $k_L a$ determination in the case of CO_2/water/n-hexadecane system with n-hexadecane volume fraction of 30%, by which $k_L a$ was determined as 0.0302 s^{-1}.

In addition, from the total pressure decrease, ΔP (cf. Figure 5.3), the overall gas solubility in the emulsions at a partial pressure of 101325 Pa can be calculated using equation 3.11 in Chapter 3.
The reported results in Chapter 6 for volumetric mass transfer coefficient ($k_L a$) and gas solubility (C^*) are mean values of at least five measurements. The experimental error considerations for the absorption of both gases are as follows:

Absorption of O_2:

- The mean relative standard deviation for $k_L a$ was 8% for n-dodecane and n-heptane emulsions, and 7% for n-hexadecane emulsions.
- The mean relative standard deviation for $C^*_{O_2}$ was always less than 5% for all emulsions.

Absorption of CO_2:

- The mean relative standard deviation for k_La was 5%, 6% and 9% for emulsions of n-hexadecane, n-dodecane and n-heptane, respectively.
- The mean relative standard deviation for $C^*_{CO_2}$ was always less than 1% for all emulsions.

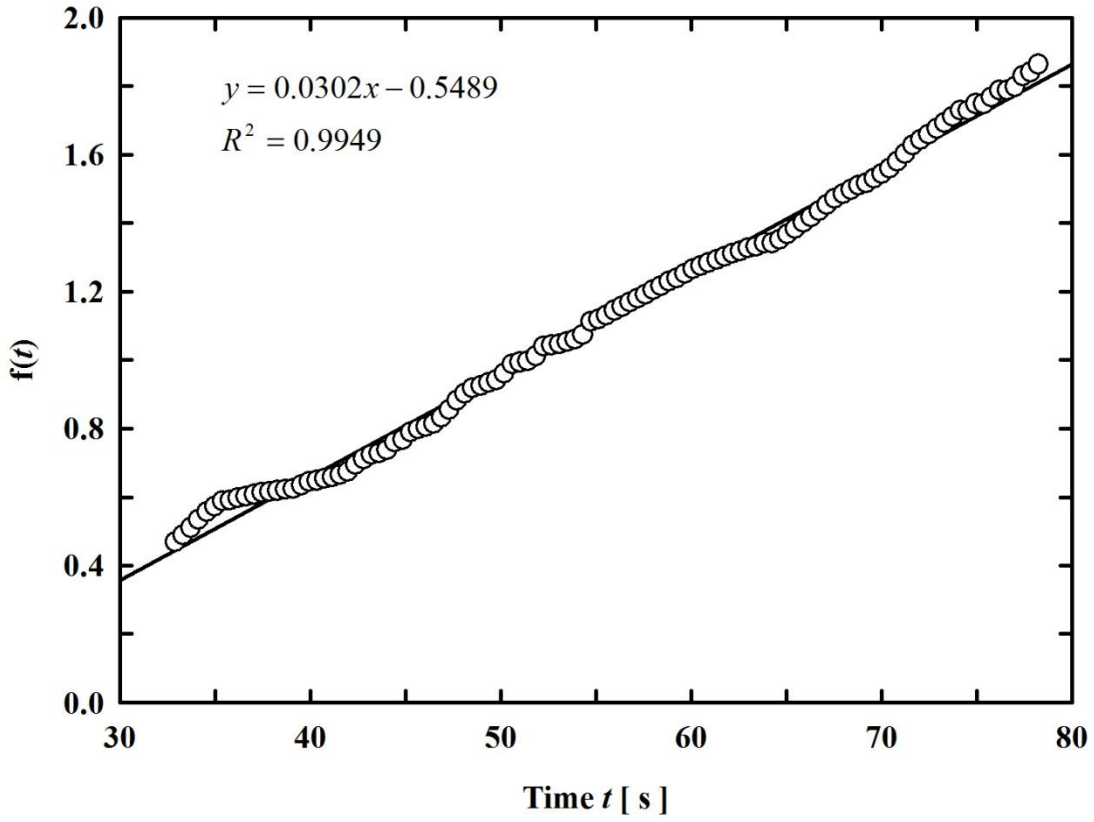

FIGURE 5.4: Example for k_La determination (using the corresponding data presented in Figure 5.3 for CO_2/water/n-hexadecane system with Φ_{oil} = 30%; solid line: linear regression line).

5.3 Measurement of $(k_La)_{GW}$

5.3.1 Experimental setup

As mentioned earlier in Chapter 3, the gas-water volumetric mass transfer coefficient, $(k_La)_{GW}$, was measured using a fluorescence-based oxygen optode for the oxygen absorption into aqueous emulsions of n-dodecane and n-hexadecane. The schematic diagram of the experimental setup for measurement of $(k_La)_{GW}$ is shown in Figure 5.5. Basically, the same experimental system as described in Subsection 5.2.1 and Figure 5.1 for measuring k_La was used, except for the following modifications:

- The model 5866 pressure controller (PC), produced by Brooks instrument, was additionally installed for performing accurately external calibration of the oxygen optical sensor. The pressure controller was operated by a control unit (WMR-compact 2, Westfall Mess-und Regeltechnik GmbH, Germany).
- The oxygen optical sensor (MOPS) was additionally installed in the glass stirred reactor at the height of about 2 cm from the reactor bottom (cf. Subsection 3.4.2, Chapter 3 for more details on the fiber optic oxygen sensor system). The analog output voltage of the optical sensor (i.e. the output voltage of the photomultiplier) was in the range of 0-1 V. This signal range was amplified to 0-10 V and recorded to a computer with the help of the KPCI 3108 A/D-Converter and the Labview 7.1 data acquisition software.
- The pressure in the glass reactor measured by the pressure sensor (PI 1) was read on the digital display (PAX S).

5.3.2 Experimental procedure

Except for a slight difference in the used chemicals, the sample preparation step was exactly the same as described above in Subsection 5.2.3 for measuring $k_L a$. Here, the water phase consisted of double-distilled water and dissolved fluorophore RuBPY (cf. Section 3.4, Chapter 3 for details) at the concentration of 0.1 kg m^{-3} (Jordan *et al.*, 2001); the feeding gas was oxygen; the oil phases were n-dodecane or n-hexadecane.

After the sample preparation, for each definite oil volume fraction, the oxygen optode had to be externally calibrated (four-point calibration method) before the absorption experiments could be performed.

- **External calibration of the optical oxygen sensor**

The photomultiplier voltage U_0 was recorded under degassing conditions (i.e. the emulsion was stirred under a vacuum of 0.0048 MPa); this voltage corresponds to the oxygen concentration in the water phase of 0% saturation. The photomultiplier voltage U_{100}, corresponding to the oxygen concentration in the water phase of 100% saturation, was recorded when the stirred emulsion was saturated after applying the initial pressure of 0.152 MPa $\pm$ 0.5% (1.52 bar $\pm$ 0.5%). This pressure value (setting point of 4.8% on the control unit of the pressure controller) was also the initial pressure for all experimental absorption curves described below.

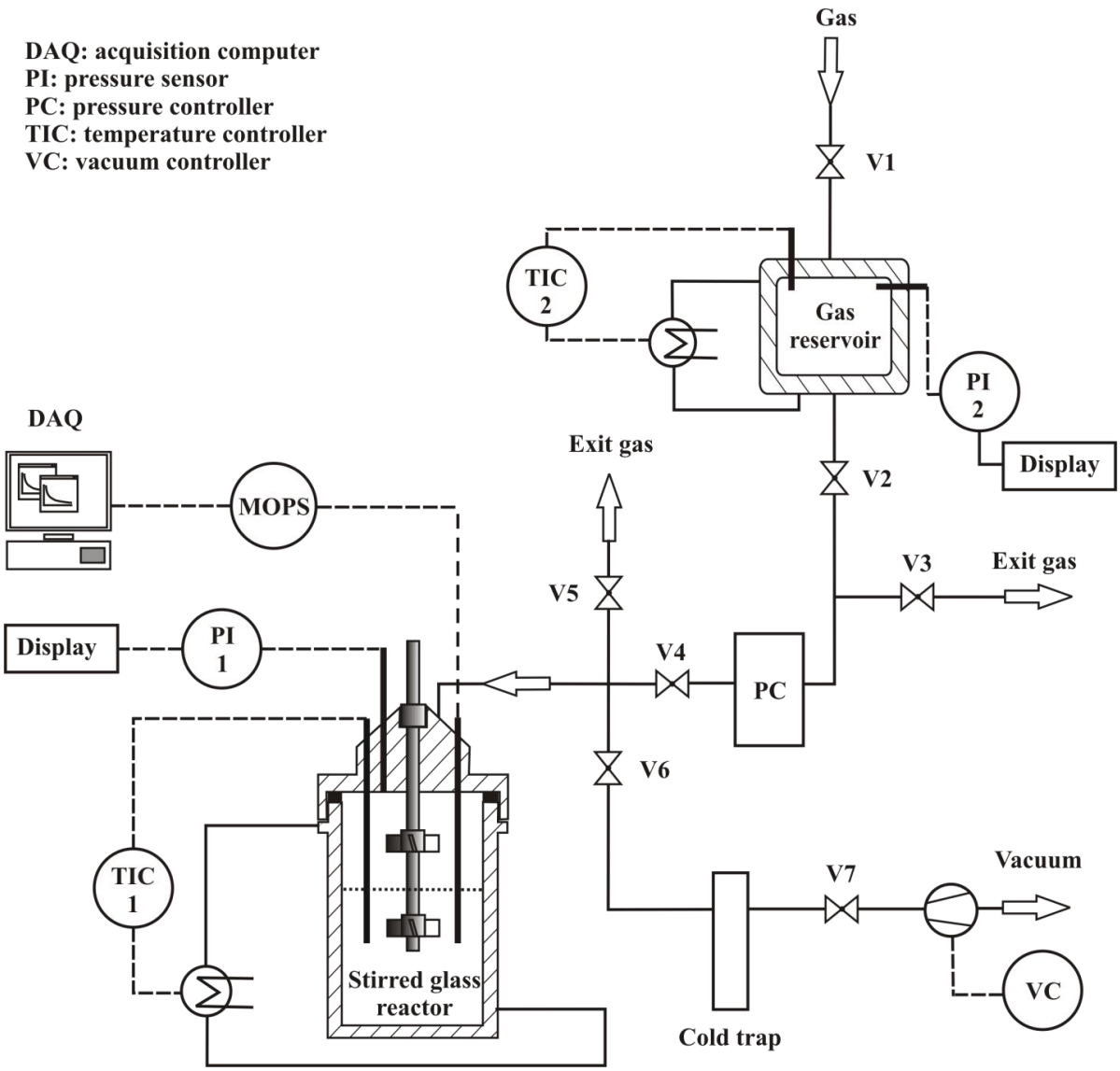

FIGURE 5.5: Experimental setup for $(k_L a)_{GW}$ measurement by fluorescence technique.

Two additional voltage values U_1 and U_2, corresponding to X_1 and X_2% oxygen saturation, were recorded when the stirred emulsion was saturated after applying the initial pressures of 0.079 MPa $\pm$ 0.5% (0.79 bar $\pm$ 0.5%) and 0.055 MPa $\pm$ 0.5% (0.55 bar $\pm$ 0.5%), respectively (setting point of 2.3% and 1.5%, respectively on the control unit of the pressure controller). The final pressures (i.e. saturated pressures) corresponding to 100, X_1 , and X_2% oxygen saturation were read on the display of the pressure sensor PI 1 (cf. Figure 5.5).

Figure 5.6 presents some examples for external calibration plots of the optical oxygen sensor, in which the relationship between U and $C_{O_2,W}$ is definitely non-linear.

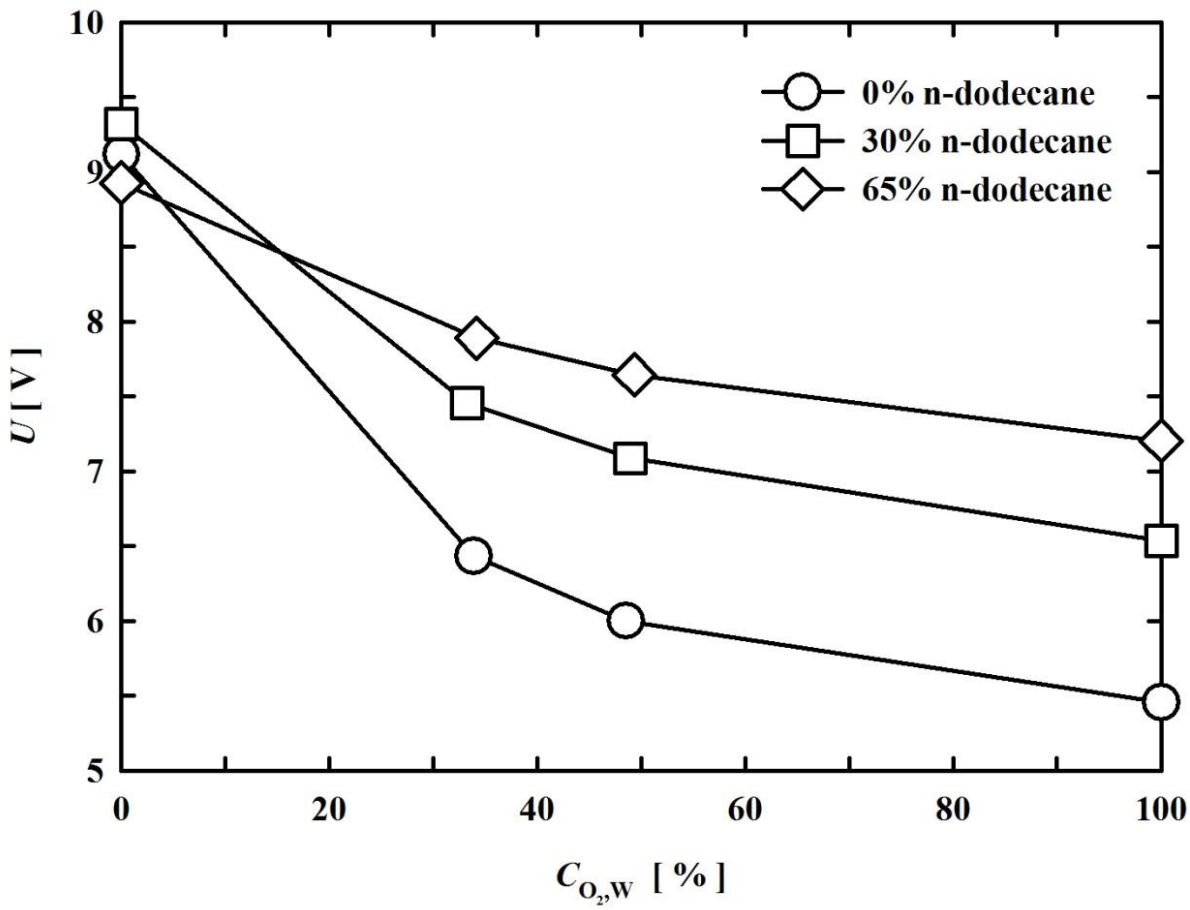

FIGURE 5.6: Examples for non-linear calibration plots of the oxygen optical sensor (pure water and two n-dodecane emulsions with Φ_{oil} = 30% and 65%).

Using the linear approach proposed in Chapter 3 (cf. Equation 3.18), linear calibration plots could be generated by plotting $1/(U_0 - U)$ against $1/C_{O_2,W}$, from which the values of K_{SV} and *const.* could be obtained (cf. Equations 3.19 and 3.20). The linear regression coefficients (R^2) were found to be always greater than 0.985 (cf. Table 5.3). The excellent linear fits of the measured data to equation 3.18 supports the validity of the proposed approach. Figure 5.7 shows the linear calibration plots corresponding to the calibration data presented in Figure 5.6, and the regression analysis results are shown in Table 5.3.

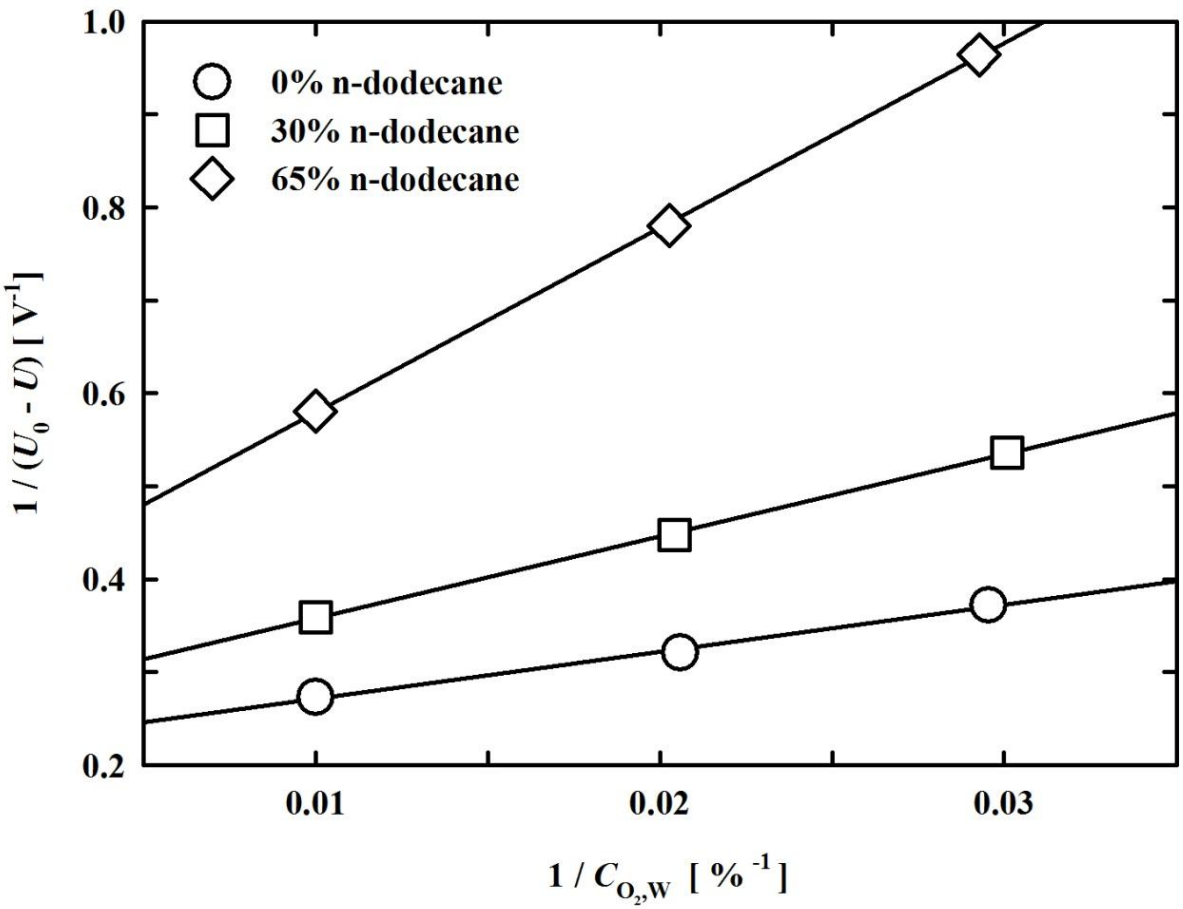

FIGURE 5.7: Linear calibration plots with corresponding calibration data presented in Figure 5.6 using the proposed linear approach (solid lines: linear regression lines).

TABLE 5.3: Examples for regression analysis results (using the corresponding calibration data presented in Figure 5.7)

Volume fraction of n-dodecane	U_0 [V]	U_{100} [V]	K_{SV} [*arbitrary unit*]	*const.* [-]	R^2
0	9.119	5.457	0.044	0.808	0.9950
0.3	9.319	6.536	0.031	0.751	0.9995
0.65	8.926	7.205	0.019	0.655	0.9998

Using the obtained values of *const.* from the above linear regression analysis, the linearity of the Stern-Volmer plots (I_0/I versus $C_{O_2,W}$) was additionally checked (cf. Subsection 3.4.1 and Equations 3.15-3.16). Quite expectedly, very good linearity was found for all emulsions of both

n-dodecane and n-hexadecane. Three Stern-Volmer plots based on the corresponding calibration data presented in Figures 5.6 and 5.7 are shown in Figure 5.8.

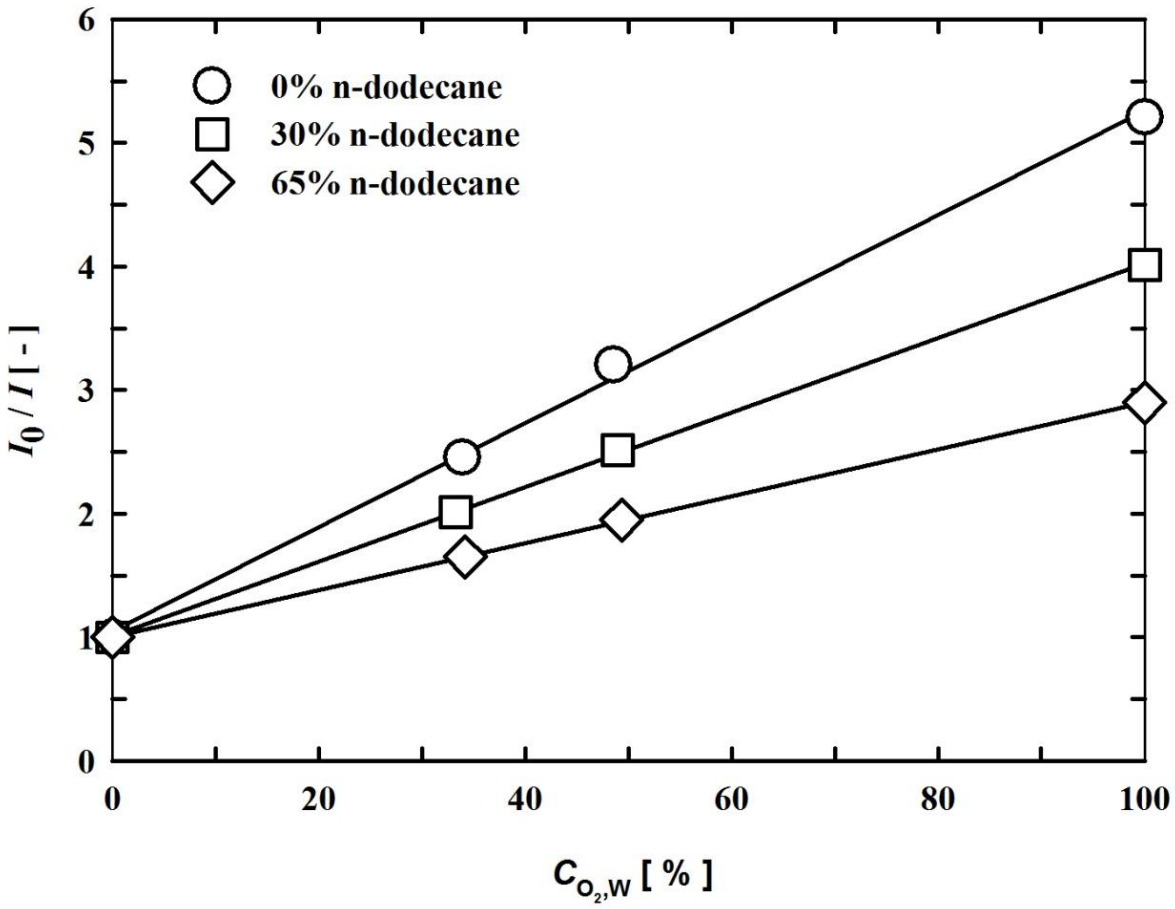

FIGURE 5.8: Stern-Volmer plots based on the corresponding calibration data presented in Figures 5.6 and 5.7 (solid lines: linear regression lines).

- **Absorption experiment**

After performing the external calibration of the oxygen optical sensor, the absorption experiments could be carried out. The experimental procedure was similar to the one used in measuring $k_L a$ by pressure method, which had been described in Subsection 5.2.3. It can be briefly summarized as follows:

1. *Degassing by applying vacuum and agitation*

The oil-water emulsion was degassed at stirring speed of 1000 min^{-1} and temperature of 298.2 $\pm$ 0.1 K by applying vacuum (V6, V7 were opened while V4 and V5 were closed). The liquid losses during degassing were determined using a cold trap with liquid nitrogen as the coolant. The losses were negligible for n-dodecane and n-hexadecane.

2. *Absorption*

After degassing, the valves V6, V7 were closed and the valve V2 was opened. The agitator was then stopped. When the liquid surface had become stable (no movement), the reactor was pressurized to 0.512 MPa $\pm$ 0.5% (1.52 bar $\pm$ 0.5%) with pure oxygen by opening the valve V4. It should be noted that the time required for charging oxygen was about 4 minutes because of the flow resistance in the pressure controller. After about 20 s, when the pressure reading had become constant, the absorption experiment was started by switching on the agitator again.

During oxygen absorption, the time course of photomultiplier-voltage (U) decrease due to the increase in oxygen concentration (i.e. increase in quencher concentration) in the water phase was recorded with the Labview 7.1 data acquisition software. The data recording rate of 2.5 s^{-1} was applied for emulsions of both n-dodecane and n-hexadecane. An example of experimental record is shown in Figure 5.9, in which the photomultiplier-voltage (U) decreases from the initial voltage U_0 (i.e. 0% oxygen saturation) down to the final voltage U_{100} (i.e. 100% oxygen saturation) with time.

It should be mentioned that, compared to pure water, the initial voltage (U_0) was actually observed not to be stable upon oil addition. For convenience in discussion of this matter, the initial and final voltages which had been measured in the external calibration stage are here expressed as U^*_0 and U^*_{100}, respectively. For the oil volume fractions in the range of 1-30%, the initial voltage U_0 was lower than U^*_0 due to a voltage decrease after degassing and stopping agitation, and a signal peak (cf. Figure 5.9) was observed at the beginning of the absorption curve. At higher oil volume fractions, the initial voltage U_0 was higher than U^*_0 and no such signal peak was observed; this is due to the fact that soon after degassing and stopping agitation, the photomultiplier voltage rapidly increased to nearly 10 V, which corresponds to the detection limit of the photomultiplier.

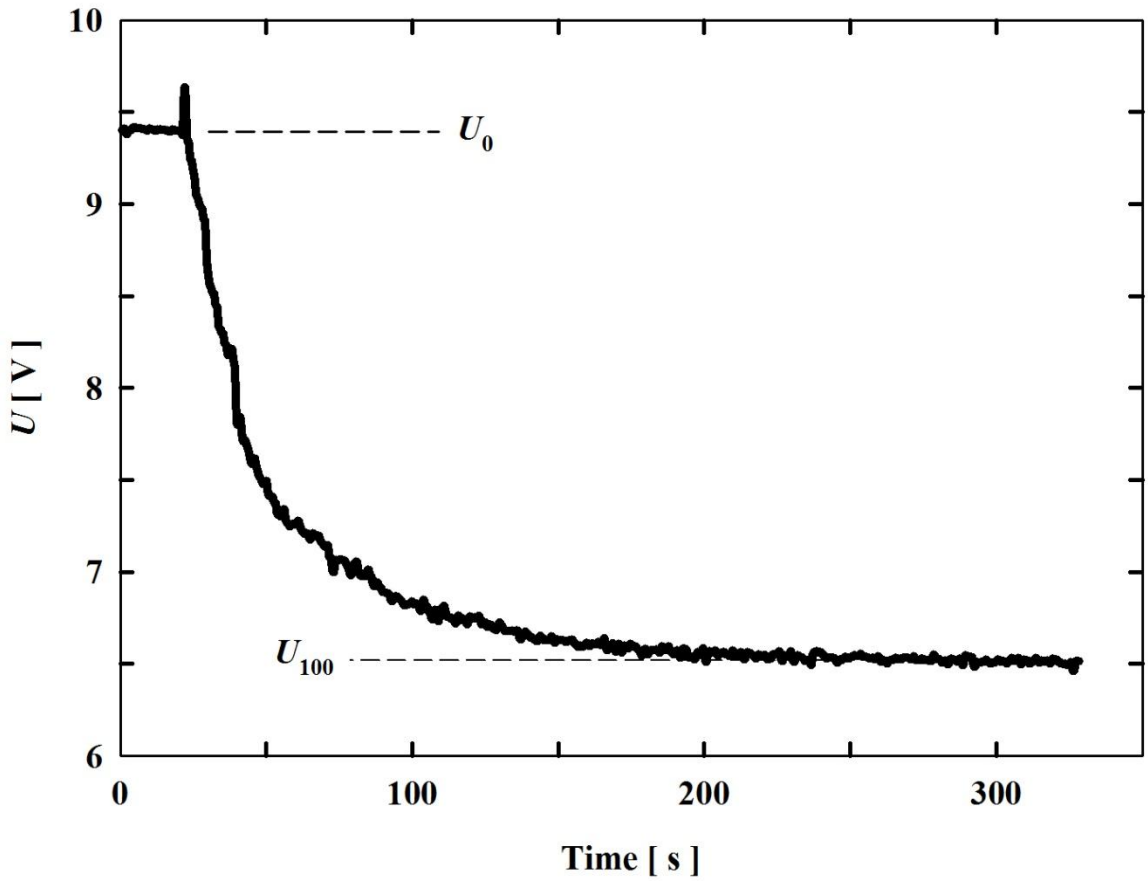

FIGURE 5.9: Example for photomultiplier voltage decrease during oxygen absorption into the water phase (n-dodecane emulsion with Φ_{oil} = 30%).

After each measurement, the agitator was stopped, the valve V5 was opened to release the pressure in the reactor to atmospheric pressure. After about 30 minutes when the water and oil phases were completely separated, the above experimental procedures were repeated for a new measurement. For each oil volume fraction, the experiment was repeated for at least five times.

The recorded photomultiplier-voltage (U) was then converted to oxygen concentration by using the modified Stern-Volmer equation 3.17 (cf. Chapter 3) and the values of K_{SV} and *const.* obtained by external calibration of the oxygen optical sensor. Due to the instability of the initial voltage signal (U_0) as described above, the initial voltage (U_0) could not be precisely read from the absorption curve. For this reason, the "true" initial voltage $(U_0)_{true}$, which was calculated based on the final voltage (U_{100}) and $\Delta U = U^*_0 - U^*_{100}$ using equation 5.2 below, was used instead.

$$(U_0)_{\text{true}} = U_{100} + \Delta U \tag{5.2}$$

Figure 5.10 represents the increase in oxygen concentration in the water phase with time converted from the corresponding experimental record in Figure 5.9, which allows determining the gas-water mass transfer coefficient $(k_L a)_{GW}$ (cf. Subsection 5.3.3 below).

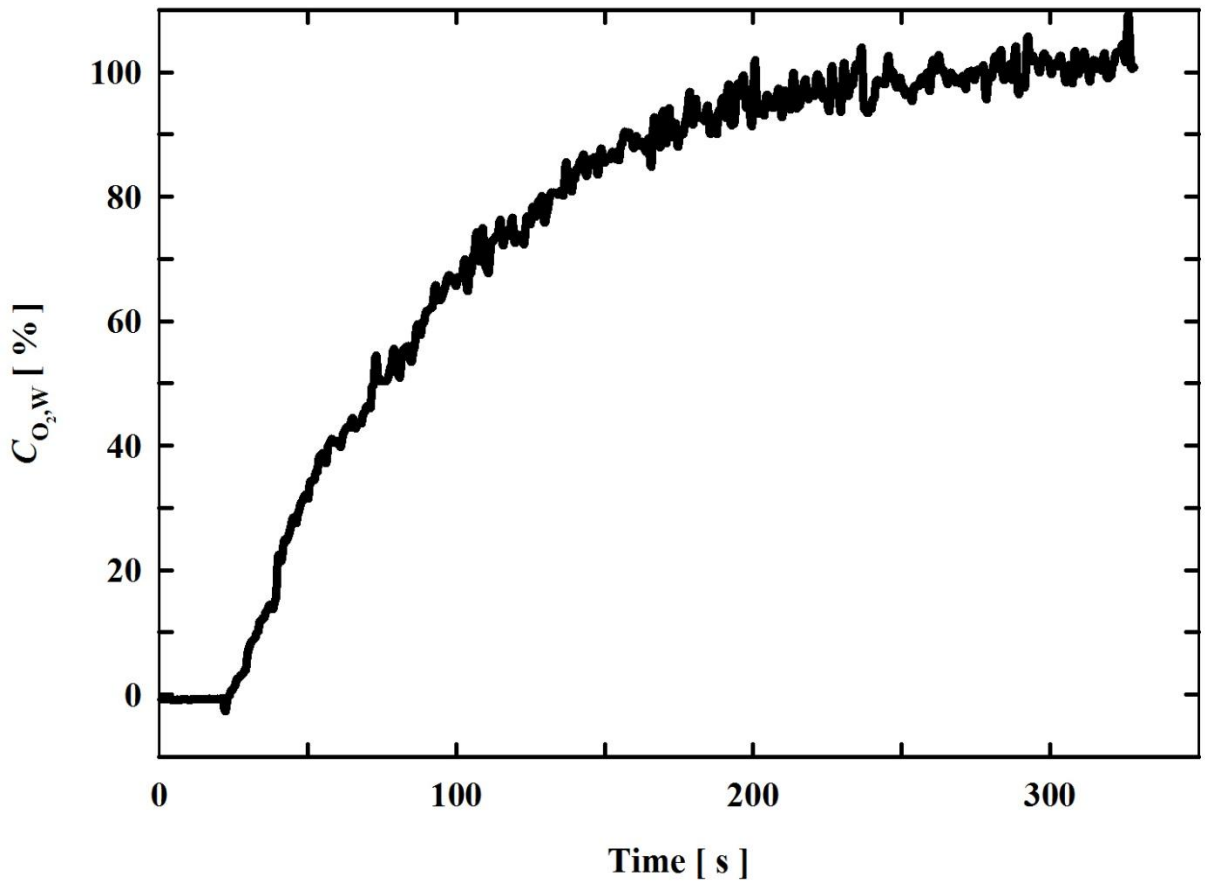

FIGURE 5.10: Oxygen concentration increase in the water phase (converted from the corresponding voltage data presented in Figure 5.9 for n-dodecane emulsion with Φ_{oil} = 30%).

5.3.3 Evaluation of $(k_L a)_{GW}$

The equation 3.23, which had been developed in Chapter 3, is mentioned below once again:

$$\ln\left(C^*_{O_2,W} - C_{O_2,W}\right) = -(k_L a)_{GW} \cdot t + C$$

This equation allows determining the gas-water volumetric mass transfer coefficient $(k_L a)_{GW}$ based on the time course of oxygen concentration increase in the water phase (cf. Figure 5.10) by plotting $g(t) = \ln\left(C^*_{O_2,W} - C_{O_2,W}\right)$ versus time *t*. The slope of the resulting linear line gives the value of $(k_L a)_{GW}$.

For all determinations of $(k_L a)_{GW}$, the data at 15% to 90% saturation was used in order to exclude the initial re-emulsification phase as well as the final phase with low driving force. It should be noted that the saturation oxygen concentration in the water phase $(C^*_{O_2,W})$ was always 100%. Figure 5.11 presents a typical example for $(k_L a)_{GW}$ determination, which used the corresponding data presented in Figure 5.10 for n-dodecane emulsion with Φ_{oil} = 30%, by which $(k_L a)_{GW}$ was determined as 0.0157 s^{-1}.

The reported results in Chapter 6 for gas-water volumetric mass transfer coefficient $(k_L a)_{GW}$ are mean values of at least five measurements with the mean relative standard deviation of 11% and 9% for aqueous emulsions of n-dodecane and n-hexadecane, respectively.

Finally, the fluorescence technique with water-soluble fluorophore could allow to measure $(k_L a)_{GW}$ reasonably up to 80% oil volume fractions; above this limitation the values of $(k_L a)_{GW}$ became unreliable.

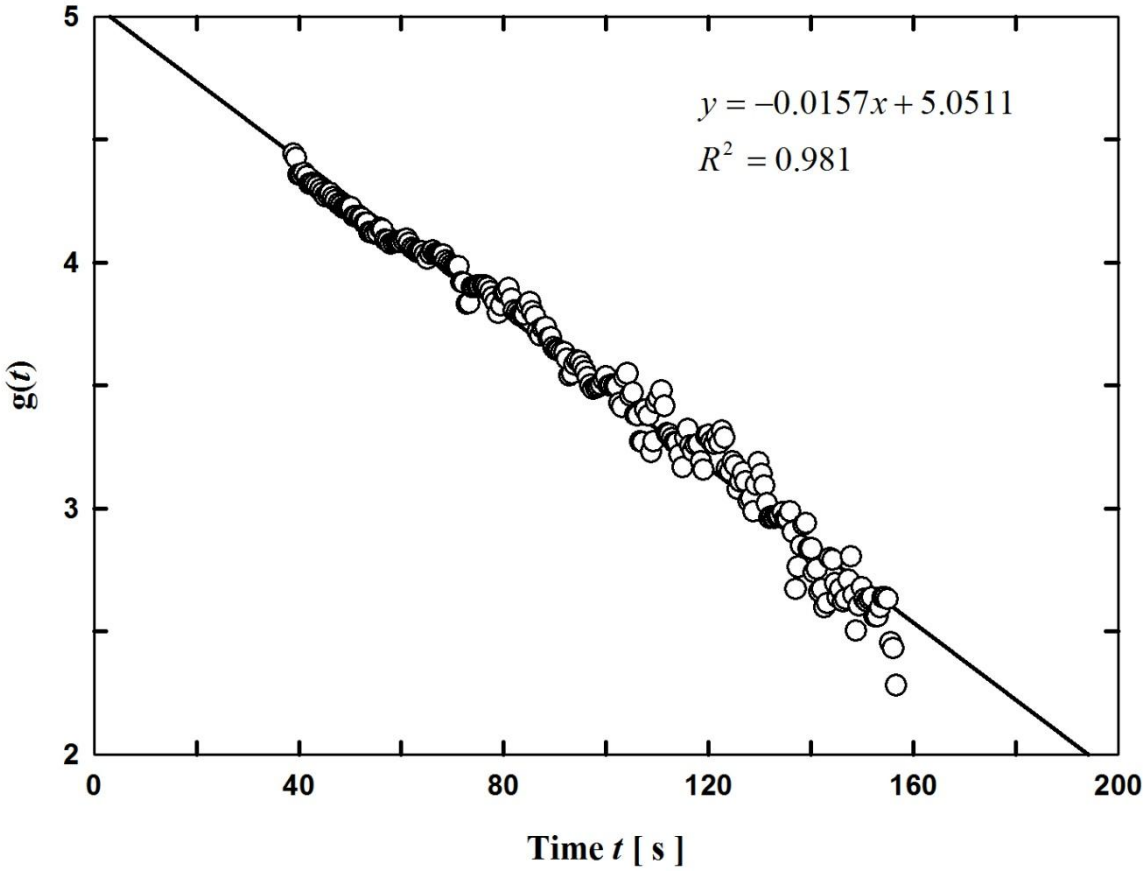

FIGURE 5.11: Example for $(k_L a)_{GW}$ determination (using the corresponding data presented in Figure 5.10 for n-dodecane emulsion with Φ_{oil} = 30%; solid line: linear regression line).

5.4 Measurement of spreading coefficient

The aim of this measurement is to explain the behavior of the oils (n-heptane, n-dodecane and n-hexadecane) used in the mass transfer experiments; therefore, no further purifications were needed for the oil phases.

The surface and interfacial tensions for pure liquids and when liquids are mutually saturated were measured at 298.15 K with the ring method using the tensiometer K11 (Krüss, Germany, Figure 5.12 B), in order to determine the spreading coefficient S or S^* (cf. Equations 2.23 and 2.24 in Chapter 2).

(A) (B)

FIGURE 5.12: Apparatus for measurement of the spreading coefficient
(A): Separating funnel; (B): Tensiometer.

The basic principle is to measure the force required to pull a circular ring from the surface or interface. The standard platinum-iridium ring (RI21), supplied by Krüss, was used for this purpose. Before each measurement, the ring had to be thoroughly cleaned with acetone and distilled water, then heated to red-color with the Bunsen burner to remove any contamination. It should be noted that the major error in this technique is caused by deformation of the ring, so that extreme care must be taken when handling the ring.

Table 5.4 shows some important parameters used in the present work. The densities of the liquids were taken from Table 5.1. For the measurements of surface tension, the density of the light phase (i.e. the air) was taken as 0.001 g cm^{-3}.

TABLE 5.4: Parameters for the ring method

Parameter	*Surface tension*	*Interfacial tension*
Measuring speed (mm min^{-1})	3	0.5
Searching speed (mm min^{-1})	20	20
Immersion depth (mm)	3	3
Immersion speed (mm min^{-1})	100	100

The saturated phases were prepared by shaking 1500 ml of pure water vigorously with 1000 ml of oil phase in a 3000 ml-separating funnel (cf. Figure 5.12 A) for about 5 minutes. The separating funnel was then stored quietly at room temperature for at least 48 hours. After that the two saturated phases were separated from each other by opening slowly the valve at the bottom.

5.4.1 Surface tension

The sample vessel (dia. 70 mm, glass) containing 70 ml of sample liquid was placed in the temperature-controlled sample holder. The clean ring (mentioned above) was then hung on the balance, positioned just above the liquid surface. After waiting for the sample reaching the desired temperature of 298.15 K (about one hour), and entering the necessary parameters from the control panel (cf. Table 5.4), the measurement was started. The ring was firstly tarred in the air, and then the measurement process was run automatically by movement of the sample holder. With the help of the software LabDesk 3.1, all the surface tension results were transferred directly to the computer, where they could be visualized and stored. The reported results in Chapter 6 are mean values of three measurements with maximum relative standard deviation of 0.25%.

5.4.2 Interfacial tension

The interfacial tension between oil and water was measured in the 'Pull' mode, which means that the ring was pulled through the interface from the water phase in the bottom layer to the oil phase in the upper layer. For this measurement, the measuring speed of 0.5 mm min^{-1} was found to be optimal; it was applied for all interfacial tension measurements (cf. Table 5.4). Working with higher measuring speed, the liquid film produced inside the ring is more likely to be broken during the movement of the sample holder.

The measurement was taken in two steps:

- Step 1: The sample vessel with 45 ml oil was placed in the sample holder, waiting for about 10 minutes until the oil surface was stable (no surface vibration), and then the ring was tarred in this oil phase. After tarring, the ring was cleaned and hung on the balance again, and the oil phase vessel was removed and covered carefully.

- Step 2: The sample vessel with 40 ml water was inserted in the sample holder. After the ring touched the water surface (i.e. immersed by about 3 mm) and waiting for about 10 minutes, the oil used for tarring in the first sample vessel was carefully layered over the

water with a syringe. After covering the water with the oil, it was waited for about one hour before the measurement of interfacial tension was actually started. Similar to surface tension, the measuring process was running automatically.

The reported results in Chapter 6 are mean values of four measurements with maximum relative standard deviation of 4%.

5.5 Identification of emulsion phase inversion

5.5.1 Measurement of electrical conductivity

As mentioned earlier in Chapter 4, the electrical conductivity method was applied in the present study to identify the phase inversion points of the emulsions. To this end, the "ultrapure water" conductivity cell LF313T (measuring range: 0.001-200 μS cm^{-1}; cell constant: 0.100 cm^{-1} ± 2%; Schott Instruments GmbH, Germany) was used to measure the electrical conductivities of the stirred emulsions. The conductivity cell was installed in the glass reactor at about half the emulsion height. After stirring the desired emulsions in the reactor at constant temperature of 298.2 K for about 4 minutes, the measurements of electrical conductivity were started. The electrical conductivity results and also the temperatures of the stirred emulsions were shown on the display of the conductivity meter Lab 960 (Schott Instruments GmbH, Germany). These data could be transferred to a computer and stored there with the help of the software MultiLab® pilot (Version 5.03). The reported results in Chapter 6 are mean values of three measurements with mean relative standard deviation of 2%.

5.5.2 Visual observation of emulsion phase inversion

- **Observation of stirred emulsions**

In some cases, the emulsion phase inversion can be visually observed due to the different appearances between O/W and W/O stirred emulsions (i.e. usually milk-white color for O/W emulsions as opposed to dull-opaque color for W/O emulsions). A mixture of oil and water with desired oil volume fractions was placed in the glass reactor. When the temperature of 298.2 K had been attained, the agitator was started. After about 4 minutes stirring, the image of the stirred emulsion was taken with a digital camera (Fuji Fine Pix 6900 zoom). To increase the clearness of the taken photos, the oil phases in the present study were colored by using the dye Sudan I (Sigma-Aldrich) with a concentration of 0.1 kg m^{-3} in oils. The taken photos showed that the

appearances of O/W emulsions (up to 60% n-dodecane) looked always brighter than those of W/O emulsions (above 65% n-dodecane). Figure 5.13 shows the different appearances between emulsions of 60% n-dodecane and 65% n-dodecane, respectively. This observation method suggested the phase inversion to be in the range 60-65% of n-dodecane volume fraction. The result was in good agreement with the one measured by electrical conductivity method (cf. Chapter 6 for more details).

(A) (B)

FIGURE 5.13: Different appearances between O/W and W/O stirred emulsions of n-dodecane (A): Emulsion at 60% n-dodecane (O/W); (B): Emulsion at 65% n-dodecane (W/O).

Unfortunately, this observation method was not successful for emulsions of n-heptane and n-hexadecane, by which no clear distinction in appearances between O/W and W/O stirred emulsions could be visualized.

- **Observation of de-emulsification**

Noui-Medihi *et al.* (2004) suggested identifying the phase inversion by simply observing the de-emulsification after switching-off the agitator. These authors studied the phase inversion for water/Sell-Sol D70 system in a stirred reactor. Shortly after the agitator was switched-off, they observed that clouds of droplets could be seen above the interface for O/W emulsion type, and that clouds of droplets were conversely seen below the interface for W/O emulsion type.

In the present study, the above suggested observation method was used to identify the phase inversion for n-heptane emulsions, for which the electrical conductivity method failed (cf. Chapter 6). A mixture of n-heptane and water with desired n-heptane volume fractions was placed in the glass reactor. When the temperature of 298.2 K had been attained, the agitator was started. After about 4 minutes stirring, the agitator was stopped, and the de-emulsification processes was recorded with the video recording function of the digital camera "Fuji Fine Pix 6900 zoom". The photos reported in Chapter 6 were extracted from the recorded videos by using the video editing software "Windows Movie Maker".

5.6 Investigation into emulsion structure by endoscope technique

In the present study, the structure of W/O emulsion at 70% n-dodecane was studied with an endoscopic photographic technique (Maaß *et al.*, 2011, 2012). The endoscopic photo-probe with a diameter of 10 mm was installed at about half the emulsion height. After about 2.5 minutes stirring (1000 min^{-1}) at constant temperature (298.2 K), photos were taken at 10 fps (frames per second). The photos were then analyzed with the SOPAT-image analysis software to calculate the surface-to-volume mean diameter of the water droplets. The time frame of the photo probe test did not allow using also the other oils.

6 Results and discussion

6.1 Spreading coefficient

Tables 6.1 and 6.2 show the measured values of initial spreading coefficient (S) and equilibrium spreading coefficient (S^*), respectively. They have been calculated from the measured data of surface and interfacial tensions by using equations 2.23 and 2.24.

TABLE 6.1: Surface tensions (σ_{WG}, σ_{OG}) and interfacial tension (σ_{OW}) measured with pure oil and water phases at 298.2 K, and calculated values of the initial spreading coefficient S

Oil	σ_{WG}	σ_{OG}	σ_{OW}	S
		$mN\ m^{-1}$		
n-Heptane	72.0	19.8	40.8	+11.4
n-Dodecane	72.0	24.7	41.4	+5.9
n-Hexadecane	72.0	26.8	42.9	+2.3

TABLE 6.2: Surface tensions (σ^*_{WG}, σ^*_{OG}) and interfacial tension (σ^*_{OW}) measured with mutually saturated oil and water phases at 298.2 K, and calculated values of the equilibrium spreading coefficient S^*

Oil	σ^*_{WG}	σ^*_{OG}	σ^*_{OW}	S^*
		$mN\ m^{-1}$		
n-Heptane	71.8	19.8	40.2	+11.8
n-Dodecane	68.2	24.6	41.6	+2.0
n-Hexadecane	71.2	26.7	42.3	+2.2

Interestingly, quite different from the literature data listed in Table 2.4, all three oils have positive values of spreading coefficient but the value for n-heptane is noticeably higher than those for n-dodecane and n-hexadecane, regardless of the spreading coefficient type (S or S^*).

The considerable differences between the measured and the literature results might be due to the fact that the oils were used as purchased without further purification prior to measurements (cf. Section 5.4). However, the apparently inconsistent results reported in the literature (cf. Table 2.4) are still not understandable due to lack of information on purification and treatment procedures of

the liquids. As mentioned earlier in Chapter 2, in most practical applications the phases are mutually saturated; therefore the equilibrium spreading coefficient (S^*) will be used throughout the following sections to discuss the effects of different oils (n-heptane, n-dodecane and n-hexadecane) on the mass transfer characteristics.

6.2 Emulsion phase inversion

The electrical conductivity of the stirred emulsions against the oil volume fraction is shown in Figure 6.1.

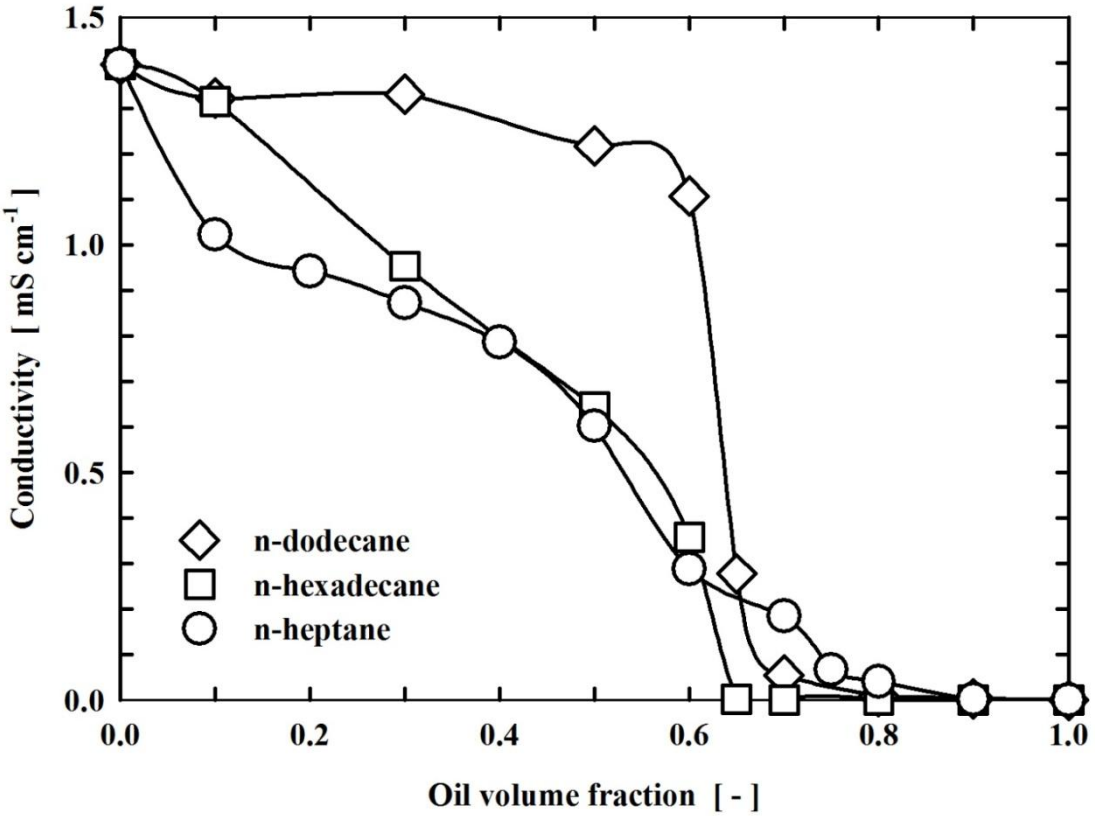

FIGURE 6.1: Conductivity of stirred emulsions.

From 60% to 65% oil volume fraction, a sudden decrease in conductivity to almost zero is found for both n-dodecane and n-hexadecane. This proves that the phase inversion from O/W to W/O occurs between 60% and 65% oil volume fraction for both n-dodecane and n-hexadecane. It can be seen that there is very good agreement between the phase inversion identification results obtained with the conductivity method and the visual observation of stirred emulsions for the case of n-dodecane emulsions (cf. Figure 5.13).

In the case of n-heptane emulsions, the conductivity decreases more gradually and comes close to zero only at oil fractions above 80%. The largest step-change in Figure 6.1 is from 50% to 60% oil volume fraction but, overall, the conductivity method is not successful in the identification of the phase inversion point of n-heptane emulsions.

Noui-Medihi *et al.* (2004) suggested identifying the phase inversion by simply observing the de-emulsification after switching-off the agitator. Shortly after stopping the agitation of n-heptane emulsions, large water drops accumulated above the interface up to 50% oil fraction whereas no drops could be seen above 60% volume fraction. Figure 6.2 is the photo of an emulsion with 50% n-heptane 2.06 s after stopping agitation. Figure 6.3 shows an image of a 60% n-heptane emulsion 1.72 s after switching off the agitator. Based on the de-emulsification observation method, the phase inversion of n-heptane emulsions would occur between 50% and 60% oil volume fraction.

FIGURE 6.2: Image of O/W emulsion of n-heptane 2.06 s after switching off the agitator (Φ_{oil} = 50%; the arrow indicates the interface).

FIGURE 6.3: Image of W/O emulsion of n-heptane 1.72 s after switching off the agitator (Φ_{oil} = 60%; the arrow indicates the interface).

6.3 Gas solubility in emulsions

From the total pressure decrease, ΔP (cf. Section 5.3), the overall gas solubility in the emulsions at a partial pressure of 101325 Pa can be calculated using equation 3.11. The solubility data of the two studied gases (O_2 and CO_2) in aqueous emulsions of n-heptane, n-dodecane and n-hexadecane are reported below.

6.3.1 Solubility of O_2 in emulsions

Figure 6.4 presents the effect of oil volume fraction on the oxygen solubility. Quite expectedly, the oxygen solubility in the emulsions increases linearly with oil volume fraction. This means that the O_2 solubility in emulsions can be simply estimated from the solubilities in the individual pure liquids. As can be seen from Figure 6.4 the oxygen solubility decreases with increasing chain length of the n-alkanes. The relative O_2 solubility, $m_{R\,(O_2)}$, (i.e. oxygen solubility in the pure oil compared to pure water) is 11.1, 7.7, and 6.5 for n-heptane, n-dodecane, and n-hexadecane, respectively.

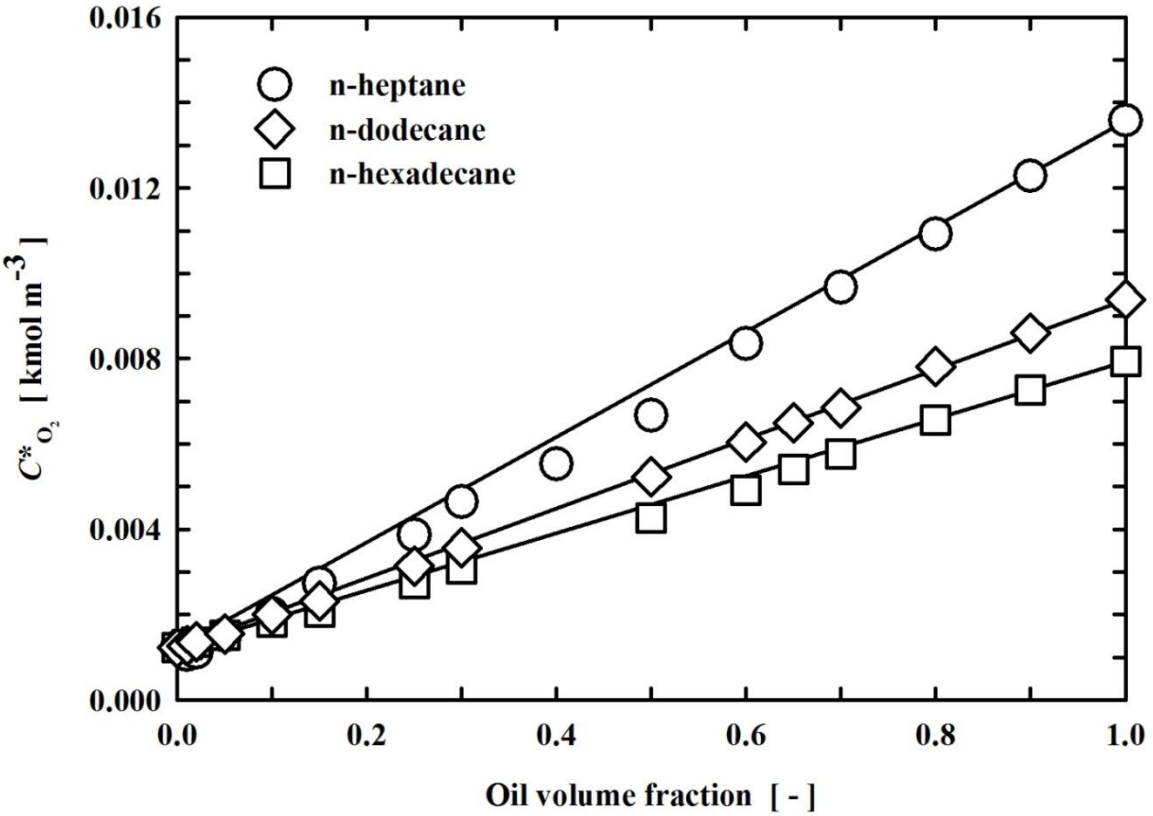

FIGURE 6.4**:** Effect of oil volume fraction on O_2 solubility at a partial pressure of 101325 Pa (solid lines: linear interpolation of the measured pure phase solubilities).

6.3.2 Solubility of CO_2 in emulsions

The effect of oil volume fraction on the CO_2 solubility is shown in Figure 6.5. Similar to the results observed with oxygen, the CO_2 solubility in the emulsions increases almost linearly with the oil volume fraction for n-hexadecane and n-dodecane emulsions. In n-heptane emulsions, the CO_2 solubility values are low as compared to linear interpolation of the measured pure phase solubilities, especially for the n-heptane volume fractions up to 30%. The relative CO_2 solubility, $m_{R\ (CO_2)}$, (i.e. CO_2 solubility in the pure oil compared to pure water) is 2.1, 1.7, and 1.5 for n-heptane, n-dodecane, and n-hexadecane, respectively.

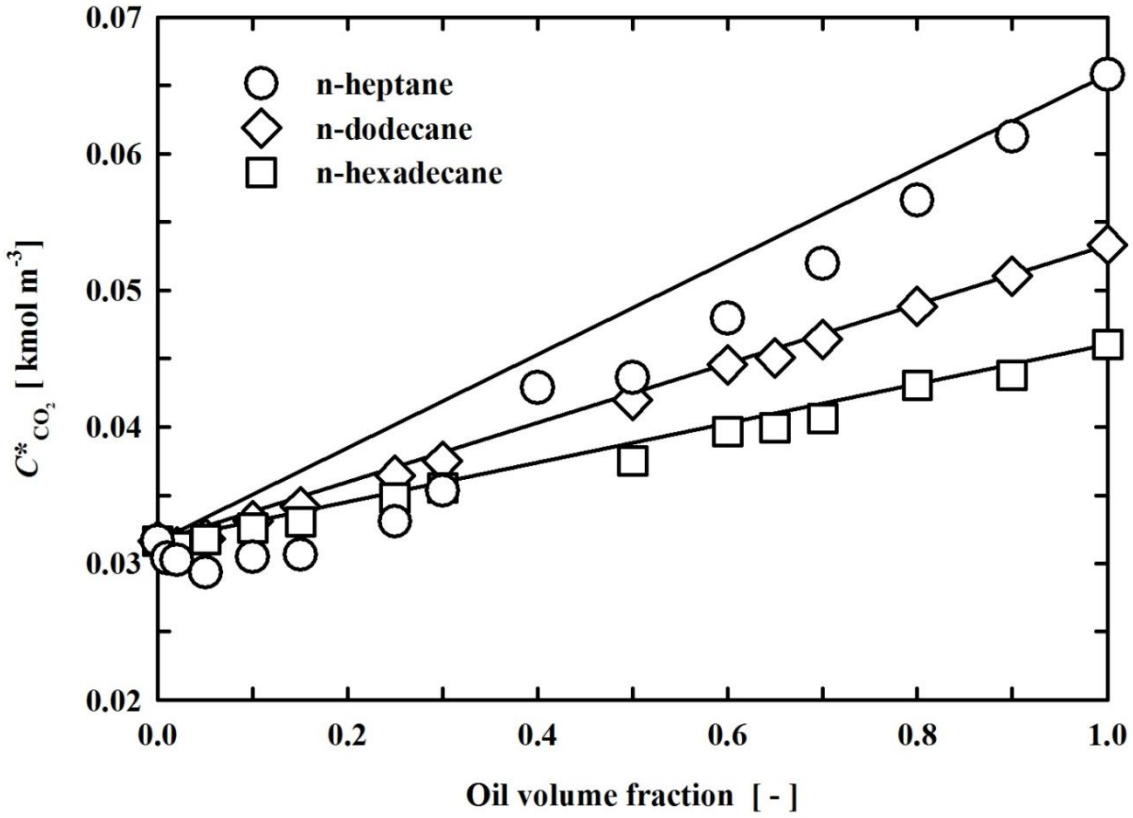

FIGURE 6.5: Effect of oil volume fraction on CO_2 solubility at a partial pressure of 101325 Pa (solid lines: linear interpolation of the measured pure phase solubilities).

6.4 Mass transfer of CO_2 into emulsions

6.4.1 Effect of oil volume fraction on k_La

In Figures 6.6-6.8, the effects of oil volume fraction on the volumetric mass transfer coefficient k_La are presented for the three oils studied.

The O/W emulsions of both n-dodecane and n-hexadecane show similar trends (cf. Figures 6.6 and 6.7): with increasing oil volume fraction, k_La first increases to a maximum at 2% (by +70% for n-dodecane and by +77% for n-hexadecane), then decreases towards the phase inversion region.

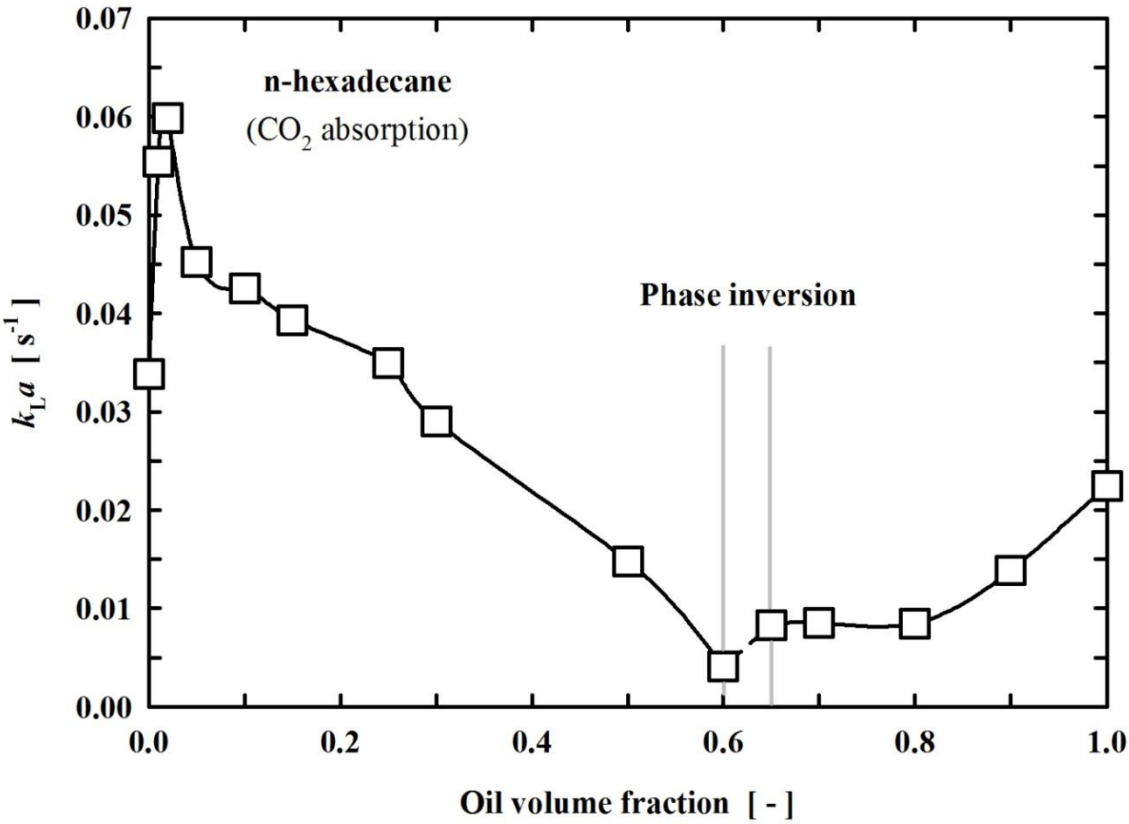

FIGURE 6.6: Effect of n-hexadecane volume fraction on k_La for CO_2 absorption.

The increase in k_La at low oil concentrations (1-2%) was also observed for oxygen absorption by several authors. Da Silva *et al.* (2006 b) reported that 1% n-hexadecane or n-dodecane increased k_La in a stirred tank by factors of 1.68 and 1.36, respectively; Kundu *et al.* (2003) concluded that addition of 1% n-dodecane or n-heptane could enhance oxygen transfer in a bubble column up to fourfold; Jia *et al.* (1999) also found a four-fold increase by 2% soybean oil in an air-lift reactor.

According to Clarke and Correia (2008), hydrocarbons tend to decrease the surface tension of the water phase, resulting in smaller bubble size, thus higher interfacial area (a), and hence higher k_La. However, as can be seen from Tables 6.1 and 6.2, the surface tension of water (72.0 mN m^{-1}) and that of water saturated with n-heptane (71.8 mN m^{-1}) or n-hexadecane (71.2 mN m^{-1}) were practically the same; only n-dodecane slightly reduced the surface tension (68.2 mN m^{-1}). This means that the 'surface tension effect' is negligible in the present study. As proposed by Bruining *et al.* (1986) and Cents *et al.* (2001), an additional transport mechanism, the so called "shuttle" mechanism (cf. Chapter 2) by very small oil droplets at low oil concentrations might be responsible for the maximum in k_La at 2% n-dodecane or n-hexadecane. Small oil droplets might

enter the mass transfer film, absorb CO_2, and then return to the bulk liquid where they discharge the absorbed CO_2.

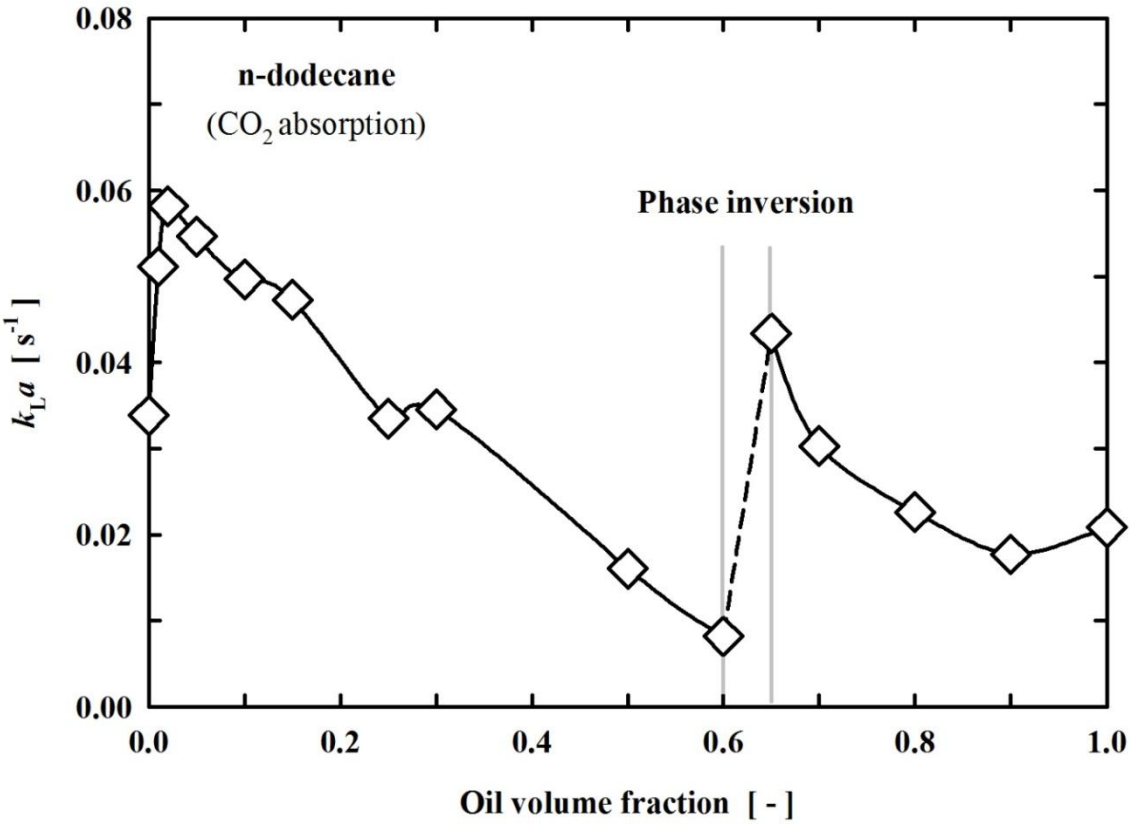

FIGURE 6.7: Effect of n-dodecane volume fraction on k_La for CO_2 absorption.

After the maximum, strong decrease in k_La is quite expected due to the increase in emulsion viscosity promoting gas bubble coalescence. The increase in O/W emulsion viscosity with increasing oil volume fraction for aqueous emulsions of n-dodecane and n-hexadecane has been illustrated in Figure 4.5.

The O/W emulsions of n-heptane behave more complicated with increasing oil fraction (Figure 6.8): k_La first increases up to 25% oil fraction, then decreases to lower value at 40% oil fraction, and increases again towards the phase inversion region. Note that all n-heptane emulsions show higher volumetric mass transfer coefficients than pure water. The highest k_La is observed at the phase inversion region (50% n-heptane). Here the k_La-value is enhanced by the factor of 5.24 compared to pure water.

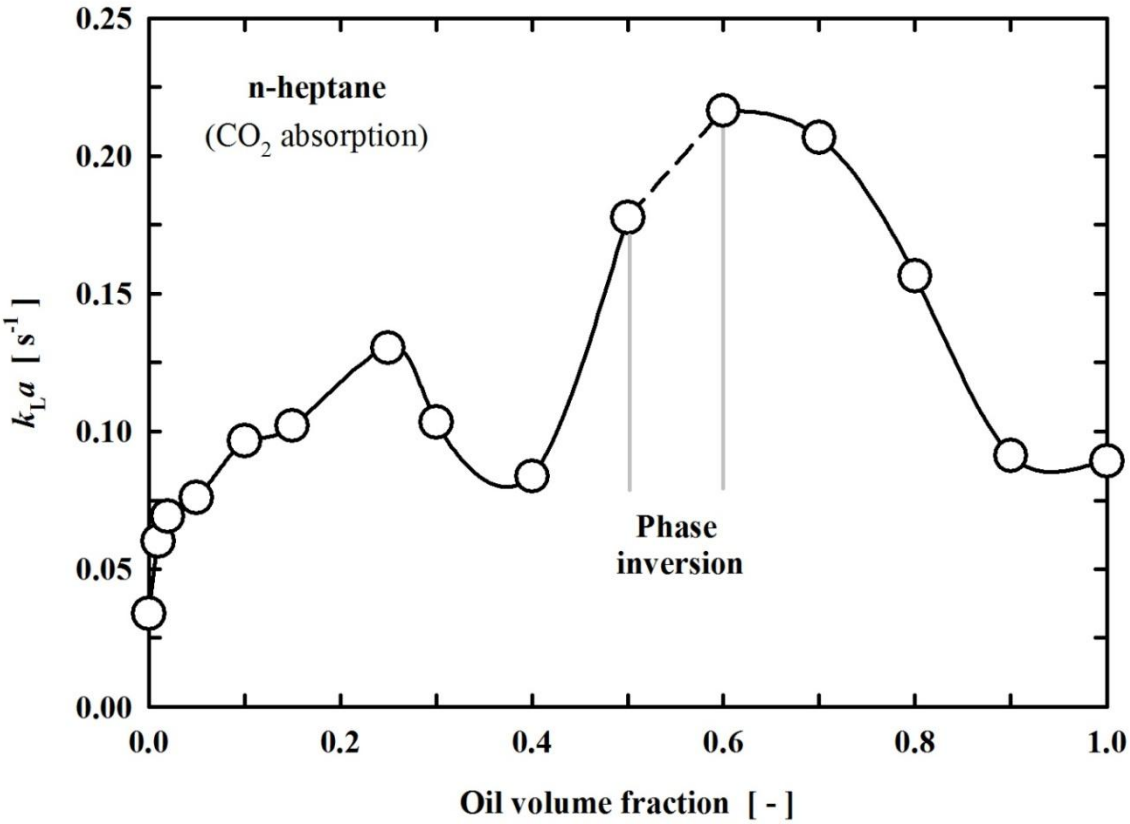

FIGURE 6.8: Effect of n-heptane volume fraction on k_La for CO_2 absorption.

The increase in k_La by +280% at 25% n-heptane fraction can probably be explained by the "bubble covering" mechanism proposed by Rols *et al.* (1991) (cf. Chapter 2 for more details). This mechanism is linked to the spreading coefficient. Pinho and Alves (2010) recently concluded that there is direct contact between gas and oil when the spreading coefficient is positive. As can be seen from Table 6.2, the high positive spreading coefficient for n-heptane (S^*= +11.8) might enable n-heptane to spread as a film on the CO_2 bubbles. As a bubble rises and finally breaks at the top surface, small CO_2-rich droplets may leave the oil film and release CO_2 to the water phase. It should be noted, however, that the solubilities of CO_2 in water and oil are more similar than those of oxygen (e.g. in n-heptane emulsions: $m_{R\ (O_2)}$ = 11.1, whereas $m_{R\ (CO_2)}$ = 2.1) and the effect should be small for the present results on CO_2.

In W/O emulsions of n-hexadecane (cf. Figure 6.6), from 100% oil volume fraction down to the phase inversion region, k_La monotonously decreases with increasing dispersed water fraction. This trend is expected based on the increase in viscosity of the W/O emulsions with increasing water content (Ngan *et al.*, 2009). The increase in W/O emulsion viscosity with increasing water

content has been illustrated in Figures 4.4 and 4.5 for emulsions of all three studied oils. Very surprisingly, for both n-heptane and n-dodecane, from 100% oil volume fraction down to the phase inversion region, $k_L a$ does not decrease, but rather increases substantially. The maximum increase in $k_L a$ compared to pure oil is found at the phase inversion region where it is +107% for n-dodecane and even +143% for n-heptane. More extensive repetitions than usual have verified these results. In addition, an attempt to study the W/O emulsion structure with an endoscopic photographic technique did not give a clue for explaining these surprising trends (cf. Section 5.6). A typical photo taken at 70% n-dodecane volume fraction is shown in Figure 6.9. In this W/O emulsion, the water drops have a surface-to-volume mean diameter of 1.16 mm (standard deviation: 0.15 mm; count: 1142 droplets). There exists no special structure like double emulsions (O/W/O) discussed earlier in Chapter 4. (It should be noted that the dispersed gas bubbles were larger than the water droplets and, therefore, appeared on photos only occasionally).

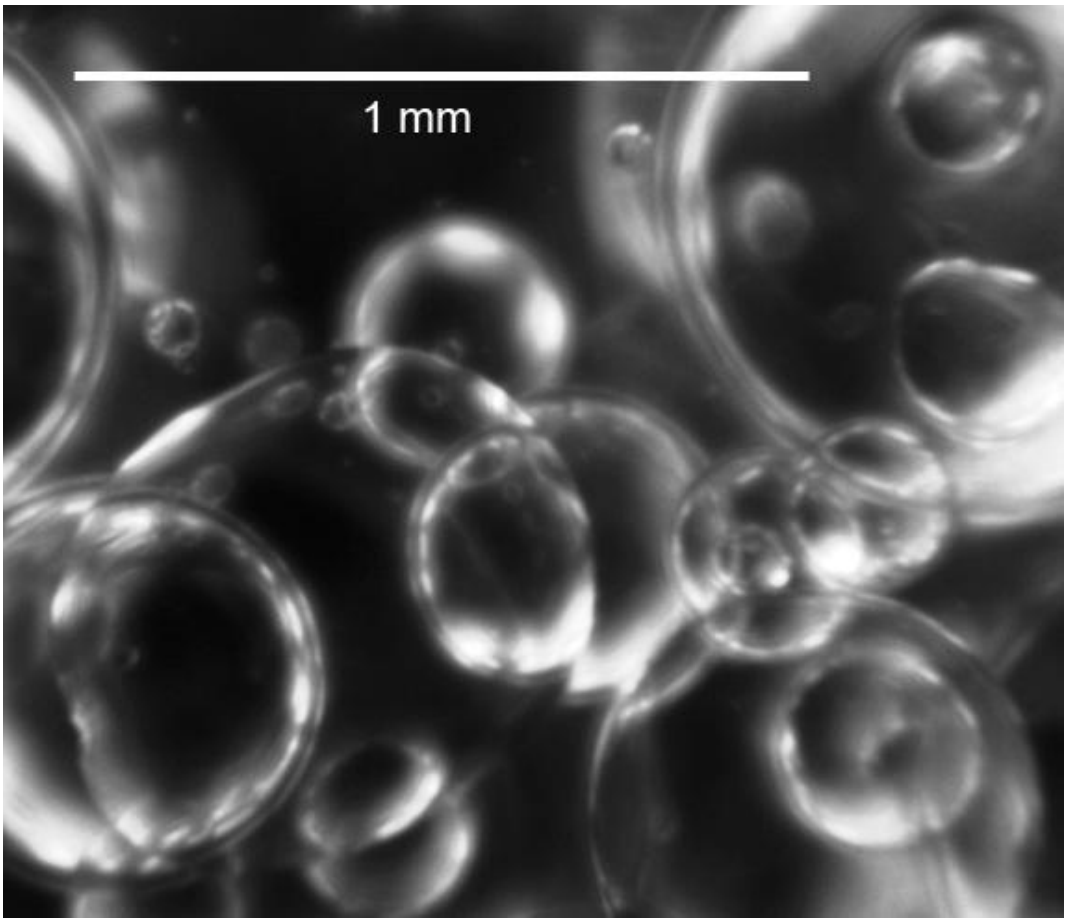

FIGURE 6.9: Photo of W/O emulsion at 70% n-dodecane taken with the SOPAT endoscope (SOPATec, Berlin, Germany).

6.4.2 Effect of oil volume fraction on enhancement factor *E*

Figures 6.10 and 6.11 present the effect of oil volume fraction on the enhancement factor *E* evaluated using equation 3.12.

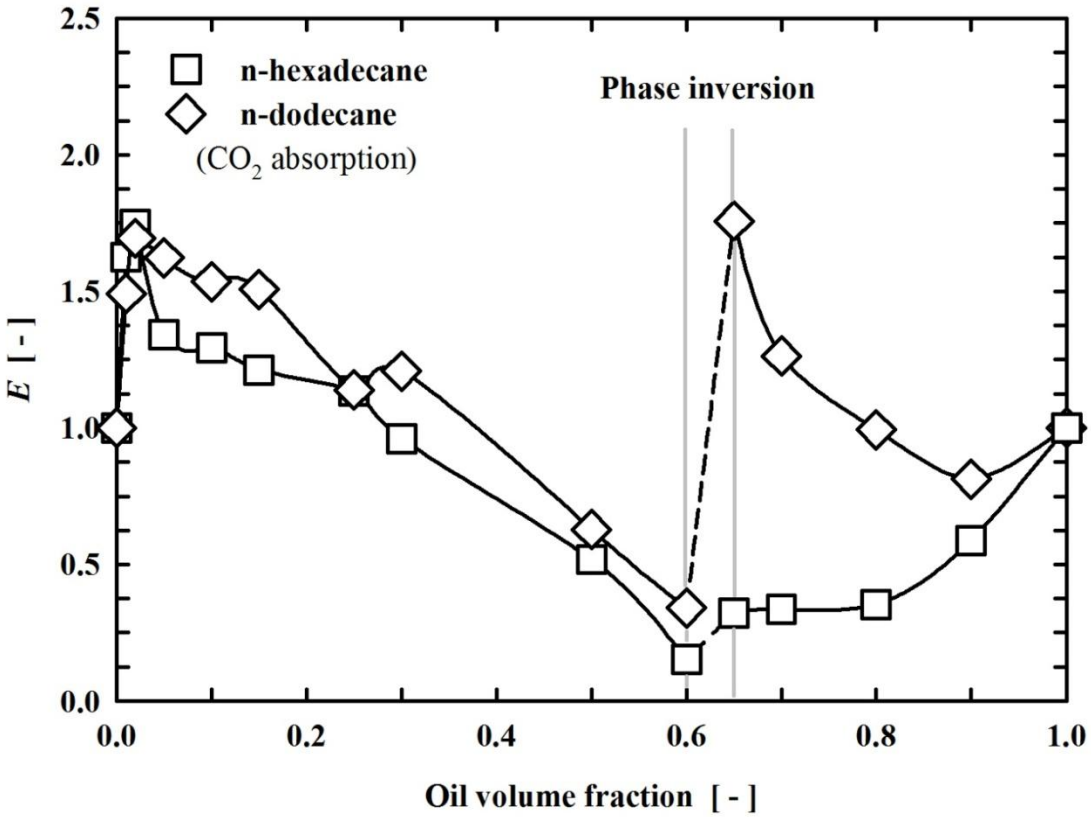

FIGURE 6.10: Variation of the mass transfer enhancement factor *E* for CO_2 with the n-dodecane and the n-hexadecane volume fraction.

It can be seen from these figures that, with increasing oil volume fraction, the trends in *E* are similar to those in $k_L a$ as reported above in Figures 6.6-6.8, for all three oils studied. This is mainly due to the fact that the solubilities of CO_2 in water and oil do not differ much ($m_{R\ (CO_2)}$ = 2.1, 1.7, and 1.5 for n-heptane, n-dodecane, and n-hexadecane, respectively).

With increasing oil volume faction towards the phase inversion region (up to 60%), the O/W emulsions of both n-dodecane and n-hexadecane show maxima in factor *E* at 2% oil volume fraction. The mass transfer rate is enhanced by factor of 1.69 and 1.75 for n-dodecane and n-hexadecane, respectively (cf. Figure 6.10). These maxima result from the corresponding maxima in $k_L a$ at these low oil volume fractions. After the maxima, the *E*-values decrease with increasing

oil volume fraction due to the decrease in k_La-values. However, it should be mentioned that some mass transfer enhancement is still observed up to about 30% n-dodecane or 25% n-hexadecane, respectively.

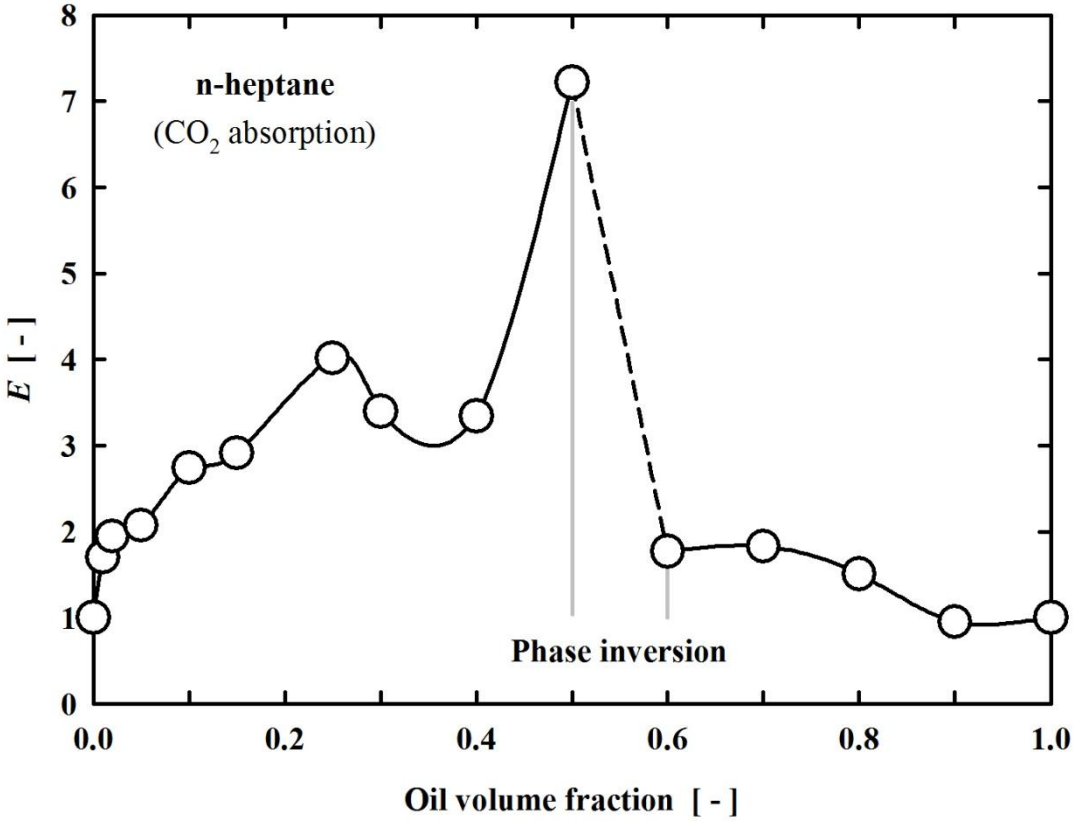

FIGURE 6.11: Variation of the mass transfer enhancement factor E for CO_2 with the n-heptane volume fraction.

In the case of O/W emulsions of n-heptane (cf. Figure 6.11), as the oil volume fraction is increased towards the phase inversion region (up to 50%), high mass transfer enhancement is always observed. This might be explained by the "bubble-covering" mechanism leading to higher k_La than pure water. The maximal mass transfer enhancement is observed at the phase inversion region (50% n-heptane) where E = 7.22. As discussed above in Subsection 6.4.1, at this n-heptane volume fraction, the k_La-value is enhanced by the factor of 5.24. This reveals that the increase in driving force (i.e. increase in CO_2 solubility) contributes only slightly to the total enhancement of the CO_2 absorption rate.

In W/O emulsions of all three oils, the trends in E with increasing dispersed water content (from 100% oil volume fraction down to the phase inversion region) are found to be similar to those in

k_La. Compared to pure oils, E is surprisingly increased for both n-dodecane and n-heptane whereas E is monotonously decreased for n-hexadecane. The maximum mass transfer enhancement factors are observed at the phase inversion regions for both n-heptane (E = 1.77 at 60% n-heptane) and n-dodecane (E = 1.76 at 65% n-dodecane).

6.5 Mass transfer of O_2 into emulsions

6.5.1 Effect of oil volume fraction on k_La

The volumetric mass transfer coefficients k_La in O/W emulsions of n-dodecane and n-hexadecane show similar trends (Figures 6.12 and 6.13): as the oil volume fraction increases, k_La first increases to a maximum at a small oil volume fraction and then decreases towards the phase inversion region. The increase in k_La at 1% n-dodecane and at 2% n-hexadecane is by +44% and +26%, respectively. An increase in k_La at low oil concentrations (1-2%) was previously also observed for oxygen by several authors (cf. Subsection 6.4.1).

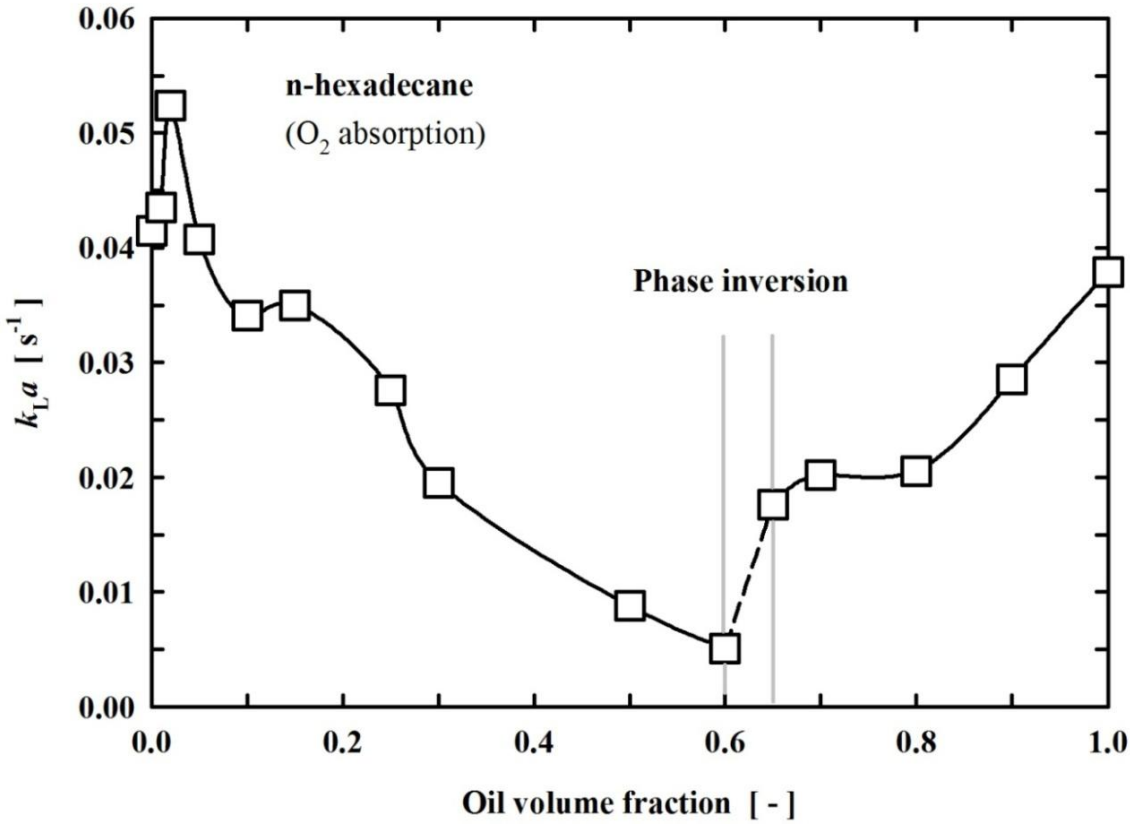

FIGURE 6.12: Effect of n-hexadecane volume fraction on k_La for O_2 absorption.

As discussed above in Subsection 6.4.1 for CO_2 absorption, the "surface tension effect" which would result in higher k_La compared to pure water is negligible for the systems studied. Therefore, the so called "shuttle" mechanism proposed by Bruining *et al*. (1986) and Cents *et al.* (2001) is likely to be responsible for the maximum in k_La at low oil concentrations (1-2% n-dodecane and n-hexadecane). Small oil droplets with higher solubility for oxygen might enter the water film at the G/L interface, absorb oxygen, and then return to the bulk water phase where the absorbed oxygen is discharged. After the maximum, the strong decrease of k_La with increasing oil volume fraction up to 60% is quite expected due to the increase of the emulsion viscosity (cf. Figure 4.5).

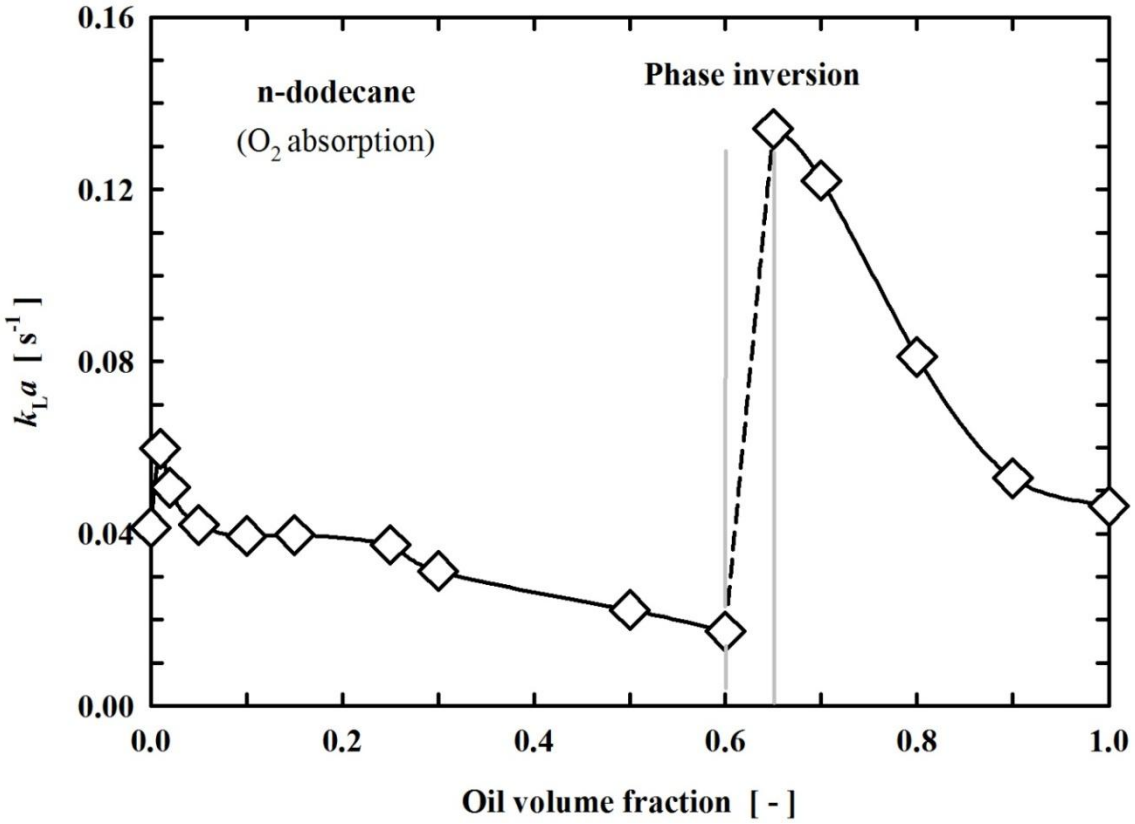

FIGURE 6.13: Effect of n-dodecane volume fraction on k_La for O_2 absorption.

The O/W emulsions of n-heptane show quite different trends with increasing oil fraction (Figure 6.14): k_La strongly increases up to 15% oil fraction and then again from 25% oil towards the phase inversion region. All n-heptane emulsions have higher volumetric mass transfer coefficients than pure water. The high k_La at 15% n-heptane volume fraction (+336% as compared to water) can probably be explained by the "bubble-covering" mechanism proposed by Rols *et al.* (1991). The considerably high spreading coefficient of n-heptane (cf. Table 6.2) might

enable n-heptane to spread as a film on the oxygen bubbles. When a bubble finally breaks at the top surface, small oxygen-rich droplets may leave the oil film and release oxygen to the water phase. It should be noted that n-heptane has the highest oxygen solubility of the three alkanes used and the k_La value in pure n-heptane is remarkably higher than that in pure water (+358%), whereas the k_La values in pure n-dodecane and in pure n-hexadecane are similar to the one in pure water. This means that if dodecane or n-hexadecane could also spread as a thin film on the oxygen bubbles, the mechanism would be less effective.

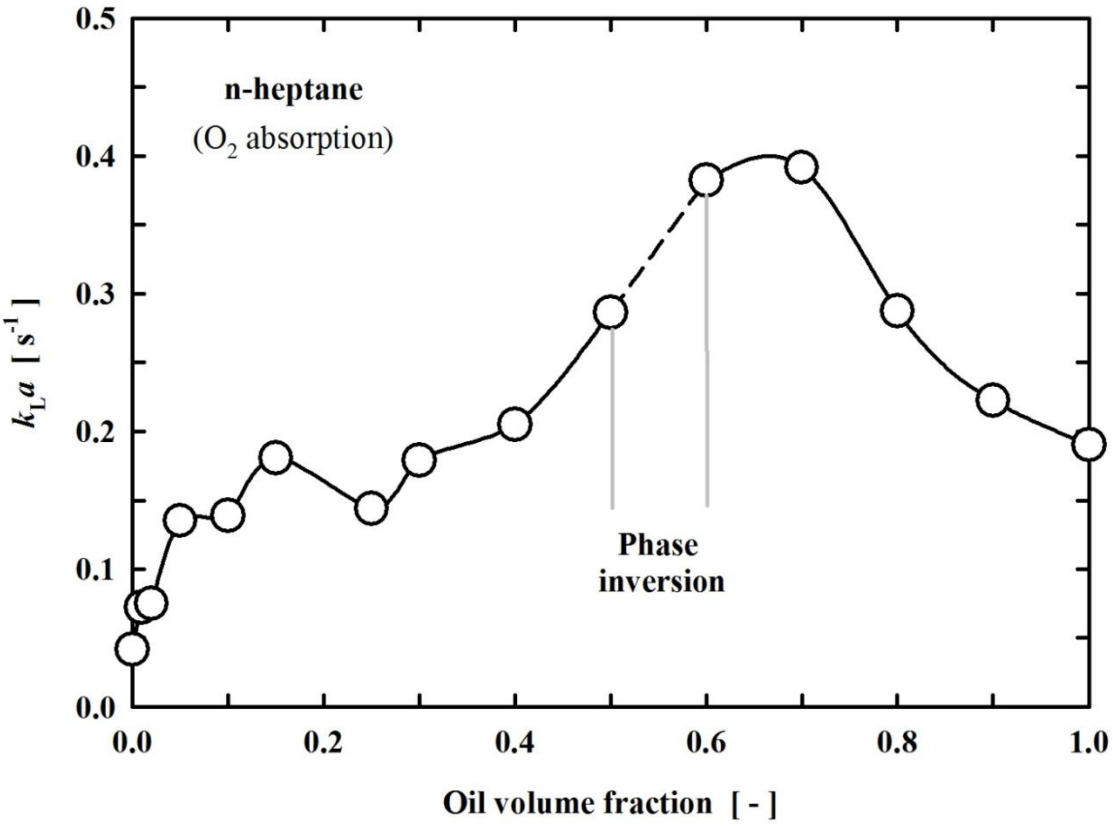

FIGURE 6.14: Effect of n-heptane volume fraction on k_La for O_2 absorption.

The differences of the k_La values in the pure oils mainly result from the viscosities of only 0.39 mPa s for n-heptane and 1.38 mPa s and 3.03 mPa s for n-dodecane and n-hexadecane, respectively (cf. Table 5.1).

In W/O emulsions, from 100% n-hexadecane down to the phase inversion region, k_La monotonously decreases with increasing dispersed water fraction. This trend is expected due to the increase in viscosity of the W/O emulsions with increasing water content (Ngan *et al.*, 2009). Figures 4.4 and 4.5 show the variation of the estimated viscosity for all studied W/O emulsions.

Very surprisingly, for both n-heptane and n-dodecane, from 100% oil volume fraction down to the phase inversion region, k_La does not decrease but increases substantially! The maximum increase in k_La compared to the pure oil is found at the phase inversion region where it is +101% for n-heptane and even +189% for n-dodecane. (For n-dodecane the k_La jump at the phase-inversion point is by a factor of 7.8). More extensive repetitions than usual have verified these results. In addition, it should be mentioned once again that no double emulsion structure (O/W/O), considered as possible reason for these surprising observations, was detected by endoscopic photographic technique (cf. Figure 6.9). The reason for these surprising results is still not clear, but the observed results are obviously very valuable for some biotechnological processes, e.g., Xanthan production by aerobic fermentation in W/O emulsions (Schumpe *et al.*, 1991; Ju and Zhao, 1993; Kuttuva *et al.*, 2004).

6.5.2 Effect of oil volume fraction on enhancement factor *E*

Figures 6.15 and 6.16 present the effects of oil volume fraction on the mass transfer enhancement factor *E*.

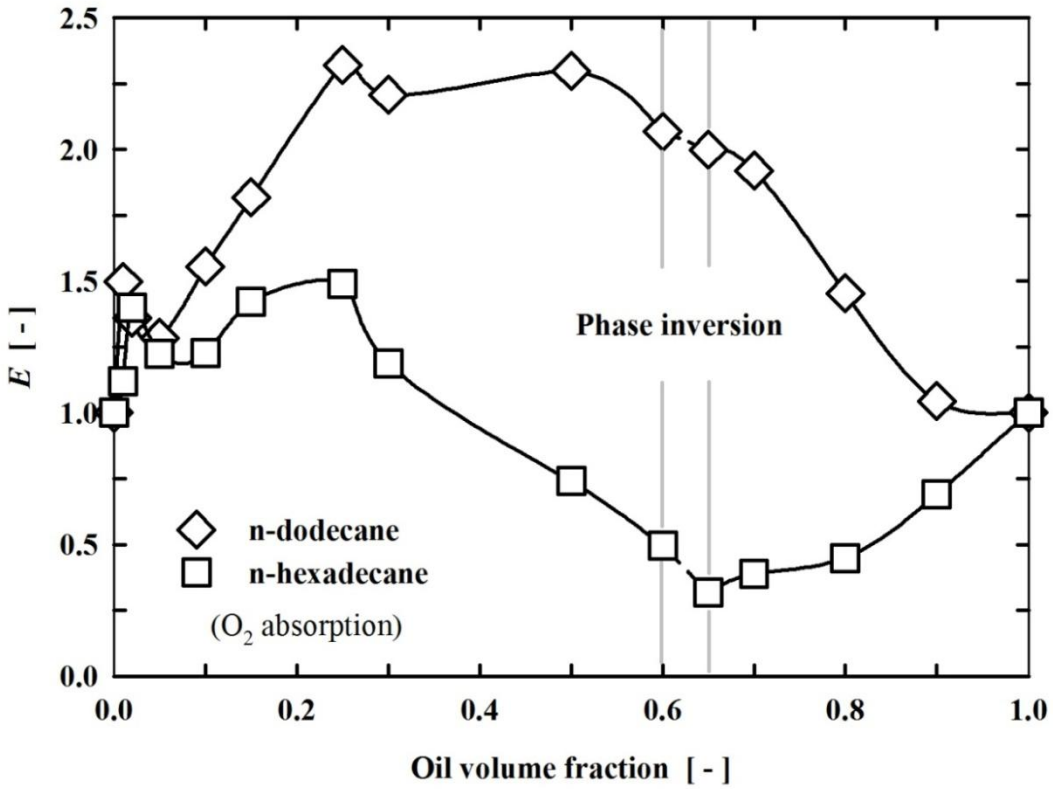

FIGURE 6.15: Variation of the mass transfer enhancement factor *E* for O_2 with the n-dodecane and the n-hexadecane volume fraction.

Somewhat different from the absorption of CO_2, in O/W emulsions of both n-dodecane and n-hexadecane, at 25% oil fraction maxima are observed. There the mass transfer rate is enhanced by a factor of 2.3 for n-dodecane and a factor of 1.5 for n-hexadecane. At further increase in the oil fraction towards the phase inversion region, the *E* value for n-dodecane decreases slightly but still shows mass transfer enhancement, whereas mass transfer retardation is observed above 40% n-hexadecane. This difference reflects the stronger k_La decrease in the case of n-hexadecane (cf. Figure 6.12) as compared to n-dodecane (cf. Figure 6.13). For example, at 60% oil fraction k_La is lower than in water by a factor of 0.12 for n-hexadecane and for n-dodecane the factor is only 0.42. In addition, the relative oxygen solubility $m_{R\ (O_2)}$ is 6.5 for n-hexadecane whereas $m_{R\ (O_2)}$ = 7.7 for n-dodecane. Both aspects lead to higher *E* values for n-dodecane emulsions (cf. Figure 6.15).

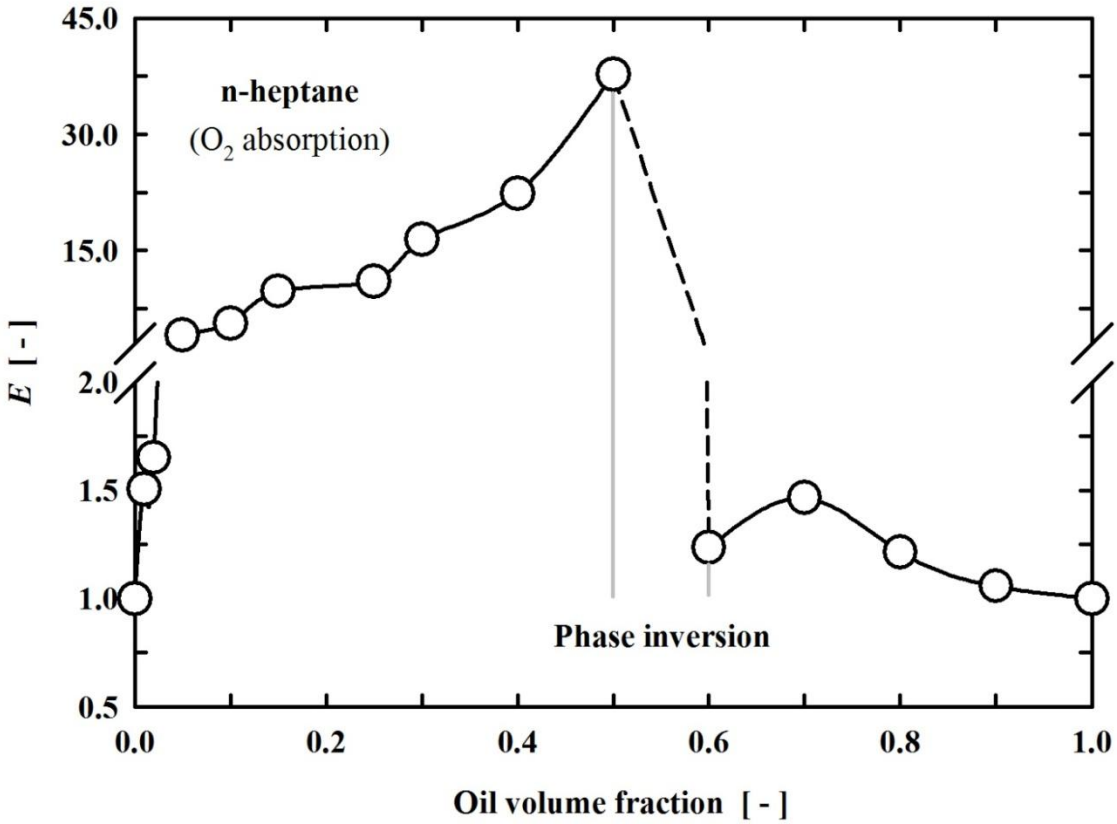

FIGURE 6.16: Variation of the mass transfer enhancement factor *E* for O_2 with the n-heptane volume fraction.

In the case of O/W emulsions of n-heptane (cf. Figure 6.16), as the oil volume fraction is increased towards the phase inversion region, high mass transfer enhancement is always observed. This reflects the high k_La values (cf. Figure 6.14) as well as the high relative oxygen

solubility ($m_{R\,(O_2)}$ = 11.1). Mass transfer is enhanced by E = 37.7 at the heptane volume fraction of 50%. The trend of E in O/W emulsions of n-heptane might be explained by the "bubble-covering" mechanism.

In W/O emulsions of all three oils, the trends of E with dispersed water volume fraction are similar to those of k_La discussed above. Compared to pure oil, the mass transfer rate is enhanced at the phase inversion by E = 2.0 (increase by +100%) and E = 1.24 (increase by +24%) for n-dodecane and n-heptane, respectively (cf. Figures 6.15 and 6.16).

6.6 Effect of gas nature on k_La

Figures 6.17-6.19 depict the effect of gas nature on k_La values as a function of oil volume fraction for aqueous emulsions of n-dodecane, n-heptane, and n-hexadecane respectively.

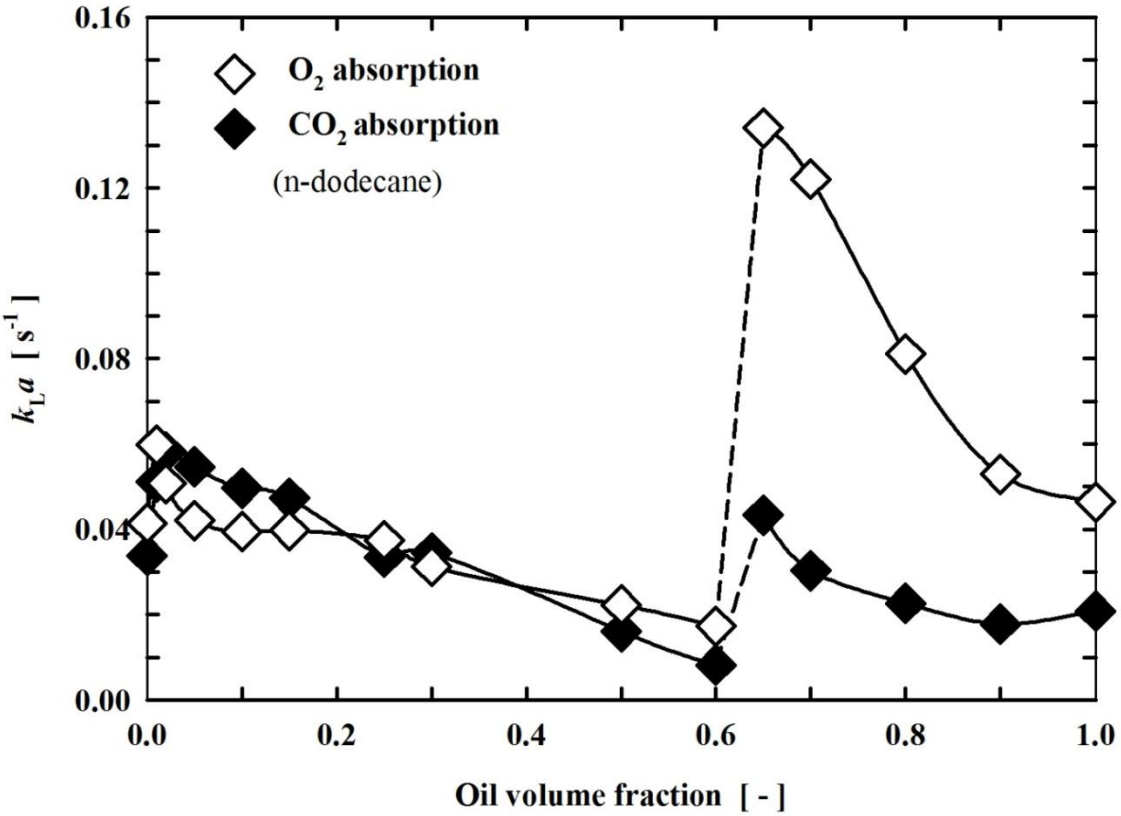

FIGURE 6.17: Effect of gas nature on k_La in n-dodecane emulsions (dashed lines indicate the phase inversion region).

Both gases (O_2 and CO_2) show similar trends in the variation of k_La with increasing oil volume fraction. This behavior might be due to the fact that the relative gas diffusivities (i.e. gas diffusivity in the pure oil compared to pure water) are practically the same for both studied gases (cf. Table 6.3). The major difference between the gases is that the CO_2 solubilities in the oils are only slightly higher than in pure water, i.e. the relative CO_2 solubility, $m_{R\,(CO_2),}$ is low.

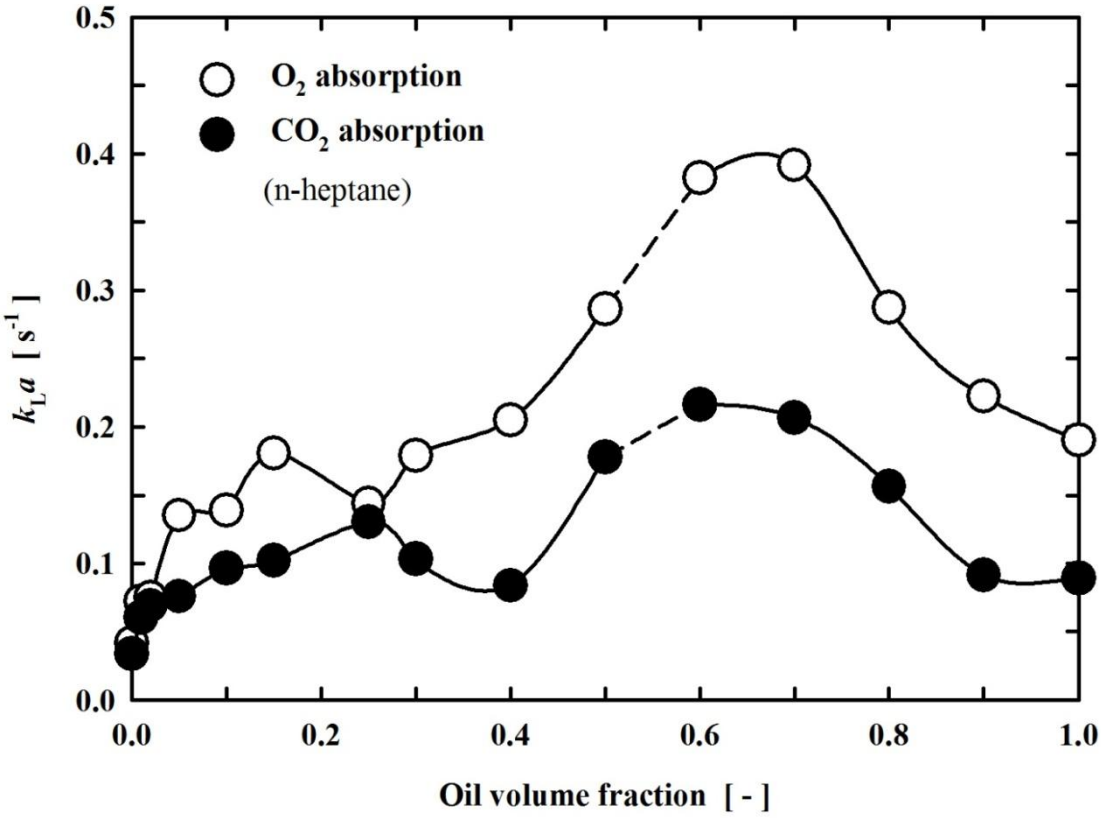

FIGURE 6.18: Effect of gas nature on k_La in n-heptane emulsions (dashed lines indicate the phase inversion region).

In the pure liquids, k_La values are lower for CO_2 than for O_2. This effect is much more pronounced in pure oils than in pure water, for instance, $k_La_{\,(O_2)}$ is higher than $k_La_{\,(CO_2)}$ by +22% in pure water, but by even +122% in pure n-heptane (cf. Figure 6.18).

In order to explain such a behavior, the diffusivities (diffusion coefficients) of both gases in all pure liquids at 298 K were estimated using equation 6.1 proposed by Díaz *et al*. (1987), and the values are given in Table 6.3.

$$(D_{AB})_{T=298\,K} = 6.02 \times 10^{-5} \left(\frac{\tilde{V}_B^{\,0.36}}{\mu_B^{\,0.61} \cdot \tilde{V}_A^{\,0.64}} \right) \tag{6.1}$$

TABLE 6.3: Estimated diffusivities of O_2 and CO_2 in studied liquids at 298 K

Gas	$D_{AB}\,x10^9$ [m^2/s]			
	Water	*n-Heptane*	*n-Dodecane*	*n-Hexadecane*
CO_2	1.83	6.62	3.68	2.52
O_2	2.2	7.97	4.43	3.03

From the values shown in Table 6.3, it is clear that O_2 has higher diffusivity than CO_2 in all studied liquids by about +20%. Compared to CO_2, the 22% higher k_La for O_2 in pure water could be explained well by higher liquid-side mass transfer coefficient k_L according to the two-film theory (cf. Chapter 2).

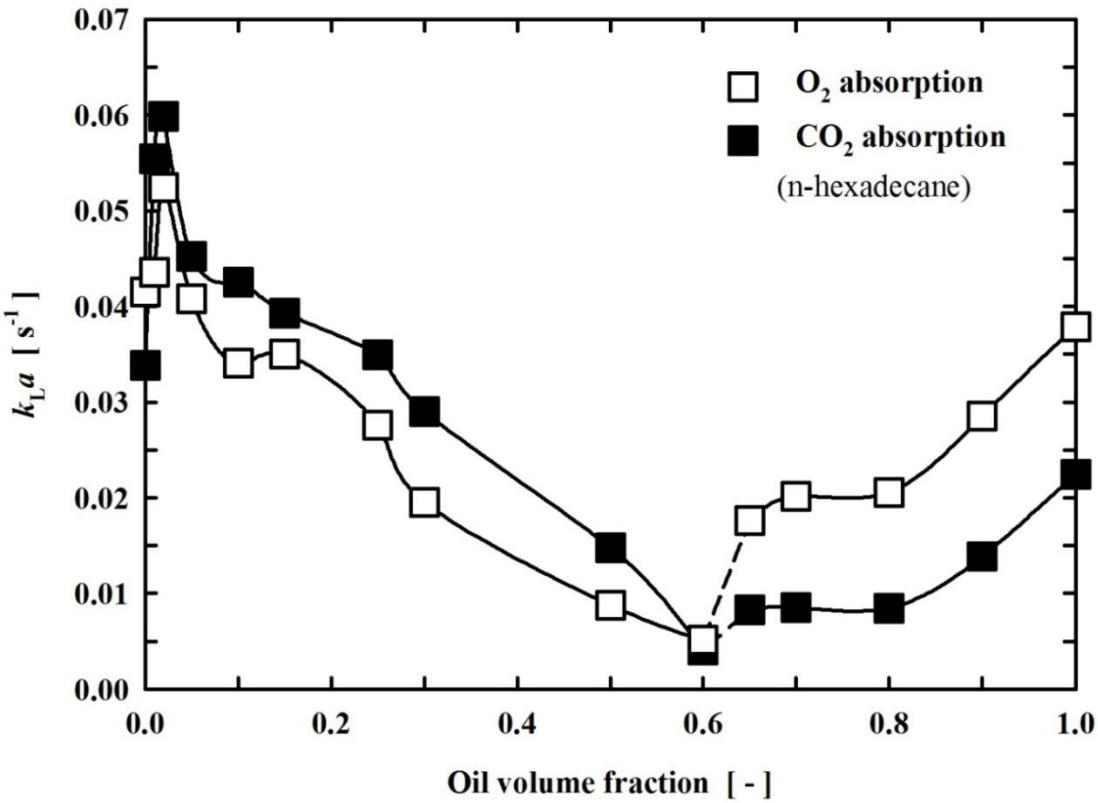

FIGURE 6.19: Effect of gas nature on k_La in n-hexadecane emulsions (dashed lines indicate the phase inversion region).

However, the diffusivities cannot reasonably explain the considerably higher k_La for oxygen in the pure oils (e.g., by +122% in pure n-heptane). This means that, in pure oils, k_La is essentially controlled by the gas-liquid interfacial area (a) rather than by the liquid-side mass transfer coefficient k_L of the gases. A possible explanation for the large difference in k_La between two gases could be that small bubbles containing CO_2 with higher solubility deplete much faster in oils than those containing O_2 resulting in a lower "effective" gas-liquid interfacial area with CO_2 (Cents *et al.* (2005).

6.7 Oxygen-water mass transfer studied by fluorescence technique

Figure 6.20 presents the effect of oil volume fraction on gas-water volumetric mass transfer coefficient $(k_La)_{GW}$ for oxygen absorption into aqueous emulsions of n-dodecane and n-hexadecane. In addition, a comparison with the gas-emulsion volumetric mass transfer coefficient k_La which has been discussed above is shown in Figures 6.21 and 6.22.

Although a quantitative comparison between k_La and $(k_La)_{GW}$ is not possible due to some small modifications of the measurement system of $(k_La)_{GW}$ as mentioned in Subsection 5.3.1, Figures 6.21 and 6.22 show that the variation of k_La and $(k_La)_{GW}$ with the oil volume fraction follows the same trend for both n-dodecane and n-hexadecane. This fact indicates that water and oil are essentially in instantaneous equilibrium during absorption.

It can be seen from Figure 6.20 that, as the oil volume faction increases from 0% to 60% (O/W emulsion region), the similar trend in $(k_La)_{GW}$ is observed for emulsions of both n-dodecane and n-hexadecane: $(k_La)_{GW}$ first increases to maxima at 1% oil volume fraction, then decreases towards the phase inversion region. Therefore, the oxygen transport to the water phase seems to follow a similar mechanism in O/W emulsions of both oils.

Compared to pure water, these maxima show an increase in $(k_La)_{GW}$ by +27% and +11% for n-dodecane and n-hexadecane, respectively. The increase in $(k_La)_{GW}$ at low oil volume fraction (3%) was also observed by Cesário *et al.* (1996) who measured $(k_La)_{GW}$ using a steady state method for the absorption of toluene in the aqueous emulsions of a perfluorocarbon (FC 40). However, as the FC 40 volume fraction further increased up to 15%, $(k_La)_{GW}$ did not decrease (as observed in the present study) but monotonously increased.

At 60% oil volume fraction, $(k_La)_{GW}$ is decreased by -78% and -88% for n-dodecane and n-hexadecane, respectively. The strong decrease of $(k_La)_{GW}$ towards the phase inversion region

implies that the oxygen transport to the water phase is not likely to follow the unique serial mechanism: gas → oil → water. If this mechanism would occur, $(k_La)_{GW}$ should expectedly increase with oil volume fraction since more gas-oil and oil-water contacts are produced.

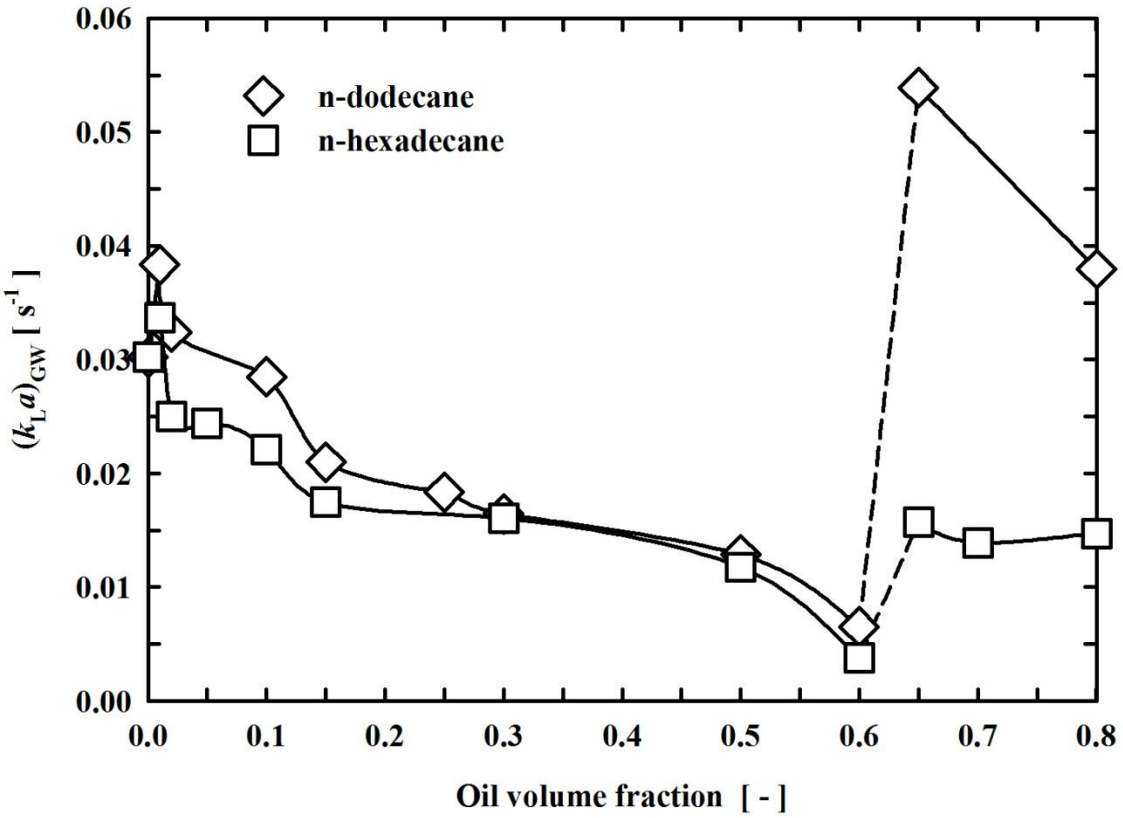

FIGURE 6.20: Effect of oil volume fraction on $(k_La)_{GW}$ for oxygen absorption into aqueous emulsions of n-dodecane and n-hexadecane (dashed lines indicate the phase inversion region).

In addition, it should be mentioned that both n-dodecane and n-hexadecane have positive values of spreading coefficient, but these values are rather low (cf. Table 6.2). This means that spreading of these oils on the oxygen bubble (i.e. direct gas-oil contact) is not likely. This conclusion is obviously supported by the strong decrease of both k_La and $(k_La)_{GW}$ with increasing oil volume fraction toward the phase inversion region. It appears that the oxygen transport mechanism to O/W emulsions of n-dodecane and n-hexadecane follows the unique serial transport: gas → water → oil.

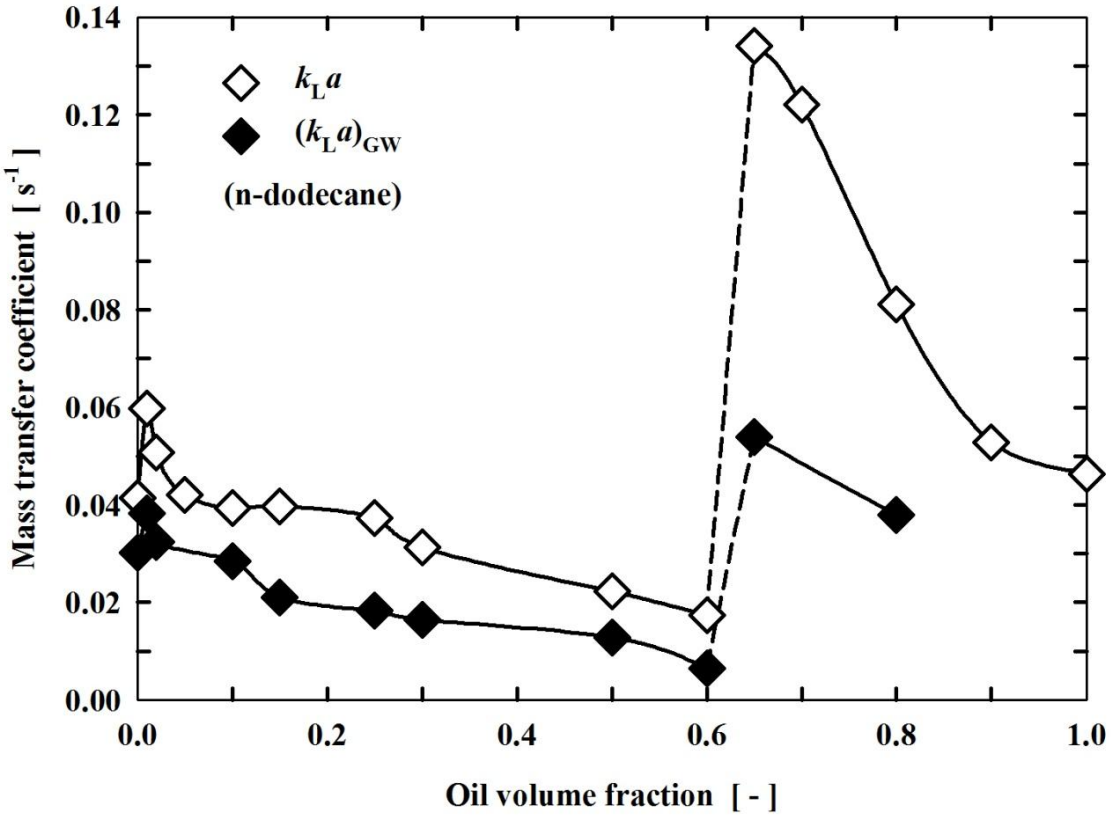

FIGURE 6.21: Comparison between k_La and $(k_La)_{GW}$ for oxygen absorption into aqueous emulsions of n-dodecane (dashed lines indicate the phase inversion region).

With further increasing the oil volume fraction up to 80%, $(k_La)_{GW}$ increases strongly for n-dodecane to a maximum at 65%, and then decreases, whereas only slight increase in $(k_La)_{GW}$ is observed for n-hexadecane. At 65% of n-dodecane, the $(k_La)_{GW}$ is increased by 78% as compared to pure water. The quite different trend in $(k_La)_{GW}$ between W/O emulsions of n-dodecane and n-hexadecane might indicate the difference in oxygen transport mechanisms between them.

Linek and Benes (1976) concluded from their study that in W/O emulsions there is a parallel transfer of gas to both the continuous oil phase and the dispersed aqueous phase, irrespective of the sign of the spreading coefficient. Due to the lower viscosity of n-dodecane, the motion of the water droplets could be more flexible in n-dodecane than in n-hexadecane, which favors the gas-water direct contacts in W/O emulsions of n-dodecane. The more direct water-gas contacts are produced, the more easily the water droplets get saturated resulting in higher $(k_La)_{GW}$ values. Therefore, the parallel transport mechanism (gas → oil and gas → water, simultaneously) would be possible in W/O emulsions of n-dodecane, whereas the unique serial transport mechanism (gas

→ oil → water) would be ascribed to W/O emulsions of n-hexadecane. However, more evident experimental results are still needed to prove these proposed oxygen transport mechanisms.

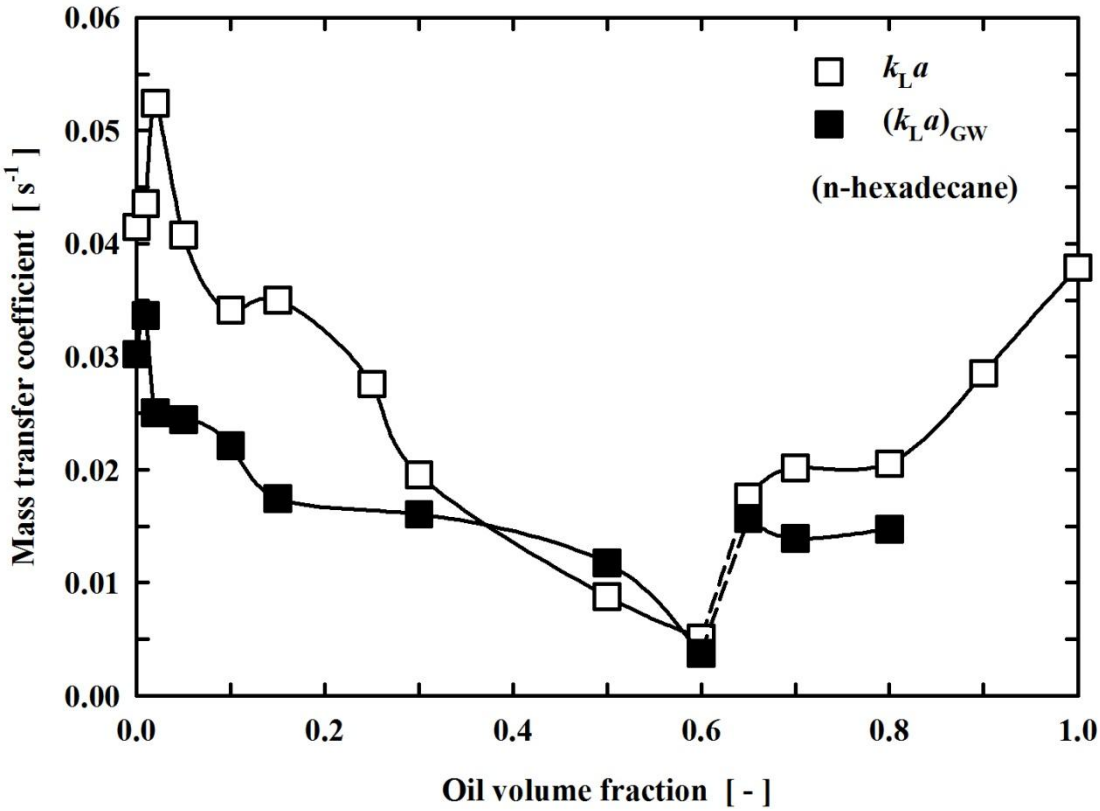

FIGURE 6.22: Comparison between k_La and $(k_La)_{GW}$ for oxygen absorption into aqueous emulsions of n-hexadecane (dashed lines indicate the phase inversion region).

7 Conclusions

Absorption of oxygen (O_2) and carbon dioxide (CO_2) into aqueous emulsions of n-heptane, n-dodecane, and n-hexadecane has been studied in the full range of oil volume fraction (0-100%) by means of dynamic pressure technique. The developed pseudo-homogenous mass transfer model allows evaluating the volumetric mass transfer coefficient $k_L a$ for the whole range of oil volume fraction. In addition, a fluorescence technique with an oxygen-sensitive fluorophore, soluble only in the water phase, has been applied to measure the oxygen-water volumetric mass transfer coefficient $(k_L a)_{GW}$ in emulsions of n-dodecane and n-hexadecane. The following conclusions can be drawn:

- **Spreading coefficient**

All three oils have positive values of initial and equilibrium spreading coefficient but the values for n-heptane are noticeably higher than those for n-dodecane and n-hexadecane. In most practical applications, the phases are mutually saturated. Therefore, using the "equilibrium" spreading coefficients (S^*) is highly recommended.

- **Emulsion phase inversion**

The electrical conductivity method can be used to identify the phase inversion region for n-dodecane and n-hexadecane (60%-65%), but fails for n-heptane. Observation of de-emulsification suggests the inversion region to be 50%-60% n-heptane.

- **Gas solubility in emulsions**

The solubility of both gases increases linearly with oil volume fraction, and can be well calculated from the solubilities in the pure liquids. Only for the CO2-water-*n*-heptane system, the values are low as compared to linear interpolation of the measured pure phase solubilities.

- **Absorption into O/W emulsions**

Both O_2 and CO_2 have similar trends in the variation of $k_L a$ with increasing dispersed oil volume fraction. A $k_L a$ maximum at low oil volume fractions (1-2%) is found for both O/W emulsions of n-dodecane and n-hexadecane; the "shuttle" mechanism might be responsible for this maximum.

Differently, O/W emulsions of n-heptane always show higher k_La than pure water; this can be explained by a bubble covering mechanism enabled by its high positive spreading coefficient.

With increasing oil volume fraction, the driving force (i.e. the gas solubility) increases strongly for O_2, but only marginally for CO_2. For O_2 absorption in O/W emulsions of both n-dodecane and n-hexadecane, maxima in enhancement factor E are observed at 25% oil fraction; there the mass transfer rate is enhanced by a factor of 2.3 for n-dodecane and a factor of 1.5 for n-hexadecane. Much stronger mass transfer enhancement never reported before is observed at 50% n-heptane, where the oxygen mass transfer rate is enhanced even by the factor of 38 as compared to pure water.

For O_2 absorption into O/W emulsions of n-dodecane and n-hexadecane, both $(k_La)_{GW}$ and k_La have the same trend with increasing oil volume fraction, which indicates that water and oil phases are essentially in instantaneous equilibrium during absorption. The low values of spreading coefficient for n-dodecane and n-hexadecane and the strong decrease of both $(k_La)_{GW}$ and k_La towards the phase inversion region suggest the serial transport mechanism: gas → water → oil.

- **Absorption into W/O emulsions**

Both O_2 and CO_2 have similar trends in the variation of k_La with increasing dispersed water volume fraction. In W/O emulsions of n-hexadecane, k_La decreases monotonously as expected due to increasing viscosity. Very surprisingly, in W/O emulsions of both n-heptane and n-dodecane, k_La increases towards a maximum at the phase inversion region. The reason for this surprising trend is not clear.

Further studies concentrating on measurements of gas bubble size and dispersed droplet size may help to find an explanation. Anyhow, these new findings could be valuable for some industrial applications of gas absorption into W/O emulsions, e.g., Xanthan production by aerobic fermentation in W/O emulsions and CO_2 capture by chemical absorption in W/O emulsions.

8 References

Albal, R. S., Y. T. Shah, A. Schumpe and N. L. Carr, "Mass transfer in multiphase agitated contactors", *Chem. Eng. Jour.*, **27**, 61-80 (1983).

Badocco, D., A. Mondin and P. Pastore, "Determination of thermodynamic parameters from light intensity signals obtained from oxygen optical sensors", *Sensors and Actuators B*, **163**, 165-170 (2012).

Badocco, D., A. Mondin and P. Pastore, "Rationalization of the behaviour of a bi-label oxygen optical sensor", *Sensors and Actuators B*, **158**, 54-61 (2011).

Baerns, M., H. Hofmann and A. Renken, *Chemische Reaktionstechnik - Lehrbuch der Technischen Chemie*, Band 1, Georg Thieme Verlag, Stuttgart, Germany (1987).

Boltes, K., A. Caro, P. Leton, A. Rodriguez, and E. Garcia-Calvo, "Gas-liquid mass transfer in oil-water emulsions with an airlift bio-reactor", *Chem. Eng. Proc.*, **47**, 2408-2412 (2008).

Brilman D. W. F., W. P. M. van Swaajj and G. F. Versteeg, "A one-dimensional instationary heterogeneous mass transfer model for gas absorption in multiphase systems", *Chem. Eng. Proc.*, **37**, 471-488 (1998).

Brilman, D. W. F., M. J. V. Goldschmidt, G. F. Versteeg and W. P. M. van Swaaij, "Heterogeneous mass transfer models for gas absorption in multiphase systems", *Chem. Eng. Sci.*, **55**, 2793-2812 (2000).

Brilman, D. W. F., *Mass transfer and chemical reaction in gas-liquid-liquid systems*, *PhD thesis*, University of Twente, The Netherlands (1998).

Bruining, W. J., G. E. H. Joosten and A. A. C. M. Beenackers, "Enhancement of gas-liquid mass transfer by a dispersed second liquid phase", *Chem. Eng. Sci.*, **41**, 1873-1877 (1986).

Cents, A. H. G., D. J. W. Jansen, D. W. F. Brilman and G. F. Versteeg, "Influence of small amounts of additives on gas hold-up, bubble size, and interfacial area", *Ind. Eng. Chem. Res.*, **44**, 4863-4870 (2005).

Cents, A. H. G., D. W. F. Brilman and G. F. Versteeg, "Gas absorption in an agitated gas-liquid-liquid system", *Chem. Eng. Sci.*, **56**, 1075-1083 (2001).

Cents, A. H. G., D. W. F. Brilman and G. F. Versteeg, "Mass transfer effects in the biphasic hydroformylation of propylene", *Ind. Eng. Chem. Res.*, **43**, 7465-7475 (2004).

Cents, A. H. G., F. T. de Bruijn, D. W. F. Brilman and G. F. Versteeg, "Validation of the Danckwerts-plot technique by simultaneous chemical absorption of CO_2 and physical desorption of O_2", *Chem. Eng. Sci.*, **60**, 5809-5818 (2005).

Cesário, M. T., H. L. De Wit, J. Tramper and H. H. Beeftink, "Dispersed organic solvent to enhance the overall gas/water mass transfer coefficient of apolar compounds in the biological waste-gas treatment. Modelling and evaluation", *Biotechnol. Prog.*, **13**, 399-407 (1997).

Cesário, M. T., H. L. de Wit, J. Tramper and H. H. Beeftink, "New technique for k_La measurement between gas and water in aerated solvent-in-water dispersions", *Biotechnology Techniques*, **10**, 195-198 (1996).

Cesário, M. T., M. Turtoi, S. F. M. Sewalt, J. Tramper and H. H. Beeftink, "Enhancement of the gas-to-water ethene transfer coefficient by a dispersed water-immiscible solvent: effect of the cells", *Appl. Mirobiol. Biotechnol.*, **46**, 497-502 (1996).

Chaudhuri, S. K. and M. M. Sharma, "Absorption of carbonyl sulfide in aqueous alkaline solutions: new strategies", *Ind. Eng. Chem. Res.*, **28**, 870-873 (1989).

Clarke, K. G. and L. D. C. Correia, "Oxygen transfer in hydrocarbon-aqueous dispersions and its applicability to alkane bioprocesses: a review", *Biochem. Eng. J.*, **39**, 405-429 (2008).

Comte, A., *Entwicklung und Einsatz eines kompakten faseroptischen Sauerstoffmessgeräts*, Diplomathesis, University Hannover (1993).

Cornils, B., "Bulk and fine chemicals via aqueous biphasic catalysis", *Journal of Molecular Catalysis A: Chemical*, **143**, 1-10 (1999).

Coulson, J. M., J. F. Richardson, J. R. Backhurst and J. H. Harker, *Chemical Engineering*, Volume 1, 4 st Edition, Pergamon Press, Oxford, England (1990).

Da Silva, T. L., A. Mendes, R. L. Mendes, V. Calado, S. S. Alves, J. M. T. Vasconcelos and A. Reis, "Effect of n-dodecane on Crypthecodinium cohnii fermentations and DHA production", *J. Ind. Microbio. Biotechnol.*, **33**, 408-416 (2006 a).

Da Silva, T. L., V. Calado, N. Silva, R. L. Mendes, S. S. Alves, J. M. T. Vasconcelos and A. Reis; "Effects of hydrocarbon additions on gas-liquid mass transfer coefficients in biphasic bioreactors", *Biotechnol. Bioprocess Eng.*, **11**, 245-250 (2006 b).

Danckwerts, P. V., "Significance of liquid-film coefficients in gas absorption", *Ind. Eng. Chem.* **43**, 1460-1467 (1951).

Das, T. R., A. Bandopadhyay, R. Parthasarathy and R. Kumar, "Gas-liquid interfacial area in stirred vessels: the effect of an immiscible liquid phase", *Chem. Eng. Sci.*, **40**, 209-214 (1985).

Demas, J. N., B. A. DeGraff and W. Xu, "Modeling of luminescence quenching-based sensors: comparison of multisite and nonlinear gas solubility models", *Anal. Chem.*, **67**, 1377-1380 (1995).

Díaz, M., A. Vega and J. Coca, "Correlation for the estimation of gas-liquid diffusivity", *Chem. Eng. Comm.*, **52**, 271-281 (1987).

Dumont, E. and H. Delmas, "Mass transfer enhancement of gas absorption in oil-in-water systems: a review", *Chem. Eng. &Proc.*, **42**, 419-438 (2003).

Dumont, E., Y. Andres and P. Le Cloirec, "Effect of organic solvents on oxygen mass transfer in multiphase systems: Application to bioreactors in environmental protection", *Biochemical Eng. J.*, **30**, 245-252 (2006 a).

Dumont, E., Y. Andres and P. Le Cloirec, "Mass transfer coefficients of styrene and oxygen into silicone oil emulsions in a bubble reactor", *Chem. Eng. Sci.*, **61**, 5612-5619 (2006 b).

Einstein, A., "Eine neue bestimmung der moleküle dimensionen", *Ann. Phys.*, **19**, 289-306 (1906).

Emig, G. and E. Klemm, *Technische Chemie - Einführung in die Chemische Reaktionstechnik*, Fünfte aktualisierte und ergänzte Auflage, Springer-Verlag, Berlin, Heidelberg, Germany (2005).

Fukui, S. and A. Tanaka, "Production of useful compounds from alkane media in Japan", *Adv. Biochem. Eng.*, **17**, 1-35 (1980).

Galaction, A. I., D. Cascaval, M. Tuernea and C. Oniscu, "Enhancement of oxygen mass transfer in stirred bioreactors using oxygen-vectors. 1. Simulated fermentation broths", *Bioprocess Biosyst. Eng.*, **26**, 231-238 (2004).

Galaction, A. I., D. Cascaval, M. Tuernea and E. Folescu, "Enhancement of oxygen mass transfer in stirred bioreactors using oxygen-vectors. 2. Propionibacterium shermanii broths", *Bioprocess Biosyst. Eng.*, **27**, 263-271 (2005).

Gómez-Díaz, D., N. Gomes, J. A. Teixeira and I. Belo, "Oxygen mass transfer to emulsions in a bubble column contactor", *Chem. Eng. Jour.*, **152**, 354-360 (2009).

Gouin, J. F., F. Baros, D. Birot and J. C. André, "A fibre-optic oxygen sensor for oceanography", *Sensors and Actuators B*, **38-39**, 401-406 (1997).

Grattoni, C., R. Moosai and R. A. Dawe, "Photographic observations showing spreading and non-spreading of oil on gas bubbles of relevance to gas flotation for oily wastewater cleanup", *Colloids and Surfaces A: Physicochem. Eng. Aspects*, **214**, 151-155 (2003).

Groeneweg, F., W. G. M. Agterof, P. Jaeger, J. J. M. Janssen, J. A. Wieringa and J. K. Klahn, "On the mechanism of the inversion of emulsions", *Chem. Eng. Res. Des. Trans. IChemE*, **76**, 55-63, (1998).

Guilinger, T. R., A. K. Grislingas and O. Erga, "Phase inversion behaviour of water-kerosene dispersions", *Ind. Eng. Chem. Res.*, **27**, 978-982 (1988).

Hartmann, P., M. J. P. Leiner and M. E. Lippitsch, "Response characteristics of luminescent oxygen sensors", *Sensors and Actuators B*, **29**, 251-257 (1995).

Hassan, I. T. M. and C. W. Robinson, "Oxygen transfer in mechanically agitated systems containing dispersed hydrocarbon", *Biotechnol. Bioeng.*, **19**, 661-682 (1977).

Haynes, W. M and D. R. Lide, *CRC Handbook of Chemistry and Physics*, 91st Edition, CRC Press: Boca Raton, Florida, USA (2010).

Higbie, R., "The rates of absorption of a pure gas into a still liquid during short periods of exposure", *Trans. Am. Inst. Chem. Eng.*, **31**, 365-389 (1935).

Ho, C. S., L. K. Ju and R. F. Baddour, "Enhancing penicillin fermentations by increased oxygen solubility through the addition of n-hexadecane", *Biotechnol. Bioeng.*, **36**, 1110-1118 (1990).

Hu, B., P. Angeli, O. K. Matar and G. F. Hewitt, "Prediction of phase inversion in agitated vessels using a two-region model", Chem. Eng. Sci., **60**, 3487-3495 (2005).

Jia, S., G. Chen, P. Kahar, D. B. Choi and M. Okabe, "Effect of soybean oil on oxygen transfer in the production of tetracycline with an airlift bioreactor", *J. Biosci. Bioeng.*, **87**, 825-827 (1999).

Jia, S., M. Wang, P. Kahar, Y. Park and M. Okabe, "Enhancement of yeast fermentation by addition of oxygen vectors in air-lift bioreactor", *J. Ferment. Bioeng.*, **2**, 176-178 (1997).

Jordan, U. and A. Schumpe, "The gas density effect on mass transfer in bubble columns with organic liquids", *Chem. Eng. Sci.*, **56**, 6267-6272 (2001).

Jordan, U., K. Terasaka, G. Kundu and A. Schumpe, "Stoffübergang in Druckblasensäulen mit organischen Flüssigkeiten", *Chem. Ing. Tech.*, **73**, 982-985 (2001).

Jordan, U., K. Terasaka, G. Kundu and A. Schumpe, "Stoffübergang in Druckblasensäulen mit organischen Flüssigkeiten", *Chem. Ing. Tech.*, **73**, 982-985 (2001).

Ju, L. -K. and S. Zhao, "Xanthan fermentations in water/oil dispersions", *Biotechnology techniques*, **7**, 463-468 (1993).

Ju, L. -K., J. F. Lee and W. B. Armiger, "Enhancing oxygen transfer in bioreactors by perfluorocarbon emulsions", *Biotechnol. Prog.*, **7**, 323-329 (1991).

Jungker, B. H., T. A. Hatton and D. I. C. Wang, "Oxygen transfer enhancement in aqueous/perfluorocarbon fementation systems: I. Experimental observations", *Biotechnol. Bioeng.*, **35**, 578-585 (1990).

Köneke, R., A. Comte, H. Jürgens, O. Kohls, H. Lam and T. Scheper, "Fiber optic oxygen sensors for use in biotechnology, environmental and food industries", *Chem. Eng. Technol.*, **21**, 666-671 (1999).

Kumar, S., "On phase inversion characteristics of stirred dispersions", *Chem. Eng. Sci.*, **51**, 831-834 (1996).

Kundu, A., E. Dumont, A. M. Duquenne and H. Delmas, "Mass transfer characteristics in gas-liquid-liquid system", *Ca. J. Chem. Eng.*, **81**, 640-646 (2003).

Kuttuva, S. G., A. S. Restrepo and L. K. Ju, "Evaluation of different organic phases for water-in-oil xanthan fermentation", *Appl. Microbiol. Biotechnol.*, **64**, 340-345 (2004).

Lakowicz, J. R., *Principles of Fluorescence Spectroscopy*, 3rd Edition, Springer, USA (2006).

Lekhal, A., R. V. Chaudhari, A. M. Wilhelm and H. Delmas, "Gas-liquid mass transfer in gas-liquid- liquid dispersions", *Chem. Eng. Sci.*, **52**, 4069-4077 (1997).

Lewis, W. K. and W. G. Whitman, "Principles of gas absorption", *Ind. Eng. Chem.*, **16**, 1215-1220 (1924).

Lide, D. R. and H. V. Kehiaian, *CRC Handbook of thermophysical and thermochemical data*, CRC Press: Boca Raton, Florida, USA (1994).

Lin, C., M. Zhou and C. J. Xu, "Axisymmetrical two-dimensional heterogeneous mass transfer model for the absorption of gas into liquid-liquid dispersions", *Chem. Eng. Sci.*, 54, 389-399 (1999).

Linek, V. and P. Benes, "A study of the mechanism of gas absorption into oil-water emulsions", *Chem. Eng. Sci.*, **31**, 1037-1046 (1976).

Little, R. J., G. F. Versteeg and W. P. M. Van Swaaij, "Physical absorption of CO2 and propene into toluene/water emulsions", *A. I. Ch. E. J.*, **40**, 1629-1638 (1994).

Liu, L., O. K. Matar, C. J. Lawrence and G. F. Hewitt, "Laser-induced fluorescence (LIF) studies of liquid-liquid flows; Part I: Flow structures and phase inversion", *Chem. Eng. Sci.*, **61**, 4007 – 4021 (2006).

Liu, L., O. K. Matar, E. S. P. de Ortiz and G. F. Hewitt, "Experimental investigation of phase inversion in a stirred vessel using LIF", *Chem. Eng. Sci.*, **60**, 85-94 (2005).

Maaß, S., J. Rojahn, R. Hänsch and M. Kraume, "Automated drop detection using image analysis for online particle size monitoring in multiphase systems," *Computers & Chemical Engineering*, **87**, 27-37 (2012).

Maaß, S., S. Wollny, A. Voigt and M. Kraume, "Experimental comparison of measurement techniques for drop size distributions in liquid/liquid dispersions," *Experiments in Fluids,* **50**, 259-269 (2011).

MacMillan, J. D. and D. I. C. Wang, "Mechanisms of oxygen transfer enhancement during submerged cultivation in perfluorochemical-in-water dispersions", *Ann. NY Acad. Sci.,* **589**, 283-300 (1990).

Mehra A., "Heterogeneous modeling of gas absorption in emulsions", *Ind. Eng. Chem. Res.,* **38**, 2460-2468 (1999).

Mehra, A. and M. M. Sharma, "Absorption with reaction in micro-emulsions: absorption of olefins", *Chem. Eng. Sci.,* **41**, 2455-2456 (1986).

Mehra, A. and M. M. Sharma, "Absorption with reaction: effect of emulsified second liquid phase", *Chem. Eng. Sci.,* **40**, 2382-2385 (1985).

Mehta, V. D. and M. M. Sharma, "Mass transfer in mechanically agitated gas-liquid contactors", *Chem. Eng. Sci.,* **26**, 461-479 (1971).

Mills, A., "Controlling the sensitivity of optical oxygen sensors", *Sensors and Actuators B,* **51**, 60-68 (1998).

Mills, A., "Optical Oxygen Sensors: Utilising the Luminescence of Platinum Metals Complexes", Platinum Metals Rev., **41**, 115-127 (1997).

Mortaheb, H. R., A. A. Nozaeim, M. Mafi and B. Mokhtarani, "Absorption of carbon dioxide in emulsions of aqueous monoethanolamine/diethanolamine solutions in kerosene/n-heptane", *Chem. Eng. Sci.,* **82**, 44-51 (2012).

Nagy, E., "Three-phase mass transfer: one-dimensional heterogeneous model", *Chem. Eng. Sci.,* **50**, 827-836 (1995).

Ngan, H. K., K. Ioannou, L. D. Rhyne, W. Wang and P. Angeli, "A methodology for predicting phase inversion during liquid-liquid dispersed pipeline flow", *Chem. Eng. Res. Des.*, **87**, 318-324 (2009).

Nielsen, D. R., A. J. Daugulis and P. J. McLellan, "A novel method of simulating oxygen mass transfer in two-phase partitioning bioreactors", *Biotechnol. Bioeng*., **83**, 735-742 (2003).

Nigam, K. D. P. and A. Shumpe, *Three-phase sparged reactors*, Gordon and Breach pulishers, The Netherlands (1996).

Noui-Mehidi, M. N., J. Wu and Y. Zhu; "A few new findings on phase inversion in a liquid/liquid system", *AIChE J.*, **50**, 3281-3283 (2004).

Oliveira, R. C. G., G. Gonzalez and J. F. Oliveira, "Interfacial studies on dissolved gas flotation of oil droplets for water purification", *Colloids and Surfaces A: Physicochem. Eng. Aspects*, **154**, 127-135 (1999).

Pacek, A. W., I. P. T. Moor and A. W. Nienow, "Video technique for measuring dynamics of liquid-liquid dispersion during phase inversion", *A.I.Ch.E. Journal*, **40**, 1940-1949 (1994).

Park, S. W., H. B. Cho, I. J. Sohn and H. Kumazawa, "CO_2 absorption into W/O emulsion with aqueous amine liquid droplets", *Sep. Sci. Tech.*, **37**, 639-661 (2002).

Pinho, H. J. O. and S. S. Alves, "Effect of spreading coefficient on gas-liquid mass transfer in gas-liquid-liquid dispersions in a stirred tank", *Chem. Eng. Commun.*, **197**, 1515-1526 (2010).

Rols, J. L., J. S. Conroret, C. Fonade and G. Goma, "Mechanism of enhanced oxygen transfer in fermentation using emulsified oxygen vectors", *Biotechnol. Bioeng.*, **35**, 427-435 (1990).

Rols, J. L., J. S. Conroret, C. Fonade and G. Goma, "Modeling of oxygen transfer in water through emulsified organic liquids", *Chem. Eng. Sci.*, **46**, 1869-1873 (1991).

Schumpe, A., S. Diedrichs, P. G. M. Hesselink, S. Nene and W. -D. Deckwer, "Xanthan production in emulsions", *Biochemical Engineering-Stuttgart* (Hrsg. M. Reuss, H. Chmiel, E. -D. Gilles und H. -J. Knackmuss), pp. 169-199, Gustav Fischer Verlag, Stuttgart (1991).

Shariati, F. P., B. Bonakdarpour and M. R. Mehrnia, "Hydrodynamics and oxygen transfer behaviour of water in diesel microemulsions in a draft tube airlift bioreactor", *Chem. Eng. Process.*, **46**, 334-342 (2007).

Taylor, R. and R. Krishna, *Multicomponent mass transfer*, John Wiley & Sons, New York, USA (1993).

Terasaka, K., D. Hullmann and A. Schumpe, "Mass transfer in bubble columns studied with an oxygen optode", *Chem. Eng. Sci.*, **53**, 3181-3184 (1998).

Toor, H. L. and J. M. Marchello, "Film-penetration model for mass and heat transfer", *A.I.Ch.E.J.*, **4**, 97-101 (1958).

Vaessen, G. E. J., M. Visschers and H. N. Stein, "Predicting Catastrophic Phase Inversion on the Basis of Droplet Coalescence Kinetics", *Langmuir*, **12**, 875-882 (1996).

Van Ede, C. J., R. Van Houten and A. A. C. M. Beenackers, "Enhancement of gas to water mass transfer rates by a dispersed organic phase", *Chem. Eng. Sci.*, **50**, 2911-2922 (1995).

Vermuelen, T., G. M. Williams and G. E. Langlois, "Interfacial area in liquid-liquid and gas-liquid agitation", *Chem. Eng. Prog.*, **51**, 85-94 (1955).

Wei, D. Z. and H. Liu, "Promotion of L-asparaginase production by using n-dodecane", B*iotechnology Techniques*, **12**, 129-131 (1998).

Xu, Xiao-Xuan, "Study on oil-water two-phase flow in horizontal pipelines", *Jour. Petrol. Sci. Eng.*, **59,** 43-58 (2007).

Yeo, L. Y., O. K. Matar, E. S. Perez de Ortiz and G. F. Hewitt, "Phase inversion and associated phenomena", *Multiphase Sci. Technol.*, **12**, 51-116 (2000).

Yoshida, F., T. Yamane and Y. Miyamoto, "Oxygen absorption into oil-in-water emulsions. A study on hydrocarbon fermenters", *Ind. Eng. Chem. Process Des. Develop.*, **9**, 570-577 (1970).

Curriculum Vitae

Personal information

Name:	Thanh Hai Ngo
Date of Birth:	21st December, 1976
Marital Status:	Married (one child)
Nationality:	Vietnamese
Email:	t-h.ngo@tu-bs.de

Educational progress

From 10.2005:	PhD Student (Mentor: Prof. Dr. Adrian Schumpe), Institute of Technical Chemistry, TU Braunschweig, Germany
04.2002-12.2004:	Master of Science in Chemistry, TU Braunschweig, Germany
09.1994-08.1999:	Engineer Diploma in Oil Refining and Petrochemicals, Hanoi University of Mining and Geology, Vietnam
09.1992-08.1994:	High-school Diploma, Tuson High-School, Vietnam

Professional experience

From 10.2005:	Scientific Co-worker, Institute of Technical Chemistry, TU Braunschweig, Germany
01.2005-09.2005:	Lecturer, Department of Oil Refining and Petrochemicals, Faculty of Petroleum, Hanoi University of Mining and Geology, Vietnam
07.2004-12.2004:	Student Assistant, Institute of Technical Chemistry, TU Braunschweig, Germany
09.1999-03.2002:	Lecturer, Department of Oil Refining and Petrochemicals, Faculty of Petroleum, Hanoi University of Mining and Geology, Vietnam